Quantifying high-resolution hydrologic parameters at the basin scale using InSAR and inverse modeling, Las Vegas Valley, NV

Meijing Zhang

Dissertation submitted to the faculty of the Virginia Polytechnic Institute and State University in partial fulfillment of the requirements for the degree of

Doctor of Philosophy
In
Geosciences

Thomas J. Burbey, Committee Chair
Jeffrey T. Borggaard
John A. Hole
Madeline E. Schreiber
Mark A. Widdowson

September 26, 2014
Blacksburg, VA

Keywords: Inverse parameterization, transmissivities, elastic and inelastic skeletal storage coefficients, the adaptive multi-scale method, DREAM MCMC, subsidence

Quantifying high-resolution hydrologic parameters at the basin scale using InSAR and inverse modeling, Las Vegas Valley, NV

Meijing Zhang

ABSTRACT

The overall goal of this dissertation is to determine and develop optimal strategies for inversely calibrating transmissivities (T), elastic and inelastic skeletal storage coefficients (S_{ke} and S_{kv}) of the developed-zone aquifer and conductance (CR) of the basin-fill faults for the entire Las Vegas basin, and to investigate future trends of land subsidence in Las Vegas Valley.

This dissertation consists of three separate stand-alone chapters. Chapter 2 presents a discrete adjoint parameter estimation (APE) algorithm for automatically identifying suitable hydraulic parameter zonations from hydraulic head and subsidence measurements. Chapter 3 compares three different inversion strategies to determine the most accurate and computationally efficient method for estimating T and S_{ke} and S_{kv} at the basin scale: the zonation method (ZM), the adaptive multi-scale method and the Differential Evolution Adaptive Metropolis Markov chain Monte Carlo scheme (DREAM MCMC). Chapter 4 outlines a fine-scale numerical model capable of capturing far more hydrologic detail than any previously developed model of Las Vegas Valley The new model is calibrated using high-resolution InSAR data and hydraulic head data from 1912 to 2010. The calibrated model is used to investigate the influence of faults and their

potential role on influencing clay thicknesses and land subsidence distributions, and to investigate future trends of land subsidence in Las Vegas Valley.

Acknowledgement

The writing of this dissertation has been one of the most significant academic challenges for me. I would never have been able to finish my dissertation without the guidance of my committee members, help from my friends, and support from my family.

I would like to express my deepest gratitude to my advisor, Dr. Thomas Burbey, for his excellent guidance, broad knowledge, encouragement, individual support and patience. I would like to thank Dr. Jeff Borggaard and Vitor Dos Santos Nunes, who cooperated with us to develop the APE algorithm. I also need to say thank you to Dr. Madeline E. Schreiber and Dr. John A. Hole for their patience and suggestions on my research and job hunting. My thanks also goes to Dr. Mark A. Widdowson for his teaching and suggestions on my research.

Thanks to all the members of the Hydrogeology group for their help, discussions and feedback during my courses and research work.

I want to thank all my friends who share with me the enjoyable time.

Specially, I would like to thank my family, who have always supported, loved and believed in me.

Table of contents

Contents

1. Introduction

Las Vegas Valley encompasses an area of about 4,150 km2 in Clark County, southern Nevada. To meet the growing domestic, irrigation and commercial water demand, groundwater has been intensively pumped since 1905, with the largest volumes of pumping commencing in the 1950s. Until 1990 water levels declined continuously throughout the valley, with a 90-m maximum decline occurring in the west-northwest part of the valley (Burbey 1995). Due to declining water levels, decreasing pore-water pressures within the aquifer system have led to significant increases in effective stress, which accounted for large-scale compaction of mostly fine-grained sediments (Terzaghi 1925, Poland and Davis 1969, Poland, Lofgren et al. 1972, Helm 1975). Land subsidence has been geodetically monitored since 1935, and is a century-long problem for this area. More than 1.70 m of total subsidence has been observed until 2000 (Bell, Amelung et al. 2002).

The compaction of the aquifer system has led to several large subsidence bowls and destructive earth fissures that have compromised many homes, roads and pipelines. What makes the problem more complex is that the major developed zones of subsidence do not coincide with the center of the greatest groundwater withdrawal. Seasonal pumping and recharging of the groundwater system has led to seasonal patterns of land subsidence and uplift that are superimposed on long-term compaction of fine-grained interbeds. Before the 1970's, groundwater was the principal water resource for the valley. To reduce the dependence on groundwater resources, surface water importation from Lake Mead commenced in 1971 and now represents over 75% of the total water use in the valley. The quantity of secondary recharge is closely related to land use and is influenced by

urban growth and importation of surface water from Lake Mead since 1972. Secondary recharge in Las Vegas Valley is primarily associated with lawn and golf course watering as well as discharge and disposal of industrial wastewater and has increased with the growing population of the Las Vegas area. The secondary recharge rate has increased considerably since 1972 (Morgan and Dettinger 1994). To help mitigate the ongoing occurrence of land subsidence, an artificial recharge program was initiated by the Las Vegas Valley Water District in 1989, which involves injecting Colorado River water into the principle aquifer during the winter months when water demand is low. This program resulted in a maximum of approximately 30 m of groundwater level increase between 1990 and 2005 (Bell, Amelung et al. 2008). Currently, water that recharges the aquifers by natural and artificial processes, including secondary recharge of the shallow aquifer, is greater than the total water withdrawals, thus helping to stabilize or increase groundwater levels in most areas of the basin; nonetheless land subsidence has not ceased in many parts of the valley because hydrodynamic lag associated with the time-dependent drainage of clay interbeds continues even as water levels of the principal aquifer increase.

Taditional bench mark surveys did not encompass the entire spatial extent of the basin and the transects missed major subsidence areas and the complex interaction of many of the faults in the region. It wasn't until the advent of InSAR and GPS that a far more complex pattern of subsidence across the basin was discovered that were not evident on earlier conventional subsidence maps (Amelung, Galloway et al. 1999, Hoffmann, Zebker et al. 2001, Bell, Amelung et al. 2002). InSAR techniques allow for the measurement of surface displacements at spatial resolutions on the order of meters or tens of meters, and can cover very large areas of up to thousands of square kilometers

(Hoffmann 2003). The subsidence investgation incorporating InSAR across Las Vegas Valley reveals that the spatial extent of subsidence is controlled by faults and clay thickness (Amelung, Galloway et al. 1999, Bell, Amelung et al. 2002). Seasonally fluctuating water levels along with detailed monthly InSAR data can be used to investigate how seasonal variations in water levels are reflected in subsidence and rebound patterns. These stress-strain signals are found to be highly diagnostic and can be used to more accurately estimate the elastic skeletal storage coefficients of the aquifer system (Hoffmann, Zebker et al. 2001, Yan 2007, Bell, Amelung et al. 2008, Yan and Burbey 2008).

Subsidence data, when used in conjunction with sparse and irregularly distributed drawdown data, can be used to improve groundwater model calibration of the hydrologic parameters such as elastic and inelastic skeletal specific storage, the compaction time constant, hydraulic diffusivity and the thickness of the compacting units (Heywood 1995, Burbey 2001, Hoffmann, Zebker et al. 2001, Hoffmann, Leake et al. 2003, Pavelko 2004, Pope and Burbey 2004). Yan and Burbey (2008) found that high spatial and temporal resolution subsidence observations from InSAR are extremely beneficial for accurately quantifying both elastic and inelastic skeletal specific storage values as well as hydraulic conductivity values, and the resulting model calibration results are far more accurate than using only water-levels as observations, or using just a few random subsidence observations (such as from GPS benchmarks).

Harrill (1976) was the first to systematically estimate basin-wide transmissivities from aquifer test data. Morgan and Dettinger (1994) developed the first valley-wide numerical groundwater model, which covered the period from 1912-1981 using the Trescott, Pinder

and Larson groundwater model (Trescott, Pinder et al. 1976). In their model, the final transmissivities were manually calibrated through trial-and-error methods and a minimum grid spacing of 2.5 km was implemented. Mean inelastic specific storage values were calculated based on groundwater level declines, clay thicknesses, and subsidence data measured at four benchmarks. The model did not capture the now known complex patterns of subsidence that exist today and likely existed at the time this model was developed. Jeng (Jen 1998) later converted the Morgan and Dettinger model to the MODFLOW model (McDonald and Harbaugh 1984) without changing any final simulated parameters from Morgan and Dettinger. Yan (Yan 2007) later updated Jeng's model by extending the simulation period to 2005 using mostly the original parameter estimates of Morgan and Dettinger as well as the same course grid spacing. Pavelko (Pavelko 2004) developed a one dimensional groundwater and subsidence model in conjunction with UCODE (Poeter and Hill 1998) to calibrate hydraulic parameters at the Lorenzi site where the USGS installed an extensometer in 1993. Until now no research has been done on calibration of the transmissivities and elastic and inelastic skeletal storage coefficients of Las Vegas Valley at the basin scale using the high-resolution InSAR data and water-level data.

Groundwater modeling software such as MODFLOW-2000, MODFLOW-2005 (Harbaugh 2005) has become an effective tool for simulating the long-term response of groundwater pumping and subsequent land subsidence, and therefore providing an important management tool for water purveyors. The application of MODFLOW-2005 with parameter estimation codes, such as UCODE_2005 (Poeter and Hill 1998) and PEST (Doherty 2004), is widely becoming a standard inverse tool in groundwater model

calibration and evaluation to simultaneously estimate multiple parameter values (Hill 1998, Poeter, Hill et al. 2005). Even with current advances in monitoring technology and software for simulation, drawbacks exist in using inverse parameter estimation techniques for model calibration. Deterministic estimation aims to find a single optimal parameter using available observed data. One widely used deterministic estimation approach is the zonation method (ZM), initially proposed by (Carrera and Neuman 1986), which involves dividing the entire study area into a number of zones, while unknown parameters are treated as uniform over each zone. However when using the ZM method, the shape and the number of the zones have to be defined by the user, which is somewhat subjective. The multi-scale method is an approach that provides criteria to discretize the zones. In multi-scale parameterization, the parameter estimation problem is solved through successive approximations by refining the zone domains during the inverse procedure (Chavent and Liu 1989, Liu 1993, Ameur, Chavent et al. 2002, Hayek and Ackerer 2007, Hayek, Lehmann et al. 2008). However during the refinement process, the number of degrees of freedom is increased, which can lead to over parameterization if they exceed the number of available observations (Ameur, Chavent et al. 2002). To overcome this drawback, Ameur et al. (Ameur, Chavent et al. 2002) developed an algorithm that uses both refinement and coarsening indicators to decide whether adding or removing some degrees of freedom is advantageous. Another important inversion approach applied in groundwater-model calibration is the pilot points method (PiPM) (De Marsily, Lavedan et al. 1984, Lavenue and Marsily 2001, Doherty 2003), which involves the perturbation of hydraulic properties at a small number of selected “pilot point” locations in an effort to better match observational data (Alcolea, Carrera et al. 2006).

The PiPM is designed to represent the hydrogeologic heterogeneity under either deterministic or stochastic conditions, while Kriging interpolation is used to generate the spatial distribution of hydraulic properties from estimated values at the pilot points. One inherent weakness in this method is that the number and location of pilot points is somewhat subjective. The deterministic estimation may become "trapped" in local minima if the initial guess is far from the optimal solution, while the stochastic estimation techniques allow for the estimation to jump out of the local minimum. Stochastic estimation techniques such as Simulated Annealing (Rao 2003), genetic algorithms (Prasad 2001) and the Markov chain Monte Carlo (MCMC) method (Fu and Jaime Gómez-Hernández 2009, Vrugt, Ter Braak et al. 2009) relies on randomness and re-trials to estimate the probability distributions of the unknown parameters and to sample the parameter space in searching for an optimal solution. Among the adaptive MCMC sampling approaches, the Differential Evolution Adaptive Metropolis (DREAM) MCMC scheme significantly improves the efficiency of MCMC simulations (Vrugt, Ter Braak et al. 2009), but compared with the deterministic method, stochastic algorithms are computationally time consuming.

Knowledge about optimal zonal distributions is often unknown even if a detailed hydrogeological description of the study area is available. To overcome the deficiency in parameter zonation definitions, we present a discrete adjoint parameter estimation (APE) algorithm in Chapter 2 for automatically identifying suitable hydraulic parameter zonations from hydraulic heads and subsidence measurements. A synthetic conceptual model containing seven transmissivity zones, one aquifer storage zone and three interbed zones for elastic and inelastic storage coefficients was developed to verify the

effectiveness of the APE algorithm.

In order to find the best strategy for calibrating optimal model parameters and providing a framework for developing an accurate hydrogeologic model for Las Vegas Valley we invoke three different inversion strategies in Chapter 3 to determine the most accurate and computationally efficient method for estimating transmissivities (T) and elastic and inelastic skeletal storage coefficients (S_{ke} and S_{kv}) at the basin scale: the zonation method (ZM), the adaptive multi-scale method and the Differential Evolution Adaptive Metropolis Markov chain Monte Carlo scheme (DREAM MCMC). A shorter term model is developed in Chapter 3 that that covers the period 1912-1987. This research represents the first effort to use parameter estimation techniques to inversely calibrate hydrogeologic aquifer parameters for the principle aquifer of the entire basin.

In Chapter 4, we have successfully extended Las Vegas Valley model to year 2010 using MODFLOW-2005 (Harbaugh 2005) incorporating the subsidence (SUB) (Hoffmann, Leake et al. 2003) and horizontal flow barrier (HFB) (Hsieh and Freckleton 1993) packages while implementing a 600m × 600m grid cell size, by far the finest scale model developed for the valley to date. We invoke the adaptive multi-scale strategy, which we developed in Chapter 3 to be an efficient and accurate strategy to calibrate the transmissivities (T), elastic and inelastic skeletal storage coefficients (S_{ke} and S_{kv}) of the developed-zone aquifer and conductance (CR) of the basin-fill faults for the entire Las Vegas basin using the high-resolution InSAR data and water-level data from 1912 to 2010. In addition, we investigate the influence of the faults and their potential role on influencing clay thicknesses and land subsidence. Then we use the calibrated parameters to investigate future trends of land subsidence in Las Vegas Valley by extending the

simulation period of the developed calibration model to year 2030. These results indicate that the rate of subsidence in the Northwest subsidence bowl will slow, but will continue even with measures implemented to increase water levels in this region. The reason for this continued subsidence is attributed to the slow draining of the thick clay interbeds in this region.

2. A New Zonation Algorithm with Parameter Estimation Using Hydraulic Head and Subsidence Observations

Meijing Zhang, Thomas J. Burbey, Vitor Dos Santos Nunes, and Jeff Borggaard

A version of this chapter was published in the journal Groundwater 52(4) 514-524

Abstract

Parameter estimation codes such as UCODE_2005 are becoming well-known tools in groundwater modeling investigations. These programs estimate important parameter values such as transmissivity (*T*) and aquifer storage values (*S*a) from known observations of hydraulic head, flow or other physical quantities. One drawback inherent in these codes is that the parameter zones must be specified by the user. However, such knowledge is often unknown even if a detailed hydrogeological description is available. To overcome this deficiency, we present a discrete adjoint algorithm for identifying suitable zonations from hydraulic head and subsidence measurements, which are highly sensitive to both elastic (S_{ske}) and inelastic (S_{skv}) skeletal specific storage coefficients. With the advent of InSAR (Interferometric synthetic aperture radar), distributed spatial and temporal subsidence measurements can be obtained. A synthetic conceptual model containing seven transmissivity zones, one aquifer storage zone and three interbed zones for elastic and inelastic storage coefficients were developed to simulate drawdown and subsidence in an aquifer interbedded with clay that exhibits delayed drainage. Simulated delayed land subsidence and groundwater head data are assumed to be the observed measurements, to which the discrete adjoint algorithm is called to create approximate

spatial zonations of T, S_{ske} and S_{skv}. UCODE-2005 is then used to obtain the final optimal parameter values. Calibration results indicate that the estimated zonations calculated from the discrete adjoint algorithm closely approximate the true parameter zonations. This automation algorithm reduces the bias established by the initial distribution of zones and provides a robust parameter zonation distribution.

2.1. Introduction

Groundwater modeling software such as MODFLOW-2000, MODFLOW-2005 (Harbaugh 2005) has become an effective tool for simulating the long-term response of groundwater pumping and subsequent land subsidence, and therefore providing an important management tool for water purveyors. The application of MODFLOW-2005 with parameter estimation codes, such as UCODE_2005, is widely becoming a standard inverse tool in groundwater model calibration and evaluation to simultaneously estimate multiple parameter values(Hill 1998, Poeter, Hill et al. 2005). UCODE_2005 compares observations with simulated equivalents to obtain a weighted least squares objective function; then a nonlinear regression algorithm is used to minimize the objective function with respect to the parameter values.

Although water levels are the most popular type data to calibrate a groundwater model, they alone are usually insufficient to obtain an adequate result(Hill 1998, Hill and Tiedeman 2006, Yan and Burbey 2008). Land subsidence caused by the compaction of sediments is a global scale problem (Johnson 1991, Barends 1995, Galloway, Jones et al. 1999). Due to declining water levels, decreasing pore-water pressures within the aquifer system have led to significant increases in effective stress, which accounted for large-scale compaction of mostly fine-grained sediments (Terzaghi 1925, Poland and Davis 1969, Poland, Lofgren et al. 1972, Helm 1975). Subsidence data, when used in conjunction with sparse and irregularly distributed drawdown data, can be used to improve groundwater model calibration of the hydrologic parameters such as elastic and inelastic skeletal specific storage, the compaction time constant, hydraulic diffusivity and the thickness of the compacting units (Heywood 1995, Burbey 2001, Hoffmann, Zebker

et al. 2001, Hoffmann, Leake et al. 2003, Pavelko 2004, Pope and Burbey 2004). Yan and Burbey (2008) found that high spatial and temporal resolution subsidence observations from InSAR are extremely beneficial for accurately quantifying both elastic and inelastic skeletal specific storage values as well as hydraulic conductivity values, and the resulting model calibration results are far more accurate than using only water-levels as observations, or using just a few random subsidence observations (such as from GPS benchmarks). Also, they found that storage estimates are far more sensitive to the deformation of the aquifer system than to changes in hydraulic head measurements. Even with current advances in monitoring technology and software for simulating subsidence, drawbacks exist in using inverse parameter estimation techniques for model calibration. Stochastic algorithms such as Simulated Annealing and Markov Chain Monte Carlo methods are computationally time consuming. The pilot points method is often used in groundwater-model calibration(De Marsily, Lavedan et al. 1984, Certes and de Marsily 1991, Lavenue and Marsily 2001, Doherty 2003, Doherty 2004, Alcolea, Carrera et al. 2006) and involves the perturbation of hydraulic properties at a small number of selected “pilot point” locations in an effort to match observational data. There are guidelines to estimate the number of points to use as pilot points based on the spacing between them and the model grid size. Variograms are used to generate the spatial distribution of hydraulic properties through from values at the pilot points. The hydraulic properties are calculated with Kriging interpolation. One inherent weakness in this method is that the number and location of pilot points is somewhat subjective. Another commonly used method is zonation, which is used in commonly used inverse models such as UCODE_2005(Hill 1998, Poeter, Hill et al. 2005). This method involves dividing

the entire study area into a number of zones and unknown parameters are treated as uniform. However the parameter zones must be specified by the user beforehand. It may lead to a good calibration of parameters with the user-defined parameter zones. However, such knowledge about optimal zonal distribution is often unknown even if a detailed hydrogeological description of the study area is available. To overcome the deficiency in parameter zonation definitions, we present a discrete adjoint parameter estimation (APE) algorithm for automatically identifying suitable parameter zonations from hydraulic head and subsidence measurements, which are highly sensitive to both elastic (S_{ske}) and inelastic (S_{skv}) skeletal specific storage coefficients. Here we develop a hypothetical model using MODFLOW-2005 in which observed measurements of land subsidence (including hydrodynamic lag) and hydraulic head data are made at selected locations and times. Using only these observations, the distributed parameter identification algorithm is called to create approximate spatial zonations of T, S_{ske} and S_{skv}. Then the approximation of parameter zonations is compared with the original (true) zonations assigned in MODFLOW-2005. Finally, UCODE_2005 is used to obtain the final optimal parameter values. The new APE algorithm, when combined with UCODE_2005, provides a new powerful tool for obtaining optimal zonations.

2.2. Formulation of the Adjoint Parameter Estimation Algorithm

The spatial variability of the storage and conductivity properties for aquifer systems are generally so complex that the investigator could not possibly identify the parameter zones in an adequate or realistic way to describe the optimal distribution of hydraulic parameters. Therefore, an algorithm which can automatically determine the parameter

zonations is necessary to produce an accurate and optimal model conceptualization. Here we present a discrete adjoint algorithm for identifying a suitable zonation scheme from hydraulic head and subsidence measurements, which are highly sensitive to both elastic and inelastic skeletal specific storage coefficients as well as transmissivity. The automatically identified parameter zonations will then be implemented into the synthetic model using MODFLOW-2005 and UCODE_2005.

Adjoint methods are widely used in areas such as optimal control theory, design optimization and sensitivity analysis(Duffy 2009). In our study, we minimize the difference between observed and simulated groundwater levels and land subsidence. The objective function can be written as:

$$J(h,q) = f(h,q) = \frac{1}{2}\left(\sum_{i=1}^{N_1} \| h(q) - h_{obs(i)} \|^2 + \sum_{j=1}^{N_2} \| Sub(q) - Sub_{obs(j)} \|^2 + \alpha \| q - q_0 \|^2\right)$$

Equation 1

where,

$$q = (S_{ske}, S_{skv}, T)$$

Equation 2

and represents the parameter vector to be optimized, S_{ske} is the elastic skeletal specific storage of the interbed, S_{skv} is the inelastic skeletal specific storage of the interbed, T is the transmissivity of the aquifer, h(q) represents the calculated water level, which is a function of q, h_{obs} represents the observed water level, Sub represents the calculated subsidence, which is a function of q, and Sub_{obs} represents the observed subsidence, N_1 is the number of observed water level, and N_1 is the number of observed subsidence. The last term of Equation 1 represents a penalty term, where α is penalty parameter; q_0 is the

initial guess or mean value of *q*. Equation 1 is subject to the groundwater flow equations

$$S_s b \frac{\partial h^a}{\partial t} = \nabla \cdot (T \nabla h^a) + \sum_j K_{vj} \frac{d\bar{h}_j^i}{dz} - W$$

Equation 3

$$S_v \frac{\partial \bar{h}^i}{\partial t} = \frac{\partial}{\partial z}(K_{vj} \frac{\partial}{\partial z} \bar{h}_j^i)$$

Equation 4

where h^a is simulated hydraulic head of the aquifer, $\bar{h}^i$ is hydraulic head in the interbed, *b* is thickness of the aquifer system, *T* is transmissivity, S_s is specific storage of the aquifer, K_v is vertical conductivity, S_v is storage coefficient of the interbed, and *W* is a source term.

After discretization of Equation 3 and Equation 4 we obtain:

$$G(q) = A(q)h^m(q) - h^{m-1}(q) - W = 0$$

Equation 5

where *G*(q) is the governing equation, *A*(q) is the matrix of parameter values, time step length and grid cell length, *m* represents the time step.

The adjoint method solves the following equation for λ .

$$\frac{\partial f}{\partial h} + \lambda \frac{\partial G}{\partial h} = 0$$

Equation 6

Then $J'(q)$ is computed

$$J'(q) = \frac{\partial f}{\partial q} + \lambda^T \frac{\partial G}{\partial q}$$

Equation 7

According to Taylor's expansion,

$$\nabla J(q_1) = J'(q_0) + J''(q_0)(q_1 - q_0)$$

Equation 8

When the cost function (1) reaches a minimum,

$$\nabla J(q_1) = 0$$

Equation 9

Then (9) is substituted into (8) to yield:

$$q_1 = q_0 - J''(q_0)^{-1} J'(q_0)$$

Equation 10

Where *J''* can be estimated with the BFGS method (named after Broyden, Fletcher, Goldfarb, and Shanno). The BFGS method is a well-known Quasi-Newton algorithm which is used for solving unconstrained nonlinear optimization problems. From Equation 10, we can calculate the parameter vector q_1 from the initial parameter guess q_0. Then, parameter vector q can be updated with the Newton method described by Equation 11until the maximum fractional change of q evaluated after three iterations is less than 0.01(Step 4 of Figure 1).

$$q_k = q_{k-1} - J''(q_{k-1})^{-1} J'(q_{k-1}) .$$

Equation 11

A procedural outline of the APE algorithm for calculating the parameter zonations is shown in Figure 1. In step 6, a "sufficient result" means that the difference between the simulated and observed water levels and subsidence is small (a value set by the user).

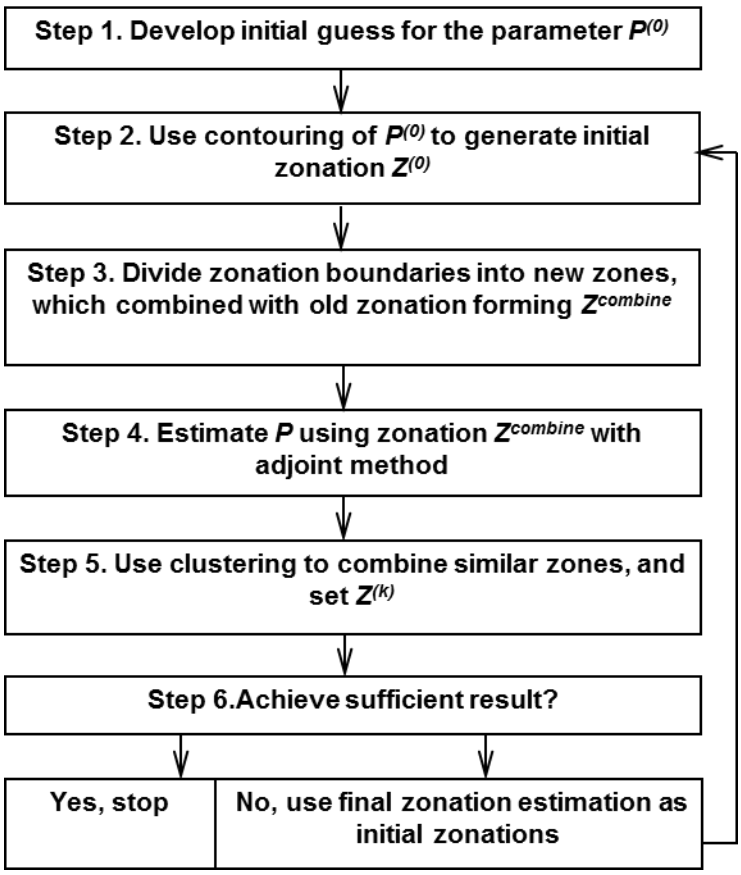

Figure 1. APE Algorithm to calculate parameter zonations

2.3. Evaluation of the APE Algorithm with MODFLOW-2005

The APE algorithm is designed to automatically identify suitable parameter zonations from hydraulic head and subsidence measurements. To evaluate the effectiveness of automated parameter zonation using the adjoint parameter estimation algorithm (APE) an areal two-dimensional hypothetical model modified from Yan and Burbey (2008) is developed using MODFLOW-2005.The model is represented as a 19 × 29 km one-layer confined aquifer, with each cell size of 1×1 km (Figure 2). This is a transient state model which simulates groundwater flow and land subsidence for 15 years. Each year is divided into two six-month stress periods. The simulated aquifer thickness is 200m. A poorly

permeable but highly compressible clay interbed of variable thickness (from 9 to 130 m) is distributed within the permeable aquifer (Figure 3). The peripheral boundaries are set as no-flow conditions. For the entire region the initial hydraulic head is 800m and the preconsolidation (previous minimum head value in the aquifer) head is 795m. Five wells are pumped at a constant rate in 6-month intervals (6 mo. on during the summer and 6 mo. off during the winter) Figure 2).

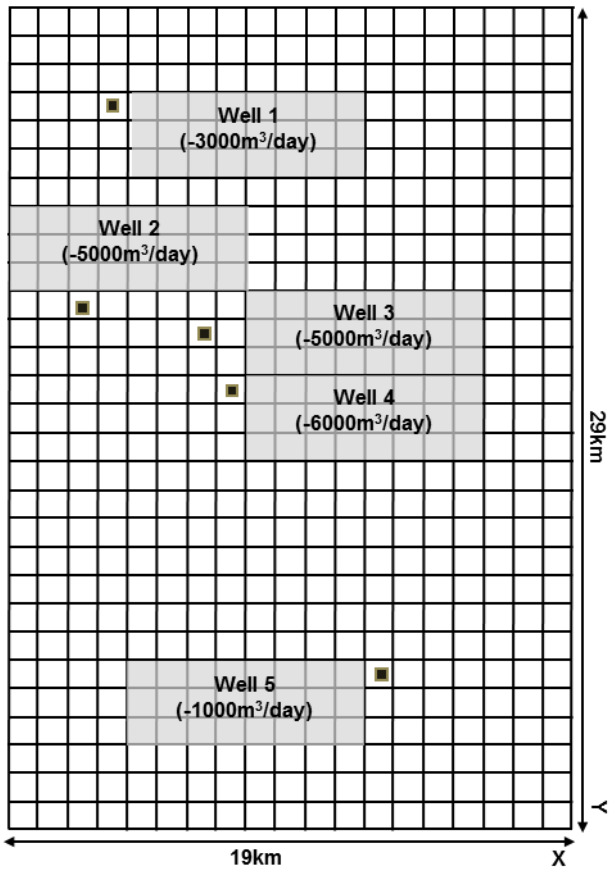

Figure 2 Areal view of the conceptual model showing the 19x29 km model grid (1x1 km cells) and well locations and pumping rate.

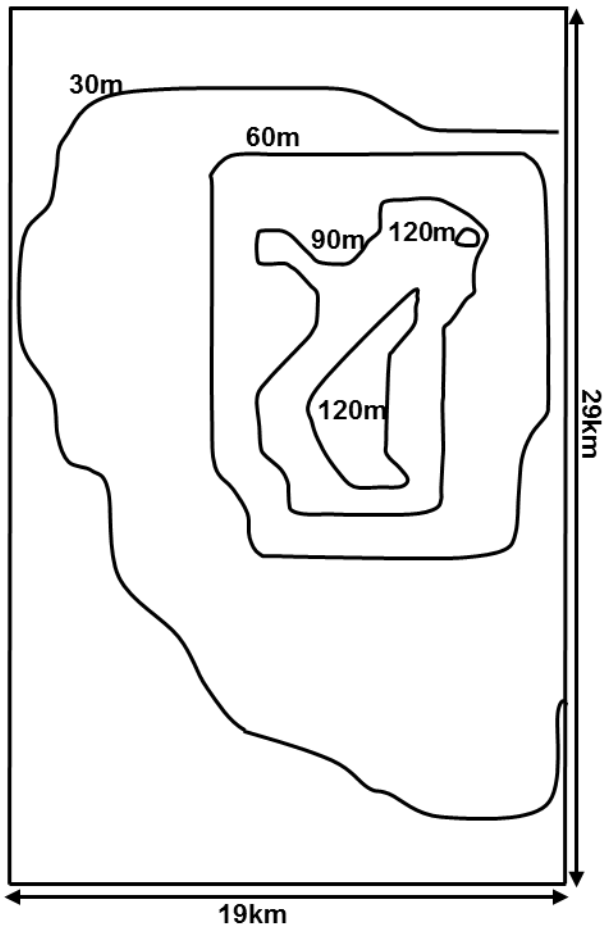

Figure 3. Conceptual model of the aquifer system containing a variably thick contiguous clay interbed with delayed drainage

The SUB package (Hoffmann, Leake et al. 2003) is used to calculate subsidence at each model cell. For the aquifer that is composed of relatively coarse-grained sand, land subsidence is simulated to occur instantaneously when groundwater levels decline. The interbed is assumed to be areally far more extensive than its thickness, and the hydraulic conductivity of the interbed is considerably lower than the aquifer, so the direction of groundwater flow within the interbed can be treated as vertical. Groundwater flow from the interbed to the aquifer occurs when the head in the aquifer declines, with the head change in the lens lagging that of the aquifer .

In the context of interbed compaction and land subsidence, the time delay caused by slow

dissipation of transient overpressures is often given in terms of the time constant, which is the time during which about 93 percent of the ultimate compaction for a given decrease in head occurs (Riley 1969). The time constant can be expressed as

$$\tau_0 = \frac{(\frac{b_0}{2})^2 S_{sk}}{K'_v}$$

Equation 12

where $b_o/2$ is one-half the thickness of the interbed, S_{sk} is the skeletal specific storage of the interbed, K'_v is the vertical hydraulic conductivity of the interbed. Laboratory consolidation tests indicate that the compressibility, and thus the skeletal specific storage, can vary greatly depending on whether the effective stress exceeds the previous maximum effective stress, which is termed as the preconsolidation stress (Johnson, Moston et al. 1968, Jorgensen 1980). Inelastic skeletal specific storage S_{skv} is used when the water level in the interbed is less than its previous minimum value, whereas elastic skeletal specific storage S_{ske} is invoked when the drawdown in the interbed is higher than the previous minimum values.

The study area is divided into 7 transmissivity zones *T*1 to *T*7 (Figure 4). Both the aquifer and interbed are treated as compressible. The storage coefficient of the aquifer is assumed to be 0.002 for the entire model region. Three separate zones are used to express the elastic (S_{ske1}, S_{ske2} and S_{ske3}) and inelastic (S_{skv1}, S_{skv2} and S_{skv3}) skeletal specific storage of the interbed. These values and the zonation distribution are shown in Figure 5. The vertical hydraulic conductivity for the interbed was assumed to be 0.00006 m/d.

An initial forward simulation using MODFLOW-2005 was conducted with known pumping rates and all true hydraulic property values described above. Hydraulic heads and subsidence values obtained from this simulation are treated as the true observation

values. We assume that high temporal and spatial resolution land subsidence data are available at each grid cell and treat them as the fictitious subsidence rates available from InSAR interferograms (Figure 6).

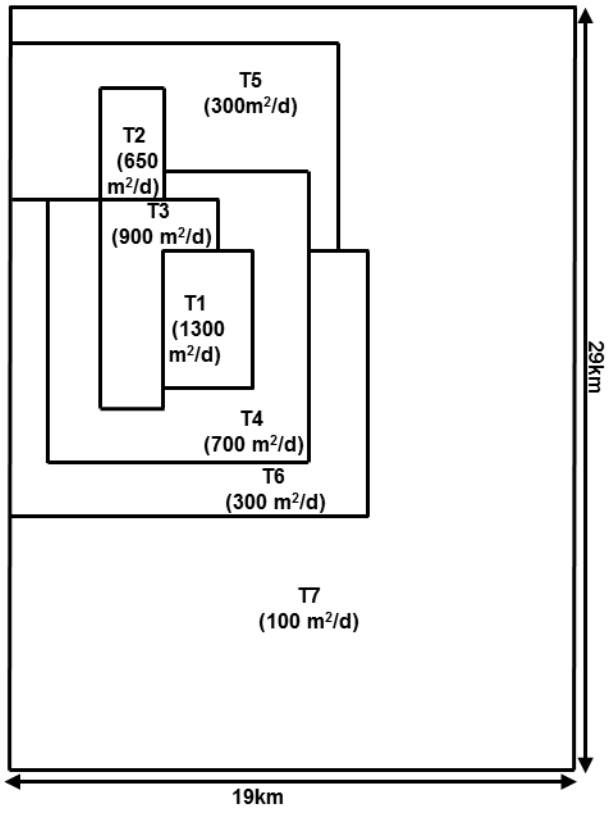

Figure 4 Transmissivity zonations and values for the synthetic model

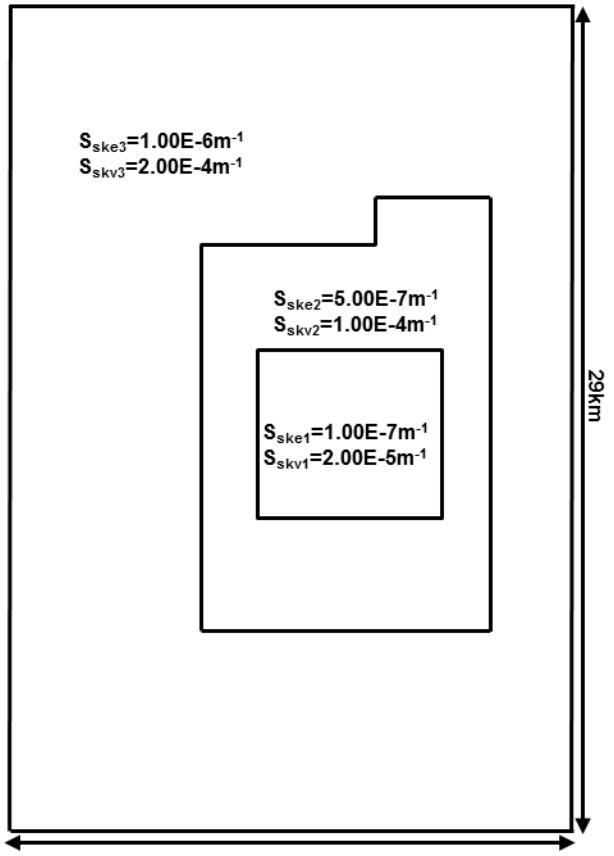

Figure 5 Zonations and values for the elastic and inelastic specific storage parameters

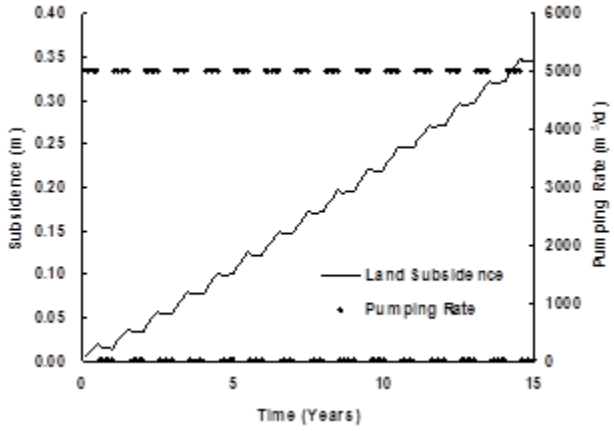

Figure 6 Cyclical pumping and resulting simulated land subsidence pattern

The APE algorithm can now be applied to calculate the zonations for transmissivity and elastic and inelastic skeletal specific storage of the interbed. For the very first call of the APE algorithm, the initial guess for the parameter $P^{(0)}$ (Step 1 of Figure 1 is estimated as follows:

(1) Incorporate the observed subsidence data to estimate an initial elastic and inelastic skeletal specific storage and set them as $S_{ske}^{(0)}$ and $S_{skv}^{(0)}$;

(2) Develop initial guesses for the transmissivity $T^{(0)}$ using Equation 13.

$$T^{(0)}(x) = \frac{S_s \frac{\partial h}{\partial t}(t,x)}{\nabla \cdot \nabla h(t,x)}$$

Equation 13

In Equation 13, we use the observed hydraulic head, *h*, only when the pumping rate is zero. The Newton method converges locally and inheritably so does the Quasi-Newton method, which is discussed thoroughly by K. Ito and K. Kunisch (2008). Thus, an initial parameter guess that is close to the local minimum will almost always guarantee convergence. In this perspective the choice of the initial guess from Equation 13 is made, since it takes advantage of the information given by Equation 13 when there is no pumping. Although this generally provides a good estimate, it is sensitive to the complexity of the problem at hand so if the zonation is highly complex, the likelihood of convergence might be lower.

2.3.1. Implementing UCODE_2005 with the APE algorithm

Once the automatically identified parameter zonations have been estimated using the APE algorithm, we implement these zones with the initial parameter values into the synthetic model using MODFLOW-2005 and UCODE_2005. UCODE_2005 is a nonlinear parameter estimation program, which compares observations with simulated equivalents to obtain a weighted least squares objective function. Then it employs a

modified Gauss-Newton method to iteratively solve a general nonlinear regression problem (Hill 1998, Poeter, Hill et al. 2005). UCODE_2005 can be used to analyze sensitivity, and calculate confidence and prediction intervals. The weighted least-squares objective function *M*(q) is defined as follows (from (Hill 1998)):

$$M(\underline{q}) = \sum_{i=1}^{ND} \omega_i \left[y_i - y_i'(\underline{q}) \right]^2$$

Equation 14

where $\underline{q}$ is a vector containing values of each of the parameters being estimated, and in this case

$$\underline{q} = (S_{ske}, S_{skv}, T)$$

Equation 15

where *ND* is the number of observations, ω_i is the weight for the i^{th} observation, y_i is the i^{th} observation being matched by the regression, and $y_i'(\underline{q})$ is the simulated value which corresponds to the *i*th observation.

UCODE_2005 yields a new set of estimated parameter values based on the zonations from the APE algorithm. The estimated parameter values calculated from UCODE_2005 are then returned to the APE algorithm as the initial guess for the parameter $P^{(0)}$ (Step 1 of Figure 1). This iterative procedure between the APE and UCODE_2005 is continued until the simulated heads and subsidence values accurately approach the true heads and subsidence values. Generally, less than 10 iterations are required to achieve convergence.

2.4. Results and Discussion

The APE algorithm (Figure 1) was applied using a portion of the water-level observations

and subsidence data produced by the synthetic model. No known information about the distribution of known parameter values (divided into specific zones where each zone represents a constant parameter value) was provided to the APE algorithm.

Initial estimates of interbed elastic and inelastic skeletal specific storage zones obtained from the APE algorithm are provided as a starting point in the iteration sequence. After estimating the distribution of S_{ske} and S_{skv} aquifer hydraulic transmissivity (T) zones are estimated. Then UCODE_2005 is used to obtain a new set of estimated parameter values based on the zonations and initial values from the APE algorithm. Then the new set of estimated parameter values calculated from UCODE_2005 are returned to the APE algorithm to recalculate S_{ske} and S_{skv} and then to obtain new estimates for T. The parameter-estimation iterations stop if the maximum fractional change in the sum-of-squared weighted residuals over three parameter-estimation iterations is less than 0.01. Generally conversion will occur after about 6 iterations between the APE algorithm and UCODE_2005. The estimated S_{ske} and S_{skv} zonations using the APE algorithm along with the true zonations that were developed from the synthetic model using MODFLOW-2005 are shown in Figure 7. Similarly, the estimated aquifer transmissivity zonations using the APE algorithm, along with the true zonations that were developed from the synthetic model using MODFLOW-2005, are shown in Figure 8.The number of zones after each iteration is listed in Table 1. These results show that after several iterations between the APE algorithm and UCODE_2005 the distributed parameter identification algorithm appears to accurately match the true spatial distributions of the zones.

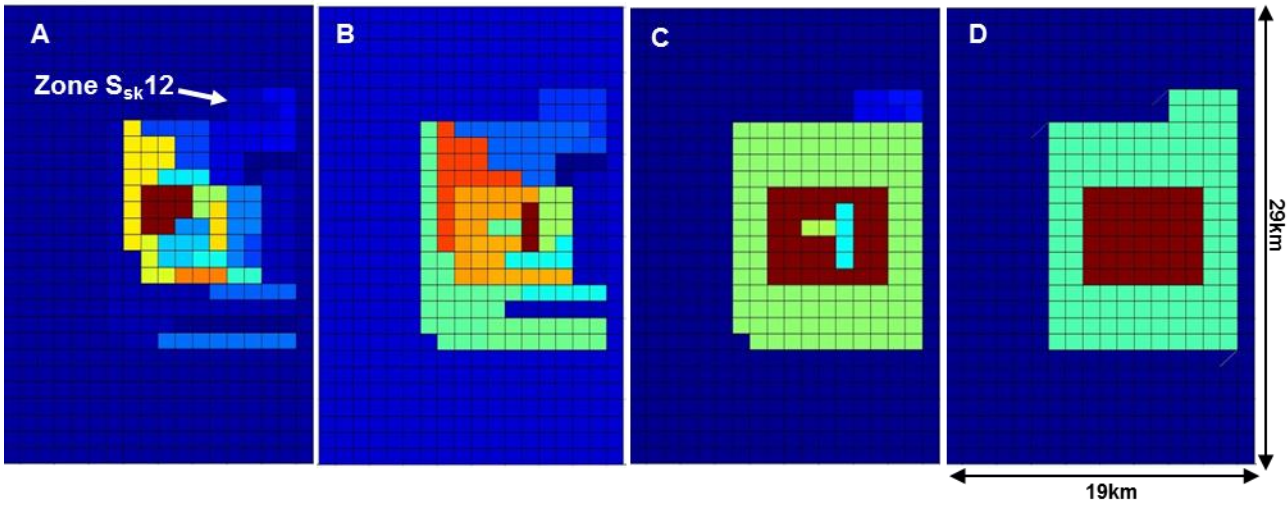

Figure 7 Estimated specific storage zonations using the APE algorithm (A) after 1st iteration, (B) after 2nd iteration, (C) after 3rd iteration compared with the (D) true specific storage zonations calculated by MODFLOW-2005 (the colors in each frame only indicate different zones and the colors (number of zones) change after each iteration)

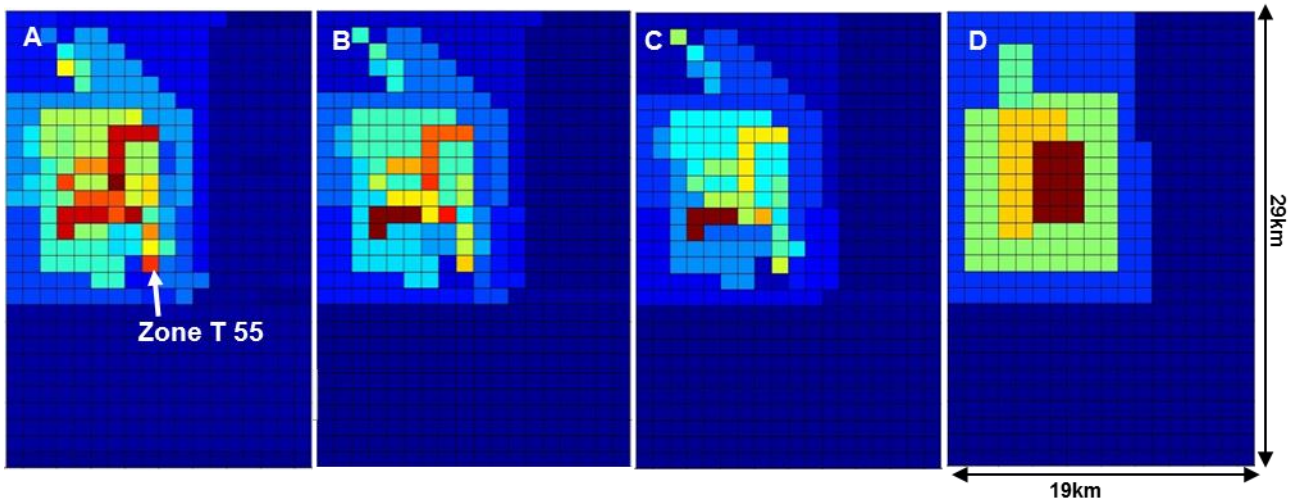

Figure 8 Estimated transmissivity zonations using the APE algorithm (A) after 1st iteration, (B) after 2nd iteration, (C) after 3rd iteration compared to the (D) true transmissivity zonations calculated by MODFLOW-2005 (the colors in each frame only indicate different zones and the colors (number of zones) change after each iteration)

Table 1 Number of calculated zones after each iteration

Iteration	Transmissivity (T)	Specific Storage (Ss)
1st Iteration	69	27

2nd Iteration	38	19
3rd Iteration	31	7
True Zones	7	3

Figure 9 shows the estimated parameter errors after each iteration where100% means the simulated value differs from the true value by a factor of 2 and a value of one means the result comes from the 1st iteration. It can be seen that calibrated transmissivity and inelastic skeletal specific storage have lower errors than the calibrated elastic skeletal specific storage. Composite scaled sensitivities (CSS) are used to measure the overall sensitivity of the observations to the parameters. CSS are calculated for each parameter using the dimensionless scaled sensitivities for all observations, which can be used to compare the amount of information provided by different types of parameters. Model simulation results will be more sensitive to parameters with large CSS relative to those for other parameters. It can also been seen from Figure 10 that transmissivity and inelastic skeletal specific storage have higher composite scaled sensitivities (CSS) than the elastic skeletal specific storage. This means that it is easier to attain accurate transmissivity and inelastic skeletal specific storage values and it is more elusive to obtain elastic skeletal specific values. This is because the relatively small amount of elastic subsidence is masked by the delayed drainage of the interbed and by the relatively large inelastic subsidence. Actually, the elastic skeletal specific storage has a high dimesionless scaled sensitivity (DSS) to land subsidence, but has low DSS to drawdown. Both inelastic skeletal specific storage and transmissivity have high DSS to both land subsidence and drawdown. Thus subsidence data are highly sensitive to elastic (S_{ske}), inelastic (S_{skv}) skeletal specific storage coefficients and transimissivity (T), which

indicates that high spatial and temporal resolution InSAR data are required to accurately calibrate parameter values.

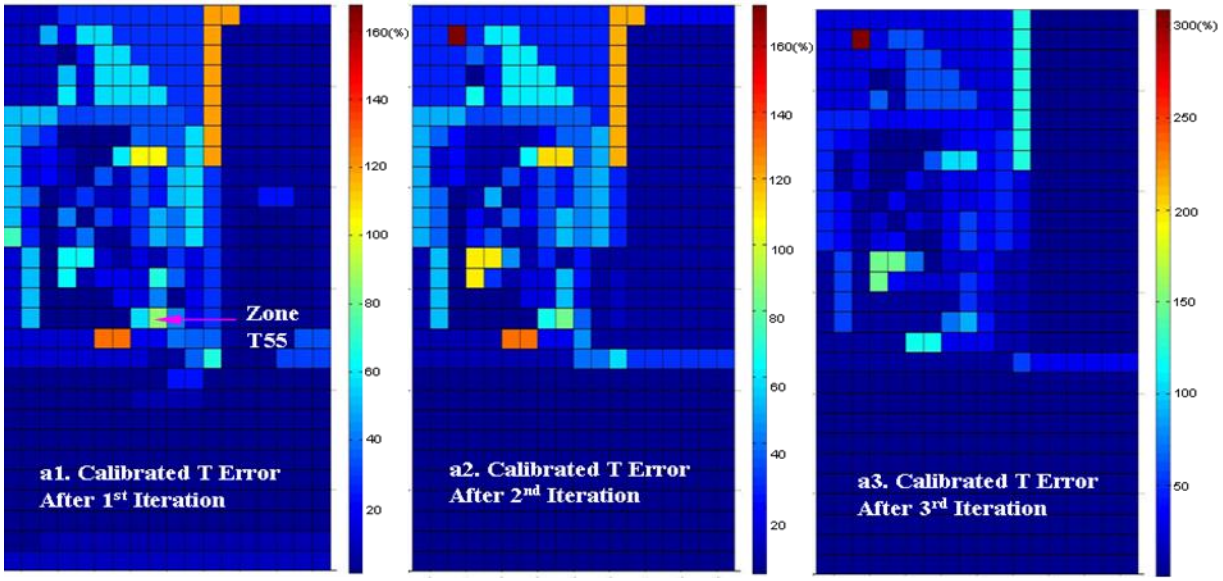

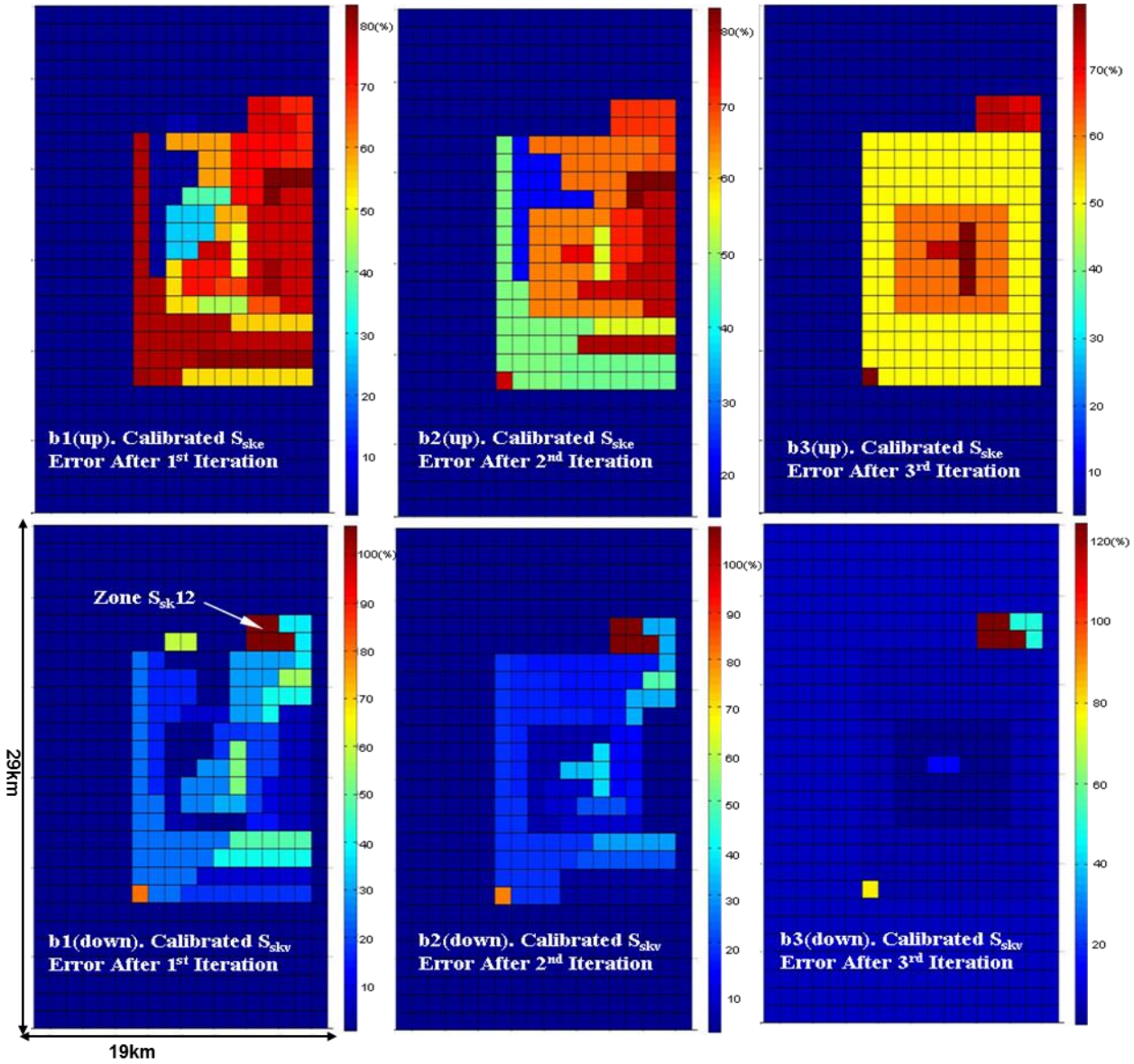

Figure 9 (a) Calibrated transmissivity errors after each iteration, and (b) Calibrated specific storage errors after each iteration.

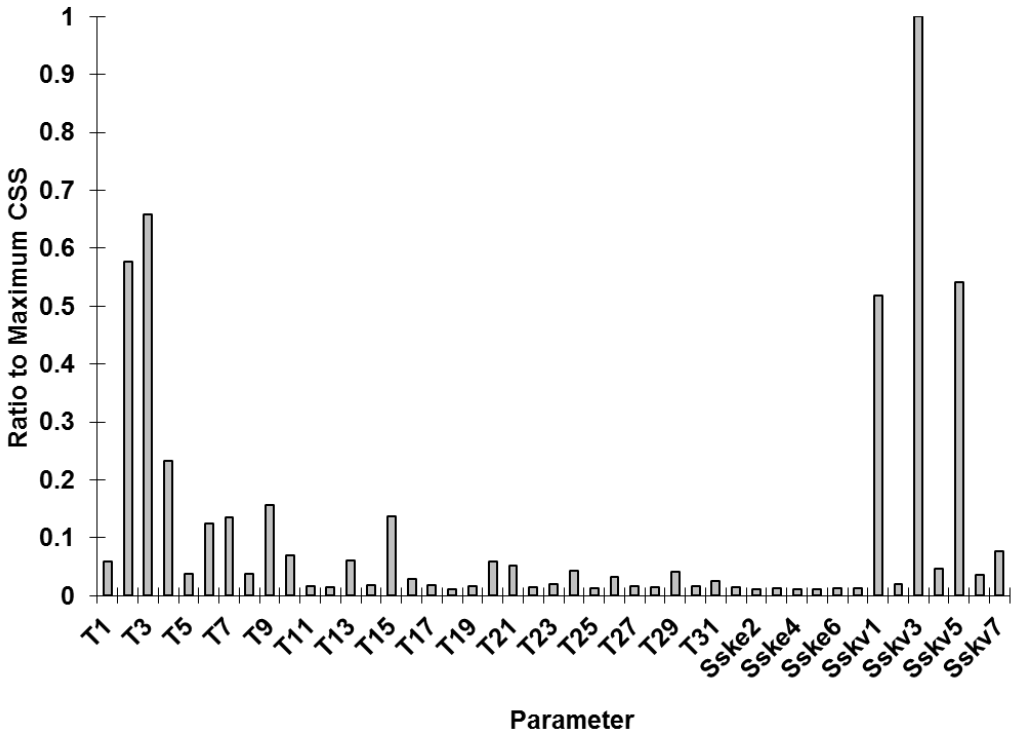

Figure 10 Composite scaled sensitivity of transmissivity and specific storage for the last iteration

The size of the parameter zones also influences the calibrated result. For example, the 1st iteration zone *T*55 covers only 1 grid cell and it leads to the largest calibrated parameter error (88%) among all the transmissivity zones (Figure 9, (a1)). Also for the 1st iteration zone $S_{sk}12$ covers only 5 grid cells leading to the largest calibrated parameter error (106%) among all the specific storage zones (Figure 9, (b1)). The requirement of further delineating small zones could easily be the result of high spatial variability of the parameters that cannot be simulated with a single value, but should be simulated with a finer representation of the spatial variability of hydraulic properties. Hence, it is important for the APE algorithm to divide the zonation boundaries into new zones after each iteration (Step 3 of Figure 1). On the other hand the requirement of further delineating smaller zones may also be an indication of combing zones with similar magnitude after each iteration (Step 5 of Figure 1). This modification to the APE

algorithm is still under investigation. Nonetheless, the APE algorithm combined with UCODE_2005 is able to provide reasonable and stable results. If some parameters have CSS that are less than about 0.01 times the largest CSS, it is likely that the regression will not converge (Hill, 1998; Anderman and others, 1996). In this model all the optimal parameters have composite scaled sensitivities that are larger than 0.022 times the largest composite scaled sensitivities (Figure 10), indicating that the parameters will likely be accurately estimated. Parameter correlation coefficients can be used to indicate whether the estimated parameter values are likely to be unique. Absolute values of parameter correlation coefficients close to 1 indicate a high degree of correlation. Thus, changing the parameter values in a linearly coordinated manner will result in the same value of the objective function. In this model, most of the parameter correlation coefficients are on the order of 10^{-2}-10^{-4} and the largest value is 0.58, suggesting that uniqueness was not a problem.

The final simulated drawdown and subsidence distributions and the true hydraulic heads and subsidence distributions are shown in Figure 11 and Figure 12. Nash-Sutcliffe efficiency (NSE) is chosen here to measure the overall fit of the hydrographs (Nash and Sutcliffe 1970). NSE is computed as

$$NSE = 1 - \left[\frac{\sum_{i=1}^{n} (Y_i^{obs} - Y_i^{sim})^2}{\sum_{i=1}^{n} (Y_i^{obs} - Y^{mean})^2} \right] \quad \textbf{Equation 16}$$

where Y_i^{obs} is the ith observation value, Y_i^{obs} is the ith simulated value, Y^{mean} is the mean of observed data, and n is the total number of observations. NSE ranges between -∞ and 1. Generally values between 0.0 and 1.0 are acceptable, with NSE=1.0 being the optimal value. In our case NSE is 0.9997 for drawdown and 0.9813 for subsidence, which

indicates that the simulated drawdown values more closely reflect the observed values than does the simulated subsidence distribution. One reason for this is that the elastic skeletal specific storage values, which control land subsidence, are less accurately estimated than other parameters. Another reason is the delayed land subsidence mechanism makes computation quite complex, so that a small error in the estimation of the parameters will lead to large differences in calculated land subsidence.

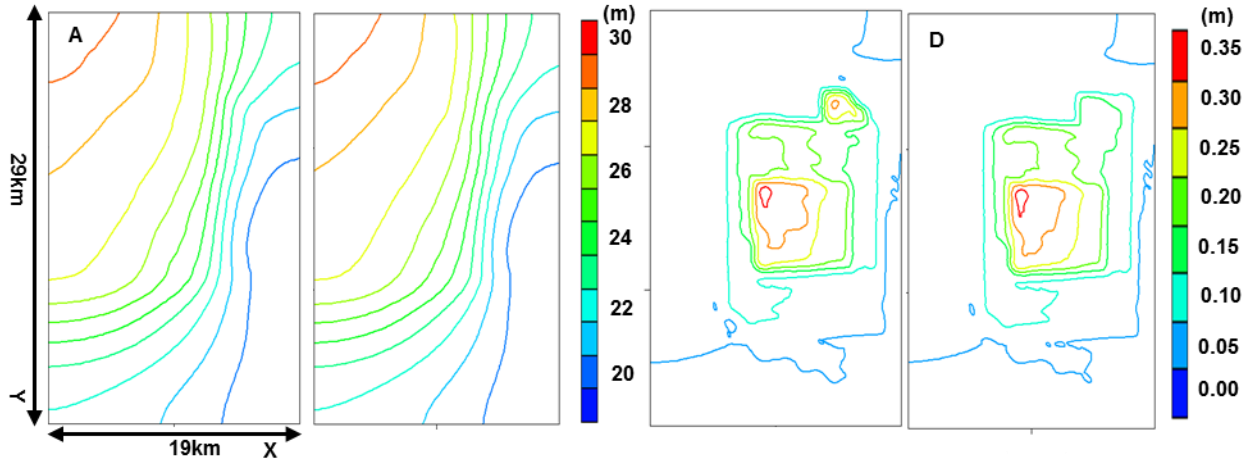

Figure 11 (A) Estimated drawdown using the estimated parameter values, (B) the true drawdown developed by MODFLOW-2005,(C) estimated subsidence using the estimated parameter values, and (D) the true subsidence developed by MODFLOW-2005

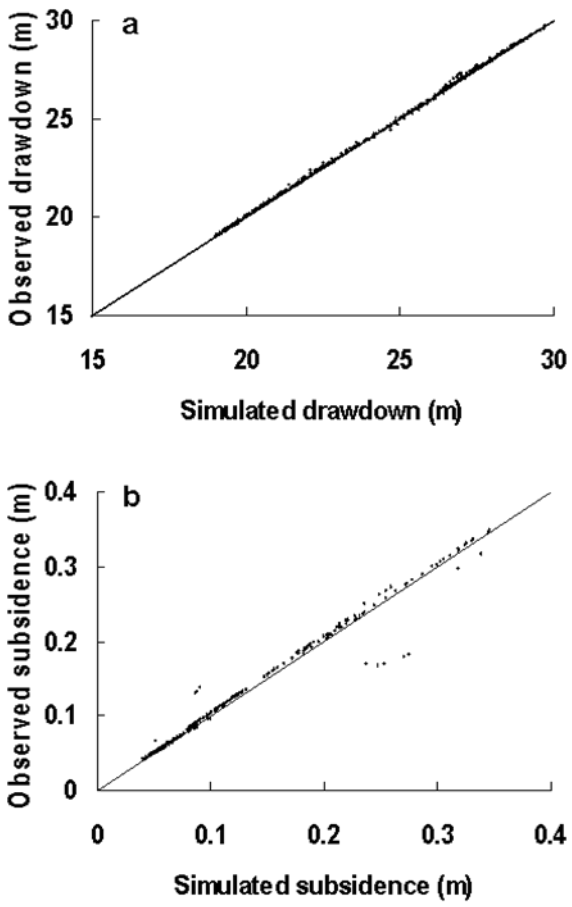

Figure 12 Observed vs. simulated (A) final drawdown, and (B) final subsidence

2.5. Conclusions

Our goal in this investigation involves applying a fully distributed parameter identification algorithm to a hypothetical model to produce results that show that this automation process can remove user bias and provide a more accurate and robust parameter zonation distribution. We have outlined an automated parameter estimation process that can greatly aid the calibration of groundwater flow models. After analyzing and comparing the results of the newly developed adjoint parameter estimation model, we make the following important conclusions:

With the advent of InSAR, basin-wide coverage of spatial and temporal subsidence and rebound measurements, which occur in response to cyclical aquifer pumping, can be

obtained where surface deformations can be expected to occur. Subsidence data are highly sensitive to both elastic (S_{ske}) and inelastic (S_{skv}) skeletal specific storage. High spatial and temporal resolution InSAR data can help reveal the heterogeneity properties of the aquifer system in ways that hydraulic head data alone cannot.

The distributed parameter identification algorithm we applied is verified to be effective. It can be seen that the estimated zones approach the spatial distribution of the true parameter zones that are developed from MODFLOW-2005. This automation process removes user bias and provides an accurate robust parameter zonation distribution. The effectiveness of the final zonation is influenced by the initial calculated zonation (Step 1 of Figure 1). Once an initial estimation of the parameters is made using UCODE_2005, the specific storage and transmissivity zonations become simplier to solve for with the APE algorithm. Thus, the algorithm presented here for the identification of appropriate zones establishes the link between improvements on zonation distribution and the limit where every point in the grid is a zone. Equation 13 represents the link between these two. The choice of the initial guess from Equation 13 takes advantage of the information given by Equation 13 when there is no pumping. Although this generally is a good estimate and typically guarantees convergence, it is sensitive to the complexity of the problem at hand, so if the zonation is highly complex the likelihood of convergence might be lower.

The size of the zone also influences the calibrated result. Small zones are likely to lead to large calibrated parameter errors. It is therefore important for the APE algorithm to divide these small zones into smaller zones or combine these small zones with larger similar zones after each iteration. The requirement of further delineating small zones

could easily be the result of high spatial variability of the parameters that cannot be simulated with a single value but rather there exists a continuum of values (as represented by a particular variogram), which points to one of the weaknesses of zonation method presented here.

Analysis of composite scaled sensitivities and parameter correlation coefficients shows that the APE algorithm combined with UCODE_2005 is able to provide reasonable, unique and stable results for the model used in this study.

The final simulated hydraulic drawdown and subsidence distribution matches the true observation distributions quite well. The simulated drawdown values more closely reflect observed values than do the simulated subsidence values. The more poorly estimated elastic skeletal specific storage values coupled with the mechanisms responsible for complex delayed drainage are the two main factors leading to larger calculated land subsidence errors.

The distributed parameter identification algorithm developed herein should be useful for the calibration of all groundwater models using multiple types of observations. However there are some limitations that were identified from this study. One limitation is that this one layer model over-simplifies the real world system. More challenges will be encountered with complex, multilayered systems. Another limitation is that we use the true land subsidence and hydraulic drawdown data developed from MODFLOW-2005 as the observations with no errors in the observed data; however, errors are impossible to avoid in real field data collection and processing (particularly with InSAR), which makes parameter estimation more difficult. Despite these limitations, this study shows that the algorithm and iterative process developed in this study can be an effective method for

model calibration.

3. A comparison of three optimization schemes for estimating basin wide transmissivities and elastic and inelastic skeletal storage coefficients for Las Vegas Valley

Abstract

Las Vegas Valley has had a long history of groundwater development and subsequent surface deformation. Much research has been done to estimate parameters within the Las Vegas basin, but this research represents the first effort to use parameter estimation techniques to inversely calibrate hydrogeologic aquifer parameters for the principle aquifer of the entire basin. Three different inversion strategies are invoked to determine the most accurate and computationally efficient method for estimating transmissivities (T) and elastic and inelastic skeletal storage coefficients (S_{ke} and S_{kv}) at the basin scale: the zonation method (ZM), the adaptive multi-scale method and the Differential Evolution Adaptive Metropolis Markov chain Monte Carlo scheme (DREAM MCMC). The three inversion methods are compared and contrasted based on quantitative measurements of model fit, computational efficiency and user flexibility. The results indicate that overall, the adaptive multi-scale method, which is able to efficiently reconstruct the T, S_{ke} and S_{kv} zones while providing more flexibility and accuracy than the other two methods, is the best strategy for calibrating optimal model parameters and providing a framework for developing an accurate hydrogeologic model for Las Vegas Valley.

3.1. Introduction

Inverse modeling involving history matching of model outputs to field measurements has been widely used in the field of hydrogeology for several decades (Hill and Tiedeman 2007) and has largely superseded trial-and-error methods. The objective of inverse modeling is to calibrate optimal model parameters, with which credible prediction can be made. Parameters such as transmissivity, hydraulic conductivity, storage coefficient, aquitard leakage and porosity, are often important parameters that are calibrated using inverse models in groundwater investigations. Although groundwater levels are the most popular type of observational data used to calibrate groundwater models, they alone are usually insufficient to obtain adequate and unique results (Hill 1998, Hill and Tiedeman 2006, Yan and Burbey 2008, Zhang, Burbey et al. 2013). Other measurement data types that are useful for calibrating a model may include fluid concentration values, flow rates, recharge rates, and land subsidence.

The inversion approach includes both deterministic and stochastic estimation. Deterministic estimation aims to find a single optimal parameter using available observed data. One widely used deterministic estimation approach is the zonation method (ZM), initially proposed by (Carrera and Neuman 1986), which involves dividing the entire study area into a number of zones, while unknown parameters are treated as uniform over each zone. This approach is commonly used in popular groundwater inversion codes such as UCODE_2005 (Poeter, Hill et al. 2005). However when using the ZM method, the shape and the number of the zones have to be defined by the user, which is somewhat subjective. The multi-scale method is an approach that provides criteria to discretize the zones. In multi-scale parameterization, the parameter estimation problem is solved

through successive approximations by refining the zone domains during the inverse procedure. When the zone refinement is complete, the refinement no longer induces a significant decrease of the objective function (Chavent and Liu 1989, Liu 1993, Ameur, Chavent et al. 2002, Hayek and Ackerer 2007, Hayek, Lehmann et al. 2008). However during the refinement process, the number of degrees of freedom is increased, which can lead to over parameterization if they exceed the number of available observations (Ameur, Chavent et al. 2002). To overcome this drawback, Ameur et al. (Ameur, Chavent et al. 2002) developed an algorithm that uses both refinement and coarsening indicators to decide whether adding or removing some degrees of freedom is advantageous.

Another important inversion approach applied in groundwater-model calibration is the pilot points method (PiPM) (De Marsily, Lavedan et al. 1984, Lavenue and Marsily 2001, Doherty 2003), which involves the perturbation of hydraulic properties at a small number of selected "pilot point" locations in an effort to better match observational data (Alcolea, Carrera et al. 2006). The PiPM is used in the parameter estimation software PEST (Doherty 2004). The PiPM is designed to represent the hydrogeologic heterogeneity under either deterministic or stochastic conditions, while Kriging interpolation is used to generate the spatial distribution of hydraulic properties from estimated values at the pilot points. One inherent weakness in this method is that the number and location of pilot points is somewhat subjective, and a considerable degree of non-uniqueness still exists. Stochastic estimation techniques such as Simulated Annealing (Rao 2003), genetic algorithms (Prasad 2001) and the Markov chain Monte Carlo (MCMC) method (Fu and Jaime Gómez-Hernández 2009, Vrugt, Ter Braak et al. 2009) relies on randomness and re-trials to estimate the probability distributions of the unknown parameters and to

sample the parameter space in searching for an optimal solution. The deterministic estimation may become "trapped" in local minima if the initial guess is far from the optimal solution, while the stochastic estimation techniques allow for the estimation to jump out of the local minimum. With the development of high performance computing and high throughput computing technology, new technologies, such as Grid computing (Foster, Kesselman et al. 2001), makes the computationally long running of stochastic calculations tractable (Renard and De Marsily 1997), however difficulties still exist, such as defining how many iterations are required to obtain an accurate statistic distribution (Ballio and Guadagnini 2004, Renard 2007). Among the adaptive MCMC sampling approaches, the Differential Evolution Adaptive Metropolis (DREAM) MCMC scheme significantly improves the efficiency of MCMC simulations (Vrugt, Ter Braak et al. 2009).

In this work, we aim to investigate the advantages and disadvantages of three different zonation-based inverse strategies applied to a groundwater flow model at the basin scale: (1) the ZM, (2) the adaptive multi-scale method and (3) DREAM MCMC. We apply each of these methods to estimate the distribution of transmissivity (T) and elastic and inelastic skeletal storage coeffieients (S_{ke} *and* S_{kv}, respectively) from observations of hydraulic head and land subsidence measurements for Las Vegas Valley between 1912-2010. A secondary objective is to find the best strategy for evaluating the model parameters for making credible predictions, and to provide a framework for developing an accurate hydrogeologic model for Las Vegas Valley.

The adjoint parameter estimation (APE) algorithm developed in Chapter 2 is useful for the calibration of groundwater models using multiple types of observations. However

there are some limitations that exist in the APE algorithm. For example, for the very first call of the APE algorithm, the initial guess for the transmissivity $T^{(0)}$ uses Equation 13, where we use the observed hydraulic head, h, only when the pumping rate is zero. However for the complex Las Vegas Valley model, there is no time that all pumping rates are zero. Although the APE algorithm generally provides a good estimate, it is sensitive to the complexity of the problem at hand so if the zonation is highly complex, the likelihood of convergence may be lower. So the APE algorithm is not considered in this Chapter.

Las Vegas Valley has had a long history of groundwater development (Harrill 1976) and subsequent land subsidence (Bell 1981, Bell, Amelung et al. 2002). The complex hydrogeological conditions and large amount of available temporal and spatial groundwater hydraulic head and land subsidence measurements since the 1930s make Las Vegas Valley area an ideal site to conduct inverse parameterization research. Harrill (1976) was the first to systematically estimate basin-wide transmissivities from aquifer test data. Morgan and Dettinger (1994) developed the first valley-wide numerical groundwater model, which covered the period from 1912-1981 using the Trescott, Pinder and Larson groundwater model (Trescott, Pinder et al. 1976). In their model, precalibration transmissivity was estimated using regression analysis from pumping tests and lithologic data interpreted by Plume (Plume 1984). The final transmissivities were manually calibrated by adjusting transmissivities and storage values so that the difference between simulated heads and observed heads was minimized as much as possible through trial-and-error methods and a minimum grid spacing of 2.5 km. Mean inelastic specific storage values were calculated based on groundwater level declines, clay thicknesses, and

subsidence data measured at four benchmarks. The model yielded a rather generalized distribution of simulated drawdown and land subsidence, but did not capture the likely complex patterns of subsidence we know exist today and likely existed at the time this model was developed. Jeng (Jen 1998) later converted the Morgan and Dettinger model to the MODFLOW model (McDonald and Harbaugh 1984) without changing any final simulated parameters from Morgan and Dettinger. Yan (Yan 2007) later updated Jeng's model by extending the simulation period to 2005 using mostly the original parameter estimates of Morgan and Dettinger as well as the same course grid spacing. Pavelko (Pavelko 2004) developed a one dimensional groundwater and subsidence model in conjunction with UCODE (Poeter and Hill 1998) to calibrate hydraulic parameters at the Lorenzi site where the USGS installed an extensometer in 1994. Hoffmann et al. (Hoffmann, Zebker et al. 2001) and Bell et al. (Bell, Amelung et al. 2008) used InSAR and PS-InSAR combined with ground water level declines to evaluate elastic and inelastic skeletal storage coefficients in Las Vegas Valley at several individual locations. Until now no research has been done on calibration of the transmissivities and elastic and inelastic skeletal storage coefficients of Las Vegas Valley at the basin scale.

In order to compensate for the deficiencies of these earlier models, we invoke three different zonation-based inversion strategies to determine best method for calibrating transmissivities and elastic and inelastic skeletal storage coefficients at the basin scale with the aim of achieving both accuracy and computational efficiency. We have successfully extended Las Vegas Valley model to year 2010 using MODFLOW-2005 (Harbaugh 2005) with the subsidence (SUB) package (Hoffmann, Leake et al. 2003) while implementing a 600m × 600m grid cell size. Observations include available

hydraulic head data and land subsidence measurements (from 1992-2010). However, due to the immense size of the model and large number of cells used, the estimation of parameters for each of these three strategies with the large number of observations (time and space) used is extremely time-consuming (especially with the accelerating DREAM MCMC method). In order to find the optimal inversion strategy for the Las Vegas Valley model, a shorter term model is used in this study that extends from 1912-1987 with the period from 1912-1981 used as the calibration period and the period from 1981-1987 represents the evaluation period.

The shorter term model is used in this investigation due to the time-dependent delayed drainage of fine-grained clay interbeds that play an important role in the complicated development and distribution of land subsidence in Las Vegas Valley. The time constant, which represents the time required for the interbed to reach 93% of its compaction for a given head change ranges from approximately 100 years to perhaps more than 1000 years for Las Vegas Valley (Pavelko 2004). Thus, any model that is to adequately simulate subsidence and hydraulic heads must coincide with the commencement of pumping in the basin. On the other hand, the subsidence rates of recent years are largely influenced by delayed drainage, making it difficult for inverse modeling techniques to accurately calibrate parameters (Yan 2007). Therefore, a shorter simulation period is used in this investigation that commences with the start of pumping in the year 1912, before the onset of subsidence in the valley. It is anticipated that this time period is sufficient for investigating the advantages and disadvantages of the various inverse methods previously described as applied to the basin scale.

3.2. Field Site and Forward Model

3.2.1. Las Vegas Valley Study Area

Las Vegas Valley encompasses an area of about 4,150 km^2 in Clark County, southern Nevada. The northwest-trending valley is bounded on all sides by various mountains. It is located in a structurally controlled alluvial basin. A series of north- to northeast-trending, east-dipping Quaternary faults cut the valley floor (Figure 13). A thick accumulation of interbedded and interfingered coarse- and fine-grained sediment fills the structural basin. In the northern, western, and southern parts of the valley, sediment consists of mainly coarse-grained sand and gravel. However sediment becomes thicker and finer-grained toward the central and eastern parts of the valley (Figure 13). The principle aquifer, composed mainly of course-grained deposits with some fine-grained low-permeable interbeds, occurs at depths ranging from 60-300 m below land surface (Malmberg 1965, Harrill 1976, Morgan and Dettinger 1994). In the vertical direction, permeability tends to decrease with depth (Maxey and Jameson 1948). Overlying the principal aquifer is a 30 m to 90 m thick sequence of clay, sand, and gravel, which is often referred to as the near-surface reservoir, which is not pumped nor used as a potable water source.

(a)

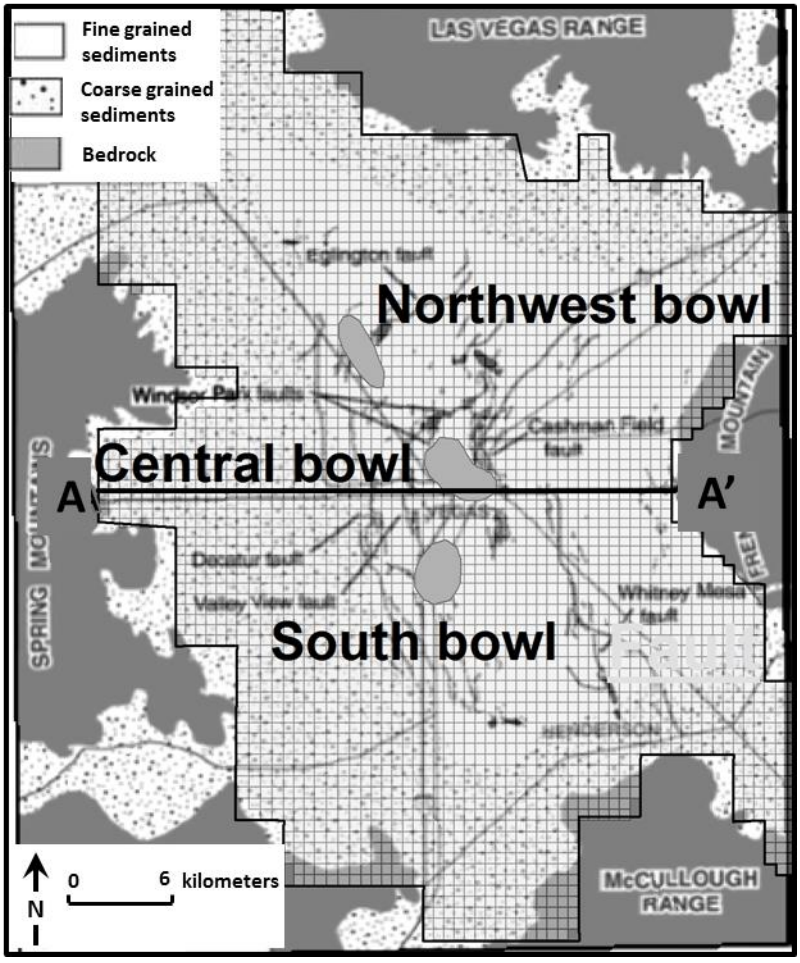
Fine grained sediments
Coarse grained sediments
Bedrock
LAS VEGAS RANGE
Northwest bowl
Central bowl
South bowl
A
A'
SPRING MOUNTAINS
MOUNTAIN
FRE
McCULLOUGH RANGE
0
6 kilometers
N

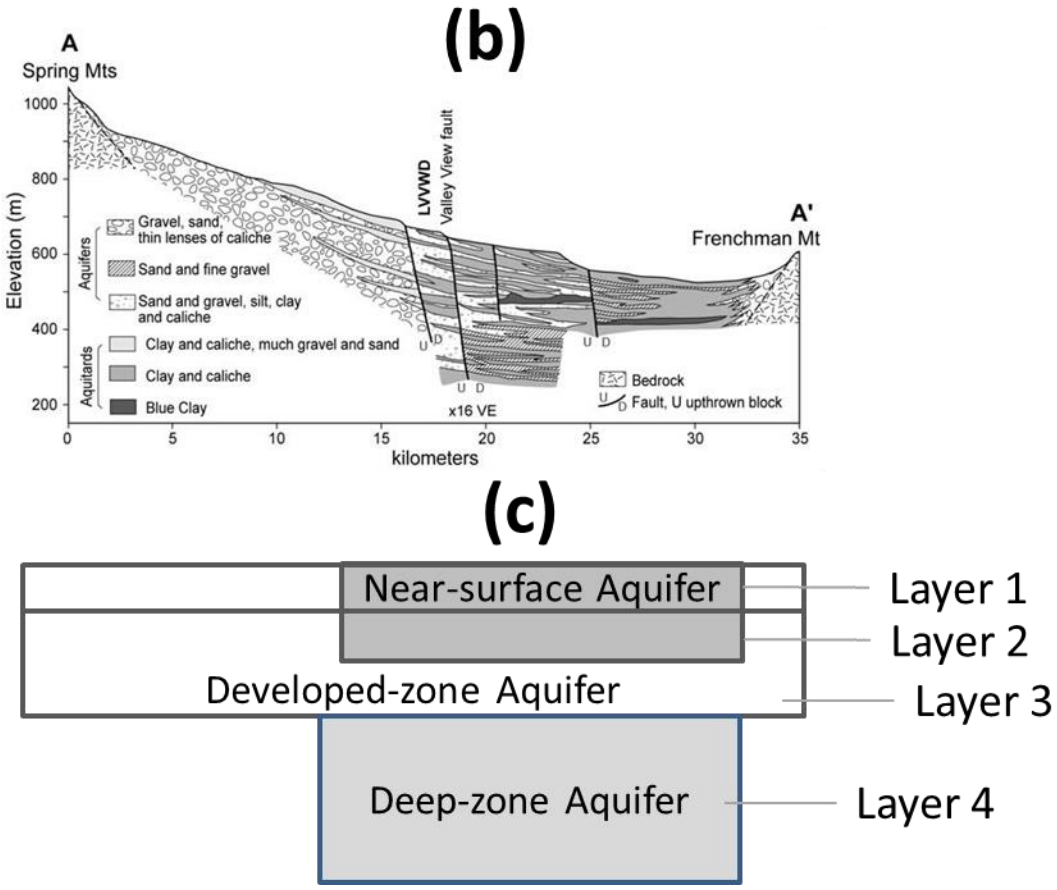

Figure 13 (a) Generalized surficial geologic map of Las Vegas Valley showing distribution of coarse- and fine-grained deposits, and principal Quaternary faults and fissures. (b) Geologic cross-section (A-A9) as modified from Bell, Amelung et al. (2002) and schematically illustrates the stratigraphic and fault relations interpreted from well log data (Bell, Amelung et al. 2002). (c) The conceptual model layer.

Groundwater has been pumped since 1905 in Las Vegas Valley area. Due to declining water levels, decreasing pore-water pressures within the aquifer system have led to significant increases in effective stress, which accounted for large-scale compaction of mostly fine-grained sediments (Terzaghi 1925, Poland and Davis 1969, Poland, Lofgren et al. 1972, Helm 1975). Because pumping has exceeded natural recharge for many years now, intensive groundwater pumping in Las Vegas has led to highly varying degrees of

land subsidence, which has resulted in surface fissures and socioeconomic problems (Bell 1981). According to benchmark surveys, an early subsidence map for the period 1935-1963 (Figure 13) shows that subsidence occurred as a singular bowl located near downtown Las Vegas (central bowl), with a maximum subsidence during that period of 67cm. For the ensuing period 1963-1980, an updated subsidence map shows that three localized subsidence bowls- the Northwest, Central and Southern bowls exist near the central part of the valley. The maximum total subsidence in 1980 was in the Northwest bowl, which was measured to be 78cm (Figure 13). For the period 1963-1987, the three principal localized subsidence bowls became more widespread and extensive. Observed subsidence of more than one and half meters had occurred in the northwest bowl by 1987 (Figure 13) (Bell, Amelung et al. 2002).

3.2.2. Forward Model

We updated Yan's (2007) model by extending the simulation period to 2010 using MODFLOW-2005 (Harbaugh 2005) with the subsidence (SUB) package (Hoffmann, Leake et al. 2003). The forward model is used to simulate groundwater flow and land subsidence at the basin scale. The new conceptual model consists of four model layers: Layers 1 and 2 represent the near-surface aquifers; layer 3 represents the developed-zone aquifer and layer 4 represents the deep-zone aquifer. Only the developed-zone (or principal) aquifer is pumped for groundwater. All four layers are assumed to be confined aquifers (Figure 13).

The groundwater flow equation of our model is given as:

$$S_s b \frac{\partial h^a}{\partial t} = \nabla \cdot (T \nabla h^a) + \sum_j K_{vj} \frac{d\bar{h}_j^i}{dz} - W$$

Equation 17

where h^a is simulated hydraulic head of the aquifer, $\bar{h}^i$ is hydraulic head in the interbed, b is thickness of the aquifer system, T is transmissivity, S_s is specific storage of the aquifer, K_v is vertical conductivity of the aquifer and W is a source term.

The interbed is assumed to be areally far more extensive than its thickness, and the hydraulic conductivity of the interbed is considerably lower than that of the aquifer, so the direction of groundwater flow within the interbed can be treated as vertical. Groundwater flow from the interbed to the aquifer occurs when the head in the aquifer declines, with the head change in the interbed lens lagging that of the aquifer and described by the diffusion equation,

$$S_k \frac{\partial \bar{h}^i}{\partial t} = \frac{\partial}{\partial z}(K_{vj} \frac{\partial}{\partial z} \bar{h}_j^i),$$

Equation 18

where S_k is skeletal storage coefficients of the interbed.

The SUB package (Hoffmann, Leake et al. 2003) is used to calculate subsidence at each model cell from a single interbed using the equation:

$$s(t) = S_k \cdot \Delta \bar{h}^i \left[1 - \frac{8}{\pi^2} \sum_{k=0}^{\infty} \frac{\exp(-\frac{\pi^2}{4} \frac{t}{\tau_k})}{(2k+1)^2} \right]$$

Equation 19

where τ_k is defined as

$$\tau_k = \frac{(\frac{b_0}{2})^2 S_{sk}}{K'_v (2k+1)^2}$$

Equation 20

where s is interbed compaction (land subsidence), t is time, $b_o/2$ is one-half the thickness of the interbed, S_{sk} is the skeletal specific storage of the interbed, K'_v is the vertical hydraulic conductivity of the interbed. The time constant τ_0 (where $k=0$ for Equation 20) represents the time required for the interbed to reach 93% of its compaction for a given head change, Δh.

The land subsidence of the entire system can be calculated by multiplying the value from Equation 19 by the factor n_{equiv}.

$$n_{equiv} = \frac{1}{\sqrt{\frac{1}{N}\sum_{i=1}^{N} b_i^2}} \sum_{i=1}^{N} b_i$$

Equation 21

Laboratory consolidation tests indicate that the skeletal specific storage, which describes the compressibility, can vary greatly depending on whether the effective stress exceeds the previous maximum effective stress, which is termed as the preconsolidation stress (Johnson, Moston et al. 1968, Jorgensen 1980). Inelastic skeletal specific storage S_{skv} is used when the water level in the interbed is lower than its previous minimum value, whereas elastic skeletal specific storage S_{ske} is invoked when the drawdown in the interbed is higher than the previous minimum values. The relationship between skeletal storage coefficient and skeletal specific storage is given as:

$S_k = S_{sk} b_0$.

Equation 22

The updated model we developed uses all the parameters from Yan (2007). However simulation result shows that the simulated drawdown and subsidence do not fit well with the observational data, hence, an inverse model, which is designed to calibrate the parameters is required to accurately describe and predict the drawdown and subsidence patterns in Las Vegas Valley.

3.3. Inversion Model and Method

3.3.1. Inversion Model, Observations, Parameters and Weighting

3.3.1.1. Simulation Period

A shorter model covering the period 1912-1987 is used in this investigation. The shorter model still covers nearly the entire pumping and subsidence history. The actual calibration period used here covers the period from 1912-1981, while the test evaluation period is from 1982-1987.

3.3.1.2. Observations

Selected measurements (including 357 hydraulic head values covering from year 1939 to 1981and 113 land subsidence measurements collected from year 1963 and 1980) from the calibration period are treated as observational data in the analysis. The evaluation period is from 1982-1987, during which 4000 hydraulic head values and 26 land subsidence measurements (from year 1987) are collected. The locations of the data are shown in Figure 14.

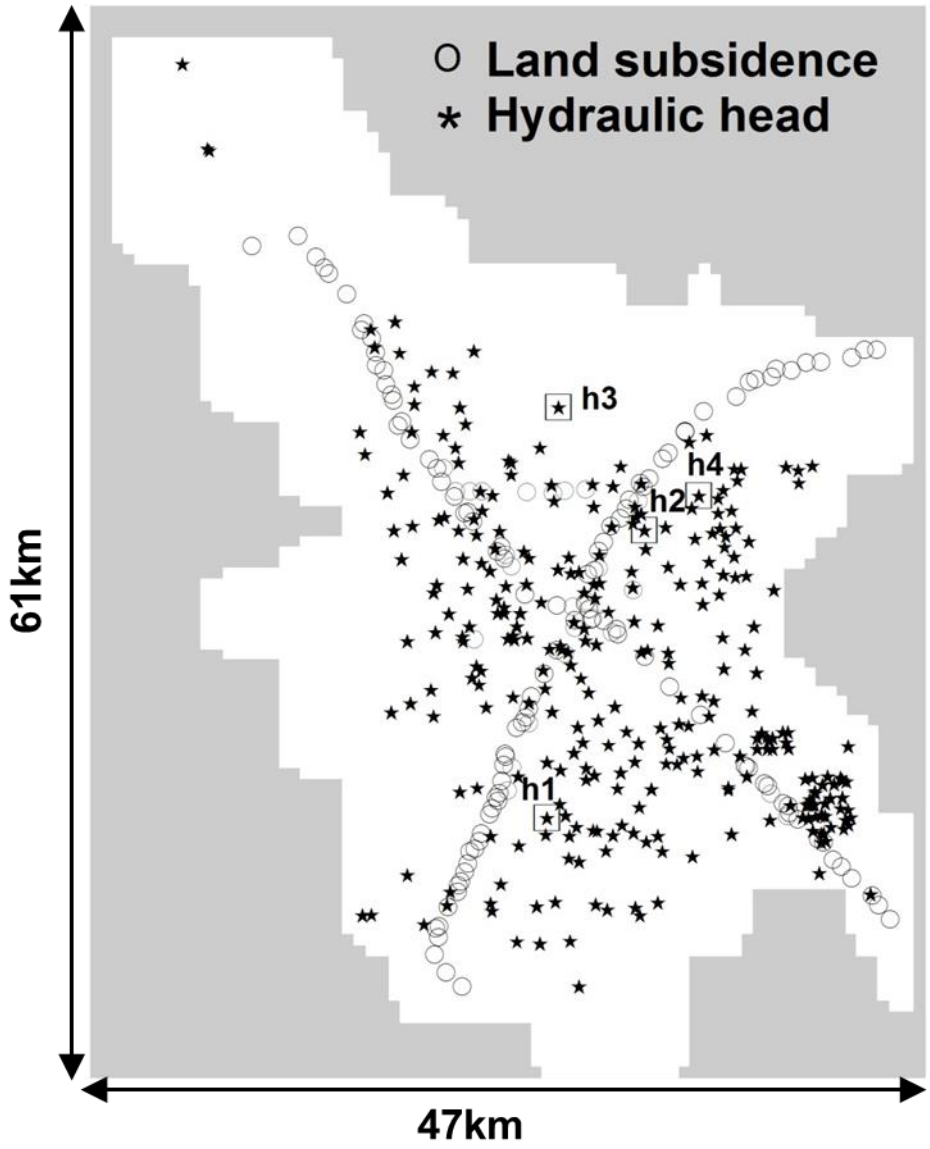

Figure 14 Groundwater and land subsidence monitoring network used as observations in the model (h1 through h4 represent four observation sites discussed in the text).

3.3.1.3. Observational Weighting

For the ZM and adaptive multi-scale strategy, the weightings used in our analyses are proportional to the inverse of the square of the observational values. The precise definition of weights generally is not required for observations. Rather, it's more

important that the sensitivity analysis results and parameter estimates be reasonably consistent over the plausible range (Foglia, Hill et al. 2009). It has been shown that choosing the weight as being proportional to the inverse of the square of the observational value is a good way to obtain accurate estimates of hydraulic parameters (Yan 2007).

For the DREAM method, the weighting is a diagonal matrix with the weight for each observation equal to $1/\sigma_i^2$, where σ_i^2 is the variance of the associated error.

3.3.1.4. Parameters

In this investigation we are interested in calibrating transmissivities (T) and elastic and inelastic skeletal storage coefficients (S_{ke} and S_{kv}) of layer 3 (the developed-zone aquifer) used in Las Vegas Valley. The principal aquifer is capable of transmitting significant quantities of ground water (Maxey and Jameson 1948, Malmberg 1965, Harrill 1976, Morgan and Dettinger 1994) and contributing to virtually all of the observed land subsidence. Seventy-two T parameters, and six S_{ke} and S_{kv} parameters were considered in Yan's model (Yan 2007), which were treated as initial estimates of both zones and parameters of layer 3 in our study. The zones and parameters of the other layers are kept the same as Yan's model (Yan 2007).

3.3.2. Inversion Method

3.3.2.1. Zonation Method (ZM)

The first inversion strategy applied in this study is the ZM. Transmissivities (T) and elastic and inelastic skeletal storage coefficients (S_{ke} and S_{kv}) of layer 3 are calibrated at the basin scale. UCODE-2005 (Poeter, Hill et al. 2005) is used to minimize the weighted

least-squares objective function defined as a least-squares misfit to the data with respect to the parameter values using a modified Gauss-Newton method. The weighted least-squares objective function can be written as:

$$J(\alpha) = \sum_{i=1}^{ND} \omega_i [y_{obs(i)} - y_i(\alpha)]^2 + \sum_{p=1}^{NPR} \omega_p [P_{prior(p)} - P_p(\alpha)]^2$$

Equation 23

where,

$$\alpha = (T, S_{ke}, S_{kv})$$

Equation 24

and represents the parameter vector to be optimized, ND is the number of observations, NPR is the number of prior information values, ω_i is the weight for the i^{th} observation, ω_p is the weight for the p^{th} prior estimate, $y_{obs(i)}$ represents the i^{th} observation, $y_i(\alpha)$ represents the simulated value which corresponds to the i^{th} observation, $P_{prior(p)}$ represents the p^{th} prior estimate, $P_p(\alpha)$ represents the p^{th} simulated value.

Prior information was used for parameter T and S_{ke} and S_{kv} on the basis of T and S_{ke} and S_{kv} distribution map provided by Morgan and Dettinger (Morgan and Dettinger 1994). The parameters were log transformed. We assume that the standard deviation is 0.349, which is used to weight the prior information. The approximate reasonable range of values for the parameter is between one fifth to five times the values provided by Morgan and Dettinger (1994) with a 95% probability. The convergence criterion was set to 0.01, which means that the regression converges if the relative change of the objective function is less than 0.01 for three sequential iterations or the fractional change for all parameters is less than 0.01 for all parameters.

If parameters have composite scaled sensitivities (CSS) that are less than about 0.01 times the largest CSS, it is likely that the regression will not converge (Hill, 1998; Anderman and others, 1996), so when minimizing the objective function using UCODE-2005, we choose to omit those parameters that have CSS lower than 0.01. The parameter nonuniqueness can be detected using parameter correlation coefficients (PCC). Absolute values of parameter correlation coefficients close to 1 indicate a high degree of correlation. Parameters with PCC's larger than 0.85 will be omitted due to their nonuniquness (Foglia, Hill et al. 2009).

3.3.2.2. Adaptive Multi-scale Strategy

The second inversion strategy applied in this study is the adaptive multi-scale algorithm, which provides criteria to reconstruct the zones by refining or coarsening the current zones. T, S_{ke} and S_{kv} of layer 3 are calibrated at the basin scale.

In this strategy we invoke the same objective function (Equation 23) for minimization. UCODE-2005 (Poeter, Hill et al. 2005) is used to minimize the weighted least-squares objective using a modified Gauss-Newton method. Both CSS and PPC analyses are conducted as previously described. The convergence criterion is the same as previously described.

3.3.2.2.1. Refinement Indicators

In order to obtain more realistic zonations based on actual hydrogeological conditions, the parameter estimation problem is solved through a series of successive approximations by refining the zone domains during the inverse procedure. The zone refinement is considered complete when it no longer induces a significant decrease of the objective

function (Chavent and Liu 1989, Liu 1993, Ameur, Chavent et al. 2002, Hayek and Ackerer 2007, Hayek, Lehmann et al. 2008). For the sake of simplicity, we assume that only one parameter is needed to be identified for each zone. The situation where additional parameters are used will be discussed later. Assuming that α_0^* and J_0^* represent the optimal parameter and objective function, respectively, corresponding to parameterization α (Figure 15a). After minimization during the first parameterization α_0, the gradient of the objective function J_0^* becomes

$$0 = \frac{\partial J(\alpha_0^*)}{\partial \alpha} \approx \sum_{i=1}^{Nz} \frac{\partial J(\alpha_0^*)}{\partial \alpha_i}$$

Equation 25

where *Nz* is the number of sub zones.

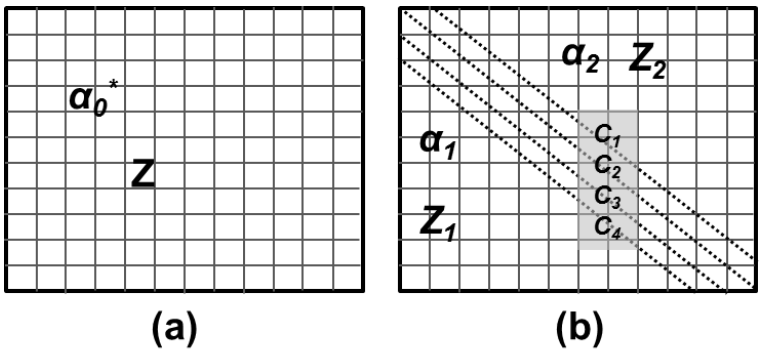

Figure 15 (a) Zone before refinement; (b) Zone after a cutting refinement

For our example, we try to split the single zone Z (Figure 15a) into two zones Z_1 and Z_2 (Figure 15b). A large number of tentative cuts can be tested (dashed line C_1, C_2, C_3 and C_4 in Figure 3b) to split the single zone Z. The refinement indicator associated with splitting the single zone Z (Figure 15a) into two zones (Figure 15b) is defined as:

$$I_0^* = \left| \frac{\partial J(\alpha_0^*)}{\partial \alpha_1} \right| = \left| - \frac{\partial J(\alpha_0^*)}{\partial \alpha_2} \right|$$

Equation 26

For zones that need to be split, the indicators associated with a large number of tentative cuts can be calculated. It can be seen from Equation 25 and Equation 26 that indicators provide first order information on the minimization of the optimal objective function, so it is recommended to select not only the highest indicator I_{max} , but also indicators whose values are greater than $\tau * I_{max}$ (Hayek and Ackerer 2007, Hayek, Lehmann et al. 2008). Here, we use τ=0.85.

Minimizing the objective function for all selected cuttings (indicators that are more than $\tau * I_{max}$). The partition with the smallest objective function is the optimal solution.

For the case where more than one parameter is needed to be identified for each zone, we use the definition provided by Hayek (Hayek, Lehmann et al. 2008), where the corresponding refinement indicator is defined as:

$$\Gamma_i = \sum_{k=1}^{N_P} \frac{I_{k,i}}{\max_i I_{k,i}}$$

Equation 27

where $I_{k,i}$ is the indicator corresponding to the parameter α_k at splitting partition i and N_P is the number of parameters needed to be identified for each zone.

3.3.2.2.2. Coarsening Indicators

During the refinement process the number of degrees of freedom are increased, which can lead to overparameterization if the number of parameters multiplied by the number of

zones exceeds the number of available observations (Ameur, Chavent et al. 2002). To overcome such a drawback, Ameur (Ameur, Chavent et al. 2002) presents an algorithm that uses both refinement and coarsening indicators to decide whether adding or removing some degrees of freedom is advantageous.

Consider the situation shown in Figure 16 where there are two zones, an interior zone Z_1 and an exterior zone Z_2 (Figure 16a). After minimization using Equation 23 using the modified Gauss-Newton method, optimal parameter values α^*_1 and α^*_2 are obtained for the interior zone Z_1 and an exterior zone Z_2. Then Z_1 is refined using the scheme provided in section 3.3.2.2.1. Suppose that refinement corresponding to the cut (dashed line) shown in Figure 16a is selected. Before choosing this new zonation (zone $Z_{1,1}$, zone $Z_{1,2}$ and zone Z_2), one must first make sure that zone $Z_{1,1}$ or zone $Z_{1,2}$ can be combined with zone Z_2, which will assure that there will not be an increase in the number of degrees of freedom According to Equation 25 this leads to:

$$\frac{\partial J(\alpha_1^*, \alpha_2^*)}{\partial \alpha_{1,1}} + \frac{\partial J(\alpha_1^*, \alpha_2^*)}{\partial \alpha_{1,2}} = 0 .$$

Equation 28

Multiplying Equation 28 by $(\alpha_2^* - \alpha_1^*)$ yields:

$$\Delta J_{1,1} + \Delta J_{1,2} = 0 .$$

Equation 29

It can be seen from Equation 29 that in theory at least one of $\Delta J_{1,i}$ is negative, which indicates that combining zones Z_2 and $Z_{1,j}$ for which $\Delta J_{1,j} < 0$ will lower the objective function. However, from Equation 25 we know that $\Delta J_{1,j}$ only provides a first order

estimate of the decrease in the optimal objective function. Thus, the decrease of the objective function can not be guaranteed, but this provides an alternative where the degrees of freedom can be unchanged during the zone reconstructing. The term $\Delta J_{1,j}$ is the coarsening indicator.

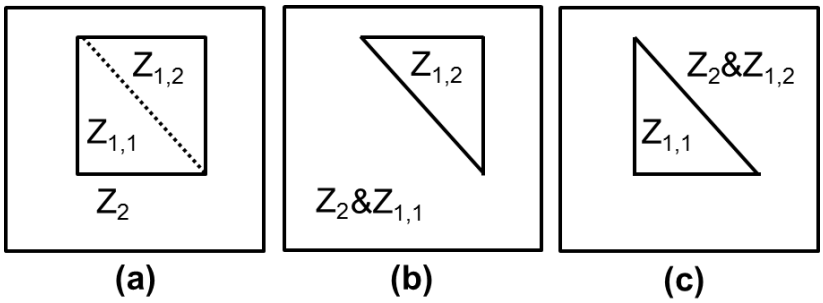

Figure 16 (a) Zone before coarsening; (b),(c) Zone after coarsening.

3.3.2.2.3. The Adaptive Multi-Scale Algorithm

In this study, we provide an alternative to using zone refinement and coarsening indicators. This alternative involves first identifying those zones where hydrogeological analysis (such as geological sediment distribution maps and interbed thickness maps) indicate where refinement or coarsening may be required, then identifying those zones that are important to fitting the observations through a sensitivity analysis (Grimstad, Mannseth et al. 2003, Foglia, Hill et al. 2009). The algorithm for this analysis is described in the following steps:

1. Choose an initial parameter zonation Z distribution (which contains N_z subzones).
2. For the current zonation Z, minimize the objective function J using UCODE and compute the optimal parameter values α^*.

3. At this point, Z contains N_z subzones. However, based on the hydrogeological and sensitivity analysis, choose a new zone Z_{chosen} that needs restructuring.
4. Choose a set of cuts that split the zone Z_{chosen}. Compute all the refinement indicators I (or Γ for multi-dimensional refinement indicator) corresponding to the chosen set of cuts. Compute I_{max} (or Γ_{max}) the largest value of all computed refinement indicators. Select all cuts whose refinement indicators are larger than 85% of I_{max} (or Γ_{max}).
5. **If** Z_{chosen} is totally inside another zone Z_{out} (as shown in Figure 16), **then** compute the corresponding coarsening indicator. Combine the subdomains where coarsening indicators allow it.

   Else go directly to step 6.
6. Minimize the objective function J using UCODE for all selected discontinuities (refinement cuts or coarsening). Notice that the number of zones is now N_{z_new}= N_z+1 for the refinement situation and N_{z_new} =N_z for the coarsening situation. The best parameterization α^*_{new} corresponds to the smallest calculated objective function J_{new}.
7. **If** the updated objective function J_{new} is sufficiently small such that a (near) perfect fit of the observed data occurs, or if the maximum number of zones is reached, or if the refinement and coarsening no longer induces a significant decrease of the objective function, **then**

   Stop iteration.

   Else $J = J_{new}$, $\alpha^* = \alpha^*_{new}$, $N_z = N_{z\_new}$ and return to step 3.

   End if

3.3.2.3. The DREAM MCMC method

The third inversion strategy involves the application of the DREAM MCMC method, which is explained by Vrugt et al. (Vrugt, Ter Braak et al. 2009). DREAM is a widely used program for Bayesian uncertainty analysis. This scheme involves performing multiple different "chains" simultaneously in order to estimate the probability distributions of the unknown parameters. Assuming multi-Gaussian distributed errors in the observations, the likelihood function for this approach is defined as (Lu, Ye et al. 2014):

$$L(\alpha \mid y_{obs}) = (2\pi)^{-ND/2} \mid C \mid^{-1/2} \exp(-\frac{1}{2}(y_{obs(i)} - y_i(\alpha)^T C^{-1}(y_{obs(i)} - y_i(\alpha)))$$

Equation 30

Where C is the covariance matrix of the measurement error. Measurement errors are taken to be uncorrelated.UCODE-2014 (Lu, Ye et al. 2014, Poeter 2014),which invokes the DREAM MCMC method, is used for estimating parameters.

Although the DREAM MCMC scheme significantly improves the efficiency of the MCMC simulation (Vrugt, Ter Braak et al. 2009), compared to the ZM and adaptive multi-scale methods, it requires significantly more computational time. In our study, UCODE-2014 takes 4.5 minutes of computational time to run one iteration with High Performance Computing (HPC) facilities at Virginia Tech. In general, DREAM MCMC takes thousands to hundreds of thousands of iterations to converge. Furthermore, additional iterations are required if more parameters are calibrated as in our case. However, with the same HPC, it takes seventy minutes to run one iteration of the modified Gauss-Newton method, which is not as efficient as the DREAM MCMC, but for our case, this method converges within 50 iterations. DREAM MCMC may not be

practical for high-dimensional models, because it requires expensive computational time (Keating, Doherty et al. 2010). Therefore, we were only able to use the DREAM MCMC method to estimate posterior probability distributions of *T* at selected zones due to the large computational time requirements.

3.3.3. Measures Used for Evaluation of Model Fit

For the ZM and the adaptive multi-scale method, the Nash-Sutcliffe efficiency index (*NS*) (Nash and Sutcliffe 1970), mass balance error (*m*), the Schulz criterion (*D*) (Schulz, Beven et al. 1999) and sum of squared weighted residuals (WSSR) are used to evaluate model fit. *NS*, *m*, *D* and *WSSR* are the commonly used measures for evaluating hydrogeologic models. *NS* is defined as (Nash and Sutcliffe 1970):

$$NS = 1 - \frac{\sum_{i=1}^{n}(y_i - y_{obs(i)})^2}{\sum_{i=1}^{n} y^2{}_{obs(i)} - \frac{1}{n}(\sum_{i=1}^{n} y_{obs(i)})^2}$$

Equation 31

where $y_{obs(i)}$ represents the i^{th} observation, y_i represents the simulated value.

When the observations are perfectly fitted by the simulated values, *NS*=1, *NS*>0.8 represents excellent fitting, 0.6<*NS*<0.8 represents very good fitting; 0.4<*NS*<0.6 represents good fitting; 0.2<*NS*<0.4 represents sufficient fitting; while *NS*<0.2 represents insufficient fitting. NS emphasizes the fit to greater observed measurements.

Another indicator, *m,* is used to evaluate whether the simulated values are generally less than or greater than the observed values, and is calculated as:

$$m = 100 \frac{\sum_{i=1}^{n} (y_i - y_{obs(i)})}{\sum_{i=1}^{n} y_{obs(i)}}$$

Equation 32

If the observations are perfectly fitted by the simulated values, m=0. When m>0 this indicates that the simulated values are greater than the observed values on average, while for the case when m<0 the simulated values are lower than the observed values on average.

Another fitting parameter, D, is calculated as (Schulz, Beven et al. 1999):

$$D = 200 \frac{\sum_{i=1}^{n} | y_i - y_{obs(i)} | y_{obs(i)}}{n(y_{obs(i),\max})^2}$$

Equation 33

where $y_{obs(i),max}$ represents the maximum of all the observations. When 0<D<3 the model fit is considered to be very good; when 3<D<10 the model fit is classified as good; when 10<D<18 the model fit is sufficient and when D>18 the model is fit is considered to be insufficient. D does not over-emphasize the larger observation values as NS does.

The standard error of regression s is a quantitative measure of overall model fit to the weighted observations (Hill 1998, Hill and Tiedeman 2006) and is calculated as:

$$s = \left(\frac{WSSR}{ND + NPR - p}\right)^{1/2}$$

Equation 34

where, *ND* is the number of observations, *NPR* is the number of prior information values, *p* is the number of estimated parameters, and *WSSR* is the sum of squared weighted residuals calculated for the diagonal weight matrix and is calculated as:

$$WSSR = \sum_{i=1}^{ND+NPR} \omega_i [y_{obs(i)} - y_i(\alpha)]^2$$

Equation 35

If the model fit is consistent with the data accuracy as reflected in the weighting, then *s* is 1.0.

For the DREAM MCMC strategy, the predictions are evaluated at the 95% credible interval using the equal-tailed method (Casella and Berger 2002) .For each prediction, the samples are ordered from the smallest to the largest values and the 95% credible interval is determined at the 2.5% and 97.5% percentiles of model predictions.

3.4. Results

3.4.1. Calibrated Transimissivity Zones and Values

3.4.1.1. The ZM Method

Transmissivities (*T*) of layer 3 are calibrated at the basin scale with the ZM. Seventy-two *T* parameters described in Yan's model (Yan 2007) are shown in Figure 17a. Calibrated *T* values obtained from the ZM are shown in Figure 17b. The results indicate that most zones have similar *T* values as those from Yan (2007), except for zones E and S located in the far eastern part of the basin where relatively higher *T* values are calculated using the ZM (

Figure 18a). Coarser-grained alluvial deposits are known to occur near point A' (Figure 13b) and in the southern part of the basin (Figure 13a), which may explain the higher simulated *T* values for zones E and S. In order to accurately describe how *T* is distributed in these zones, a much finer zone distribution based on hydrogeological conditions is required. Sensitivity analysis shows that all parameters have CSS values larger than 0.04 times the largest CSS (

Figure 18a), which indicates that the model and the observed data provide sufficient information to estimate the parameters. The PCC analysis shows that no parameter have

correlation coefficients larger than 0.83, indicating that the estimated parameters are unique given the information provided by the observations.

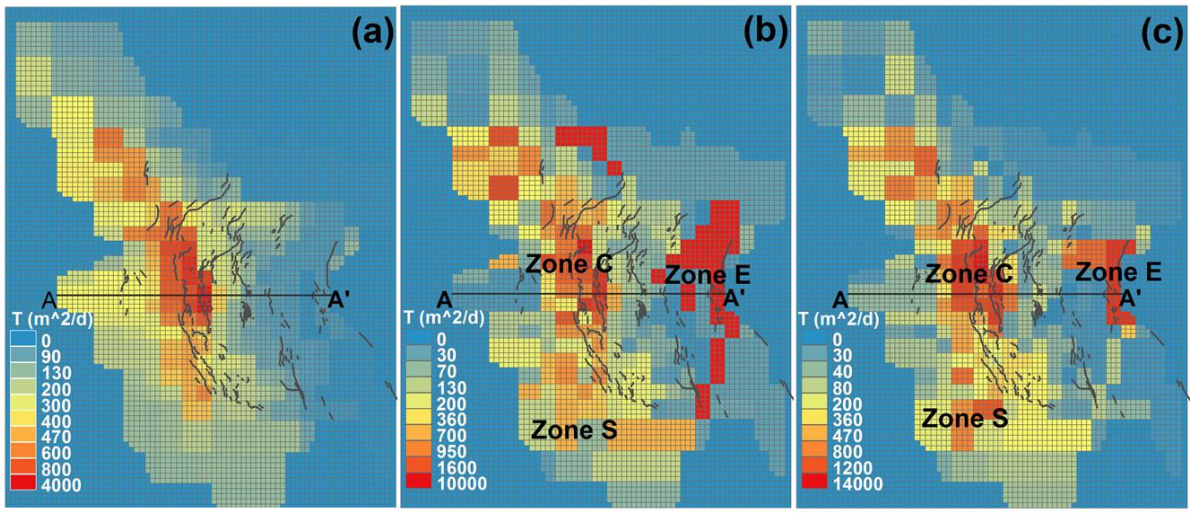

Figure 17 (a) Transmissivity zones and values from Yan (2007); (b) Transmissivity zones and values calibrated with ZM; (c) Transmissivity zones and values calibrated with DREAM MCMC.

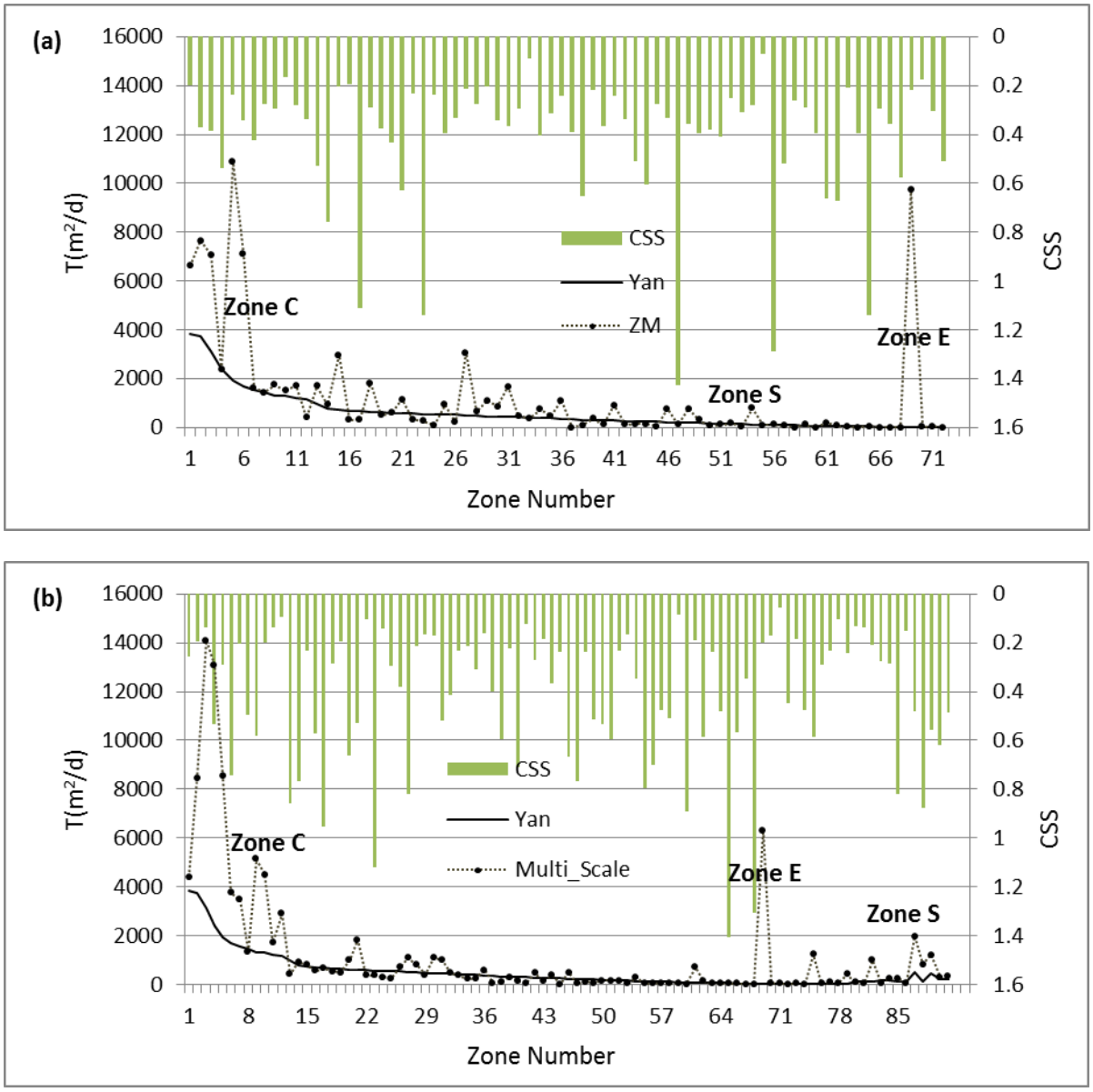

Figure 18 A comparison of transmissivity values (a) from Yan (2007) and calibrated with ZM; (b) from Yan (2007) and calibrated with the multi-scale strategy. Zones C, E and S are shown in Figure 5. CSS represents the composite scaled sensitivities

3.4.1.2. The Adaptive Multi-scale Strategy

In order to obtain more realistic zonations based on actual hydrogeological conditions, the adaptive multi-scale algorithm is applied to reconstruct the *T* zones of layer 3 at the basin scale. The parameter estimation problem is solved through 13 iterations of

successive approximations by refining the zone domains (especially zone E and zone S in the eastern part of the basin) during the inverse procedure. The final zone distributions and zone values are shown in Figure 17c. Most zones have similar *T* values as that from Yan (2007), except at zones E and S (Figure 18b). The sensitivity analysis shows that all parameters have CSS value larger than 0.03 times the largest CSS (Figure 18b), indicating that the model and the observed data provide sufficient information to estimate the parameters. A PCC analysis shows that no parameter has a correlation coefficient larger than 0.80, which indicates that the estimated parameters are unique given the information provided by the observations

3.4.1.3. The DREAM MCMC method

Due to the significant computational time required for the global optimization method, we were only able to use this method to calibrate *T* at selected zones. For our test, we calibrate *T* at zones a, b, c and d (Figure 19). Uniform prior information (*T* ranges from 1 to 15,000 m^2/d) is used for all parameters. A total of four Markov chains are used to generate candidate samples.

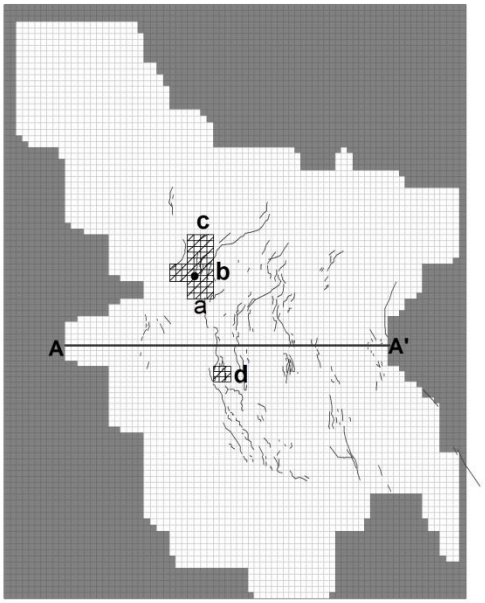

Figure 19. Transmissivity zones calibrated with DREAM MCMC (Zones with slash).

Figure 20 illustrates the numerical evolution of the sampled *T* values at zones a, b, c and d. The four chains converged to a limiting distribution within 400 evaluations. The convergence is then evaluated by the Gelman-Rubin values, which are shown to be continuously less than 1.2 after 400 iterations. The final *T* values from Yan (2007), the ZM and Adaptive Multi-scale methods are also shown in Figure 20 for comparison. *T* values calibrated with the ZM and the Adaptive Multi-scale method are within one order of magnitude of the values obtained with DREAM MCMC. This outcome is reasonable because *T* values are calibrated at only four selected zones with DREAM MCMC, but for the entire basin with the other two methods.

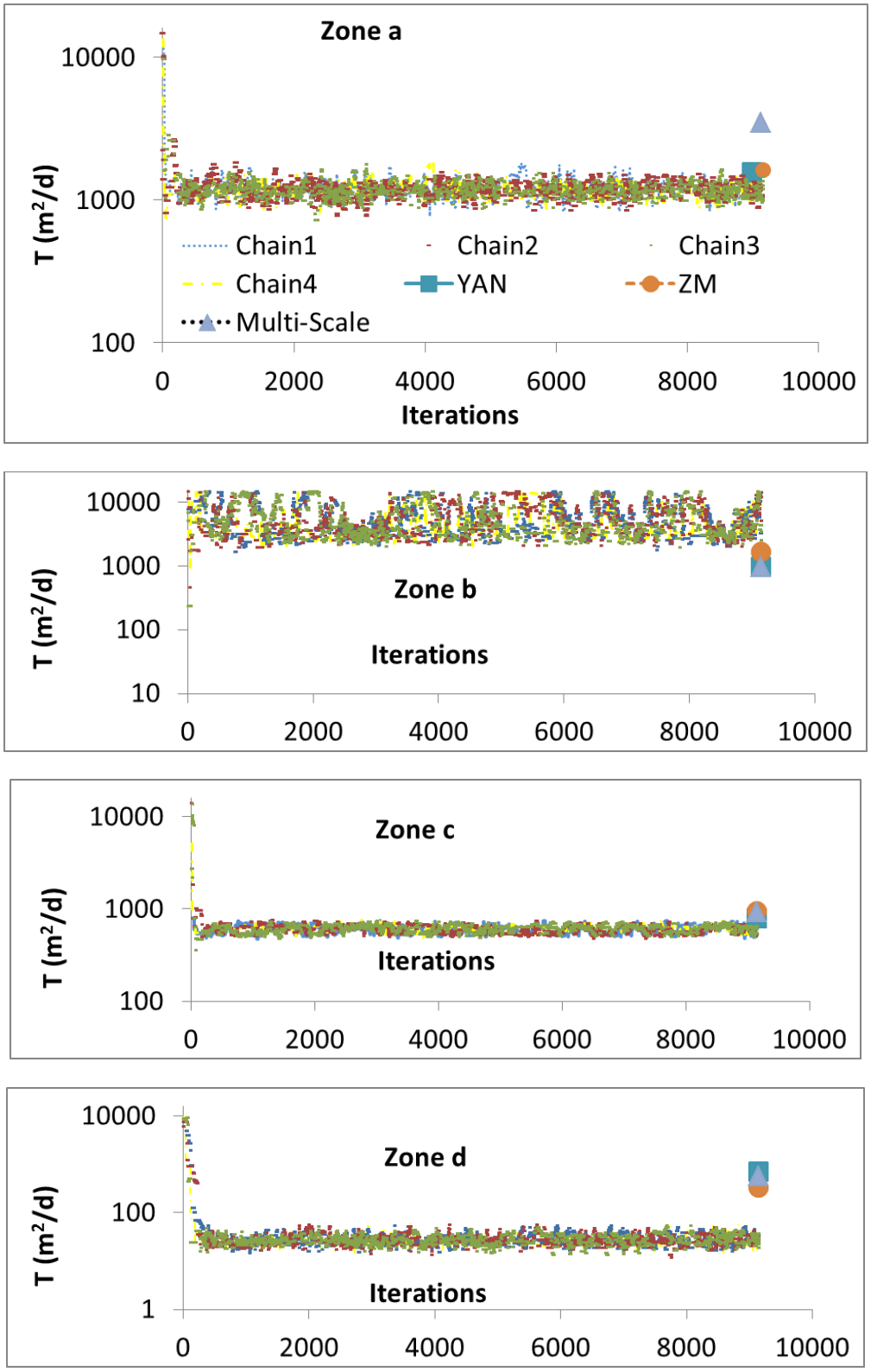

Figure 20. Numerical calibration of sampled *T* values for zones a, b, c, d using DREAM MCMC.

With the sufficient parameter samples after chain convergence, the last 50% of the samples in the four chains (0.5×4×9,000=18,000samples) are used to construct histograms for each individual parameter (Figure 21). The *T* at zones a and d have only one mode, which are Gaussian-like and exhibit negligible skewness. While the simulated *T* at zone b has one mode, which is Gaussian-like with positive skewness. The posterior distribution of *T* at zone c has two modes, which may indicate that the formal likelihood Gaussian function assumption may not hold. This is reasonable, because only the covariance matrix of the measurement error is considered in Equation 30, however the Las Vegas Valley model is extremely nonlinear and complex, with multiple sources of uncertainty including model structural error, input error, etc. The PCC between two parameters is shown in Figure 22. All the PCC are smaller than 0.7, indicating that the parameters are weakly correlated. This is consistent with the result obtained from the ZM method and the adaptive multi-scale method.

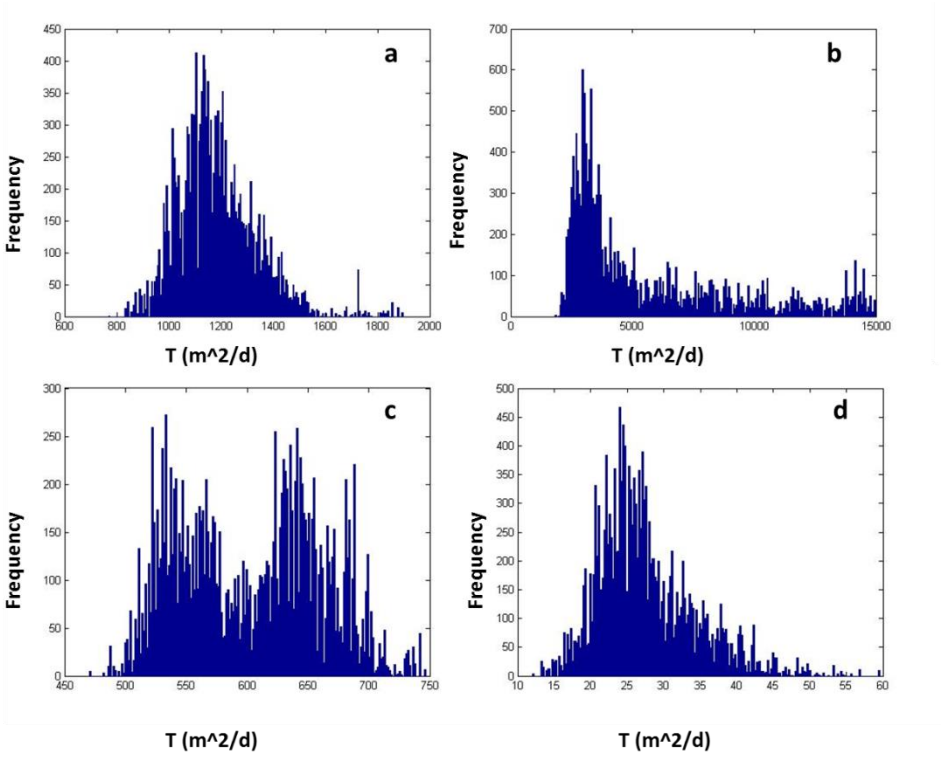

Figure 21. The simulated marginal posterior distributions of the four transmissivity zones.

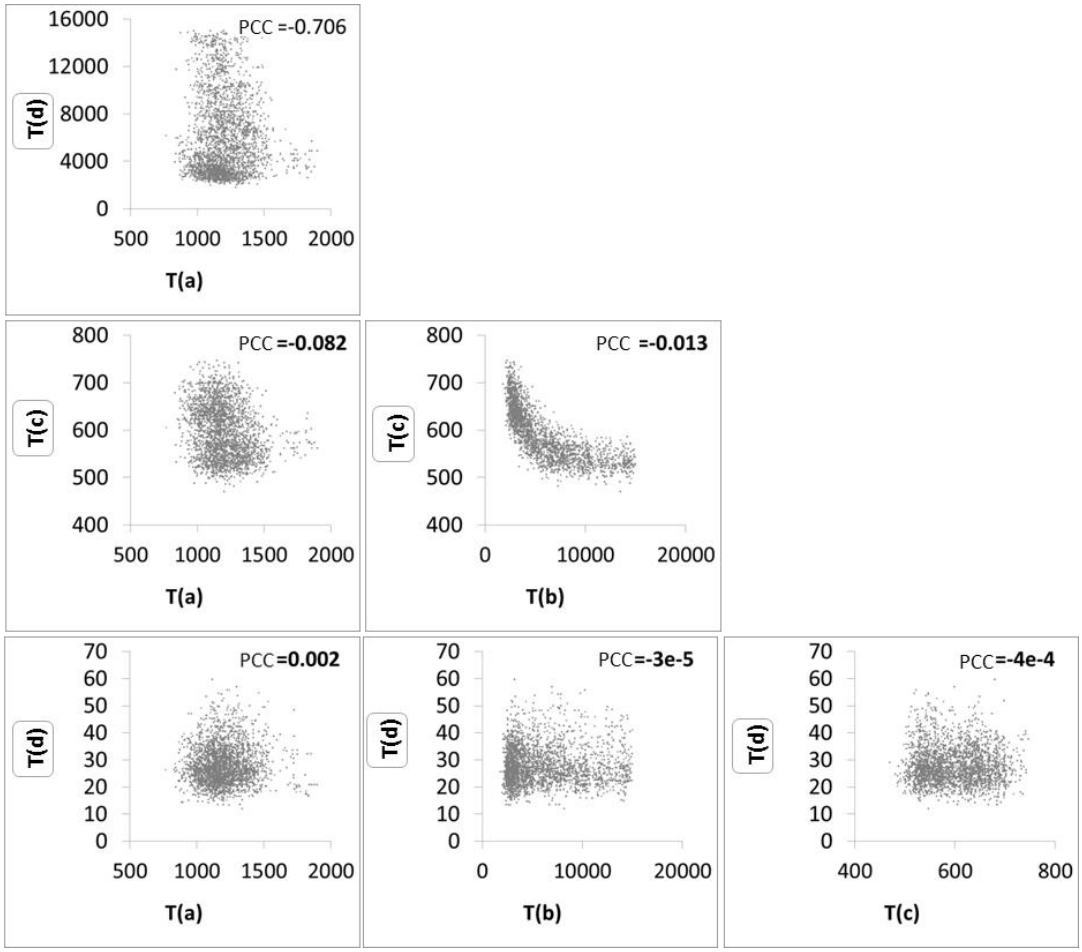

Figure 22. The parameter correlation coefficients (pcc) between each of the transmissivity parameters

3.4.2. Calibrated Ske and Skv Zones and Values

The parameters S_{ke} and S_{kv} of layer 3 are calibrated at the basin scale using the ZM and the multi-scale strategy. Six pairs of S_{ke} and S_{kv} parameters described in Yan's model (Yan 2007) are shown in Figure 23a. The S_{ke} and S_{kv} parameters that Yan used are from Morgan and Dettinger (1994). The interbed thicknesses that are used to calculate S_{ke} and S_{kv} are inferred for many locations within the basin where data are limited, especially in the northwest part of the basin (See Figure 3.3.4-1 and 3.3.4-2 of (Morgan and Dettinger

1994)), hence, in order to obtain a better model fit, reconstructing S_{ke} and S_{kv} zones and calibrating parameter values based on actual hydrogeological conditions is preferred. Calibrated S_{ke} and S_{kv} values using the ZM are shown in Figure 23b. The zones are the same as in Yan's model. However, S_{ke} and S_{kv} values are lower than those calibrated by Yan. In order to obtain more realistic zonations based on actual hydrogeological conditions, the adaptive multi-scale algorithm is applied to reconstruct the S_{ke} and S_{kv} zones of layer 3.The parameter estimation problem is solved through four iterations of successive approximations by refining or coarsening the zone domains (especially in the northwest part of the basin where initial estimates were largely unknown) during the inverse procedure. The final calibrated zone distributions and values are shown in Figure 23c. Sensitivity analysis shows that all parameters have CSS values larger than 0.18 times the largest CSS with S_{kv} exhibiting the largest CSS, which suggests this parameter is highly sensitive to observations and important in the calibration process. PCC analysis shows that no parameter has correlation coefficients larger than 0.83, indicating that the estimated parameters are unique and relatively unaffected by the model given the information provided by the observations.

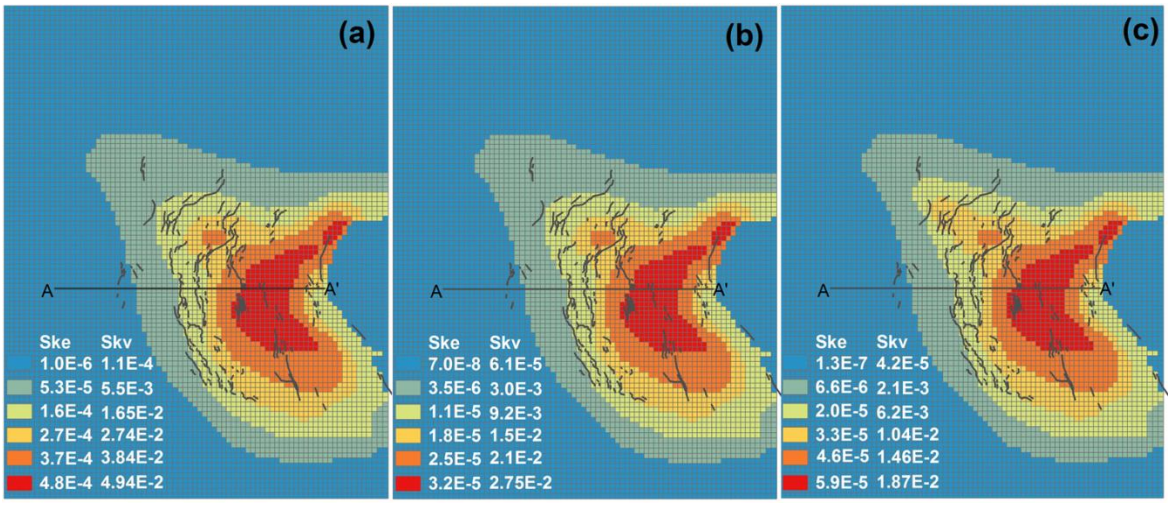

Figure 23. Elastic and inelastic skeletal storage coefficient zones and values (a) from Yan (2007); (b) calibrated with the ZM; (c) calibrated with the adaptive multi-scale strategy.

3.4.3. Evaluation of Model Fit

The final T, S_{ke} *and* S_{kv} values from the ZM and the adaptive multi-scale strategy are used to calculate simulated hydraulic heads and basin-wide land subsidence. For the DREAM MCMC strategy, the predictions are evaluated and their 95% credible intervals limits are determined using the equal-tailed method (Casella and Berger 2002) for each of the 18,000 converged parameter samples (Figure 21).

Figure 24 shows plots that compare observed versus simulated hydraulic heads for the calibration period from the ZM and adaptive multi-scale strategies. The results show that the ZM and adaptive multi-scale methods produce a better model fit than Yan's model. A quantitative assessment of the model fit is listed in Table 2. The *NS* criteria indicates that the fit is excellent with the ZM and the adaptive multi-scale methods. The *m* criteria indicate that on average, the simulated hydraulic heads are larger than the observed heads. The *D* criteria indicates that the fit is very good with both the ZM and adaptive multi-scale inversion strategies. The *s* criteria is shown to be decreasing with the ZM and the adaptive multi-scale methods, which represents an improved overall model fit to the weighted observational data. Based on the quantitative assessment results (Table 2) the adaptive multi-scale method is shown to be superior to the ZM inverse method.

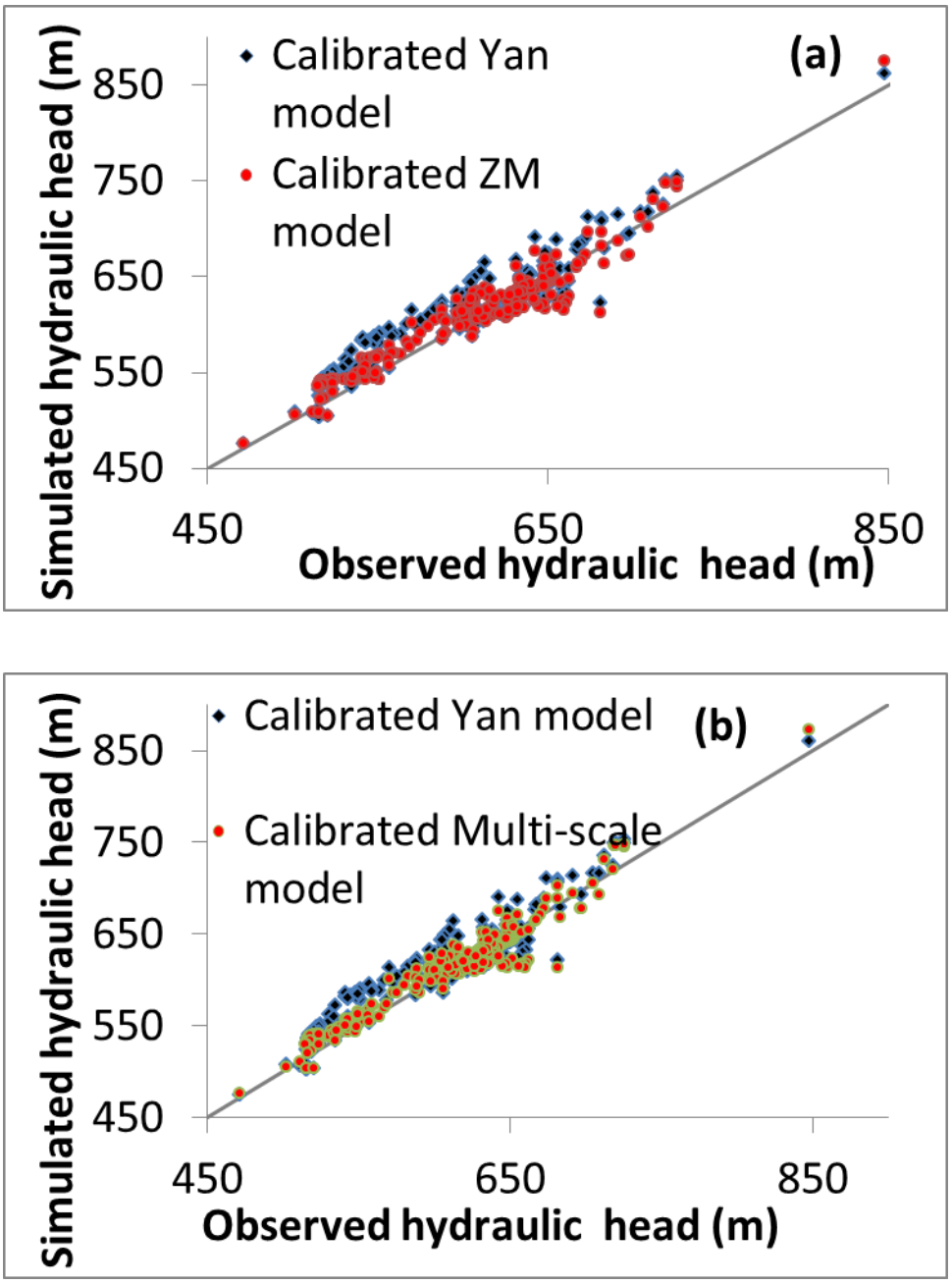

Figure 24. Observed vs. simulated hydraulic heads for the calibration period using (a) ZM, and (b) the adaptive multi-scale method.

Table 2. Measures of model fit[a] between observed and simulated hydraulic head and land subsidence.

Model		Hydraulic head				Land Subsidence			
		NS	*m*	*D*	*s*	*NS*	*m*	*D*	*s*
YAN	C	0.73	1.09	2.02	2.01	0.61	-16.93	5.26	5.56
	P	0.90	0.84	2.50	2.48	0.16	-32.67	22.85	5.28
ZM	C	0.86	0.54	1.48	1.39	0.73	-22.09	4.74	3.35
	P	0.93	0.12	2.12	2.02	0.01	-43.43	26.74	4.12
Adaptive multi-scale method	C	0.88	0.27	1.33	1.29	0.77	-24.16	4.65	3.13
	P	0.93	-0.06	2.08	1.98	-0.05	-48.78	27.77	4.05

[a] NS is the Nash-Sutcliffe efficiency index; m is the mass balance error; D is the Schulz criterion; s is the quantitative measure of overall model fit to the weighted observations; C represents calibration period; P represents prediction period.

Figure 25 shows plots comparing observed versus simulated hydraulic heads at sites h1-h4 (Figure 14), where more than two observations are available for the calibration period. The results show that the adaptive multi-scale method produces the best model fit at sites h1-h4 (Figure 25).

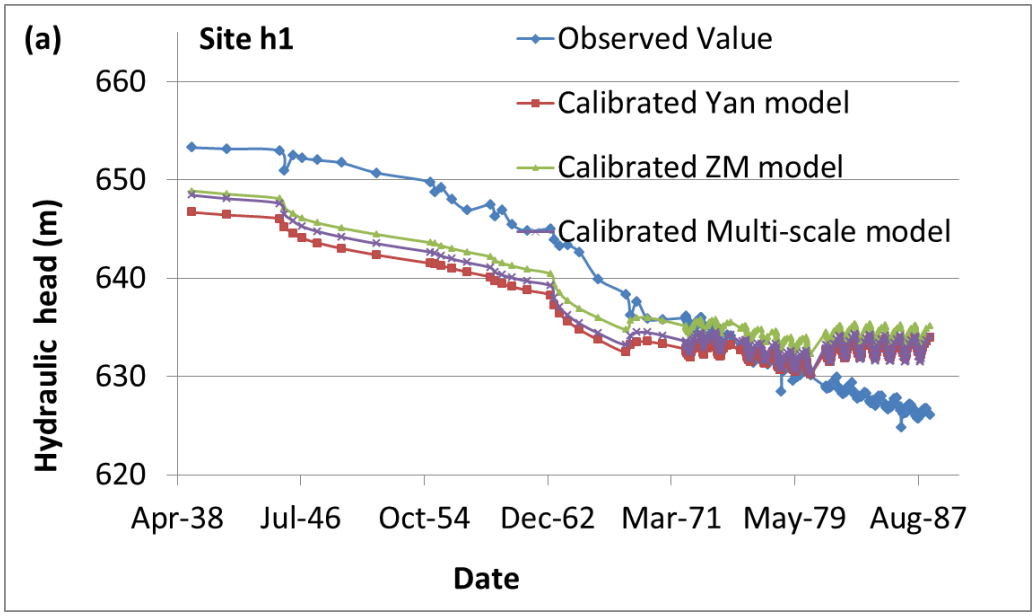
(a)
Site h1
Observed Value
Calibrated Yan model
Calibrated ZM model
Calibrated Multi-scale model
660
650
640
630
620
Hydraulic head (m)
Apr-38
Jul-46
Oct-54
Dec-62
Mar-71
May-79
Aug-87
Date

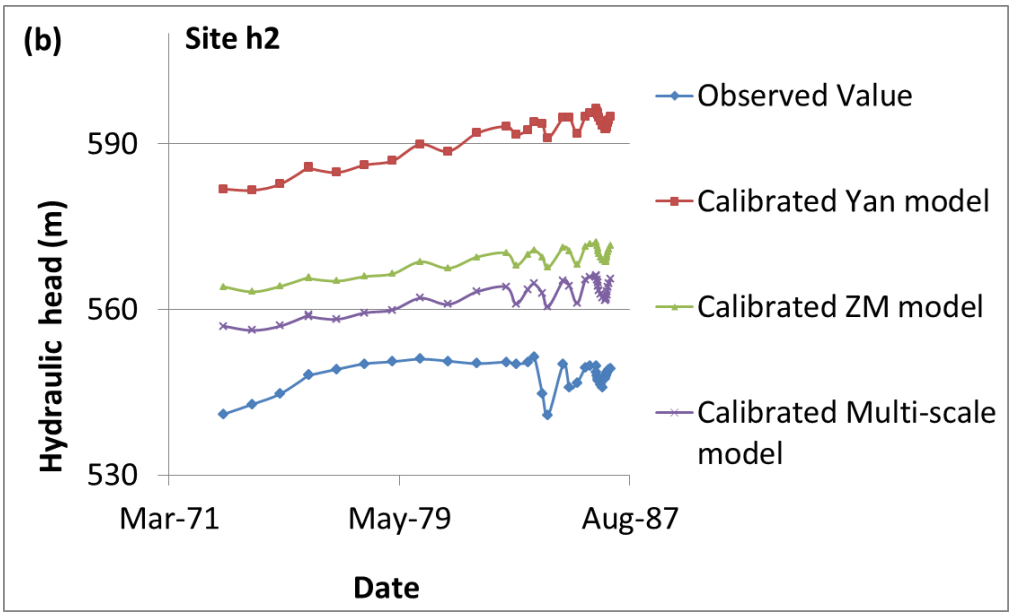
(b)
Site h2
Observed Value
Calibrated Yan model
Calibrated ZM model
Calibrated Multi-scale model
590
560
530
Hydraulic head (m)
Mar-71
May-79
Aug-87
Date

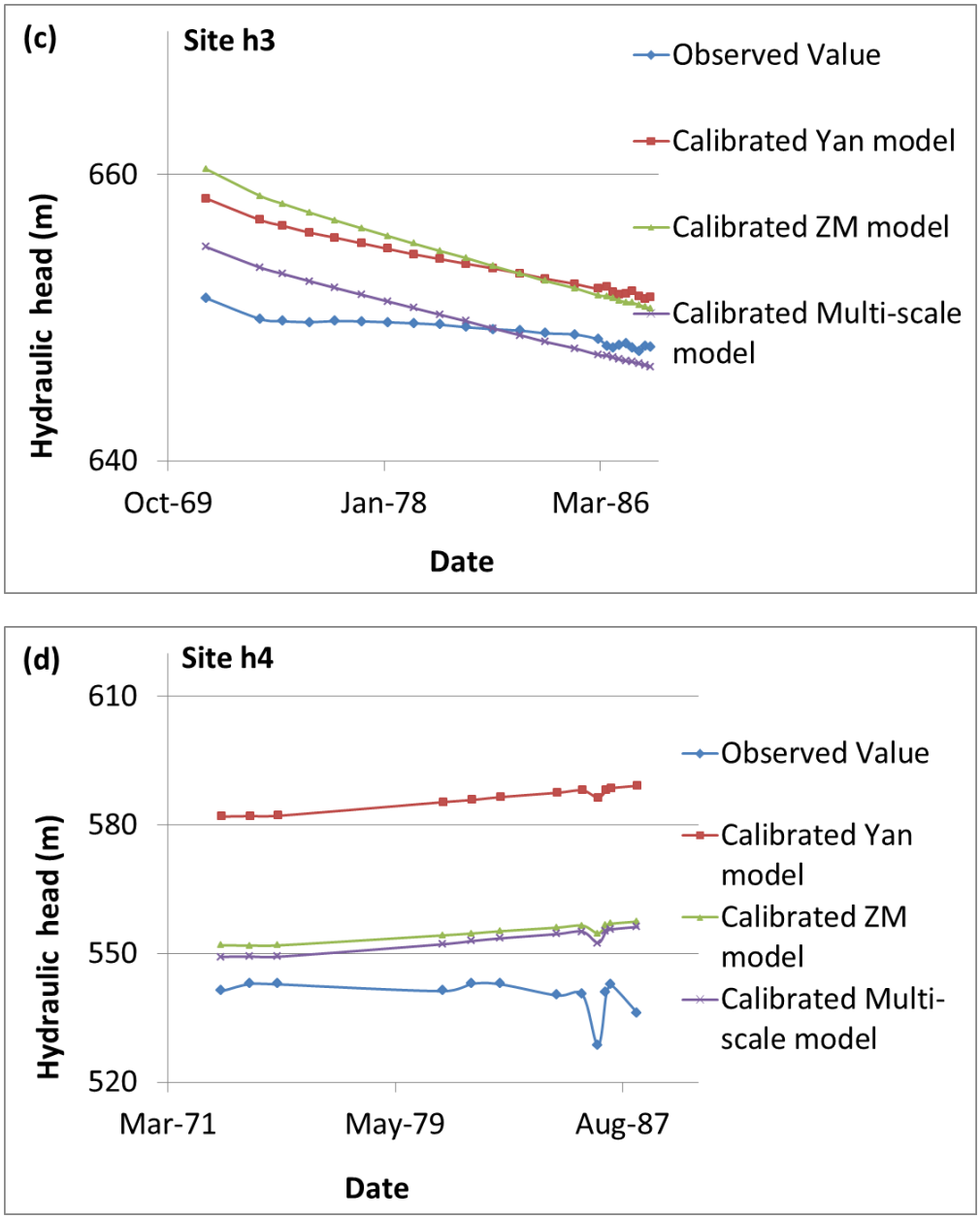

Figure 25. Observed hydraulic head vs. simulated hydraulic head at (a) site h1, (b) site h2, (c) site h3 and (d) site h4 for the three evaluated calibration strategies.

Observed and simulated land subsidence values for the calibration period using the ZM and the adaptive multi-scale strategies are shown in Figure 26. It can be seen from Figure

26a and Figure 26b that the ZM and the adaptive multi-scale methods fit the observed values more closely than Yan's model, especially where the observed land subsidence values are small. Quantitative assessment of the model fitting is listed in Table 2. The *NS* criteria indicates that the fit is very good for both the ZM and the adaptive multi-scale inversion methods. The *m* criteria indicates that on average, simulated subsidence values are smaller than the observed ones. The *D* criteria indicate that the fit is good with all two inversion strategies. The *s* criteria is decreasing with the ZM and the adaptive multi-scale method, suggesting that the overall model fit to the weighted observational data has improved. The adaptive multi-scale method appears to be superior to the ZM method based on *NS*, *D* and *s* criteria (Table 2).

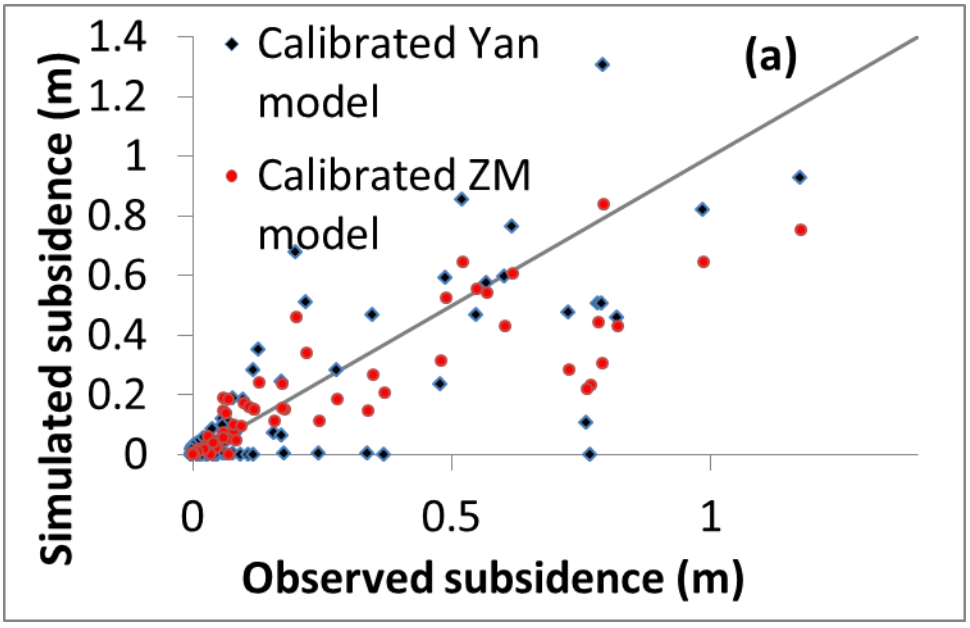

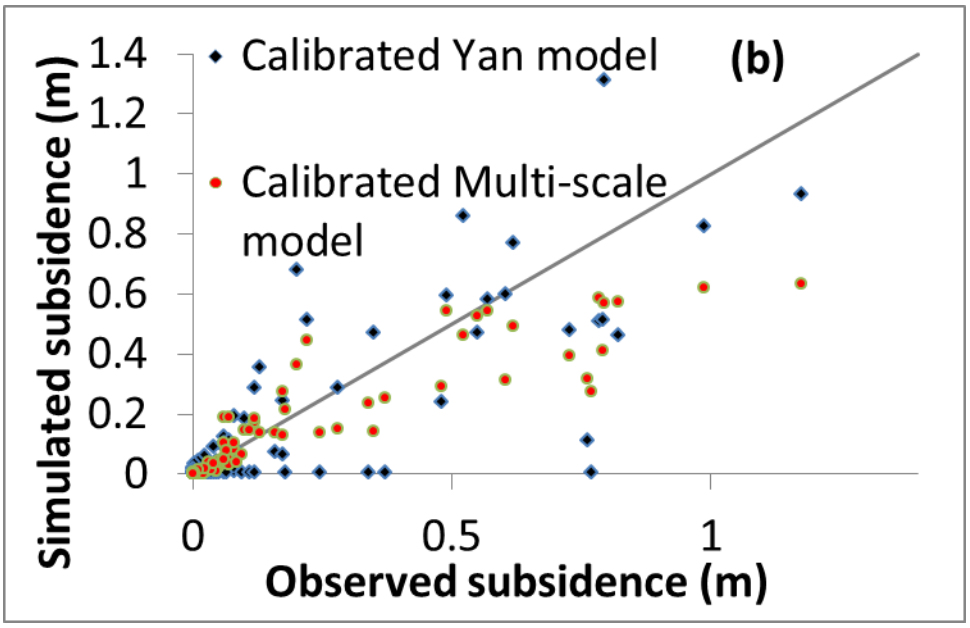

Figure 26. Observed vs. simulated land subsidence for the calibration period with (a) ZM, and (b) adaptive multi-scale method.

Observed versus simulated hydraulic heads for the evaluation period for the ZM and the adaptive multi-scale strategy are shown in Figure 27. The results indicate that the ZM and adaptive multi-scale methods yield superior results (better fitting) when compared with Yan's model. The quantitative assessment of model fit is listed in Table 2. The *NS* criteria indicates that the fit is excellent for the ZM and the adaptive multi-scale inversion methods. The *m* criteria indicates that on average, the simulated hydraulic heads are lower than the observed heads for the ZM, while simulated heads are higher than observed heads for the other two methods. The *D* criteria indicate that the fit is very good for both the ZM and the adaptive multi-scale inversion strategies. The *s* criteria is decreasing with the ZM and the adaptive multi-scale method. Based on quantitative assessment results (Table 2), the adaptive multi-scale method is shown to be superior to

the ZM method based on these criteria. Figure 25 shows that the adaptive multi-scale method produces the best model fit at sites h1- h4. Figure 28 shows plots that compare the observed versus predicted hydraulic heads at sites h3 and h4 (Figure 14) using the DREAM strategy. The results show that the 95% credible intervals are too narrow to include in the observed data. The mean predictions (the center of the intervals) are close to the observation data at site h3, but far from the observation data at site h4.

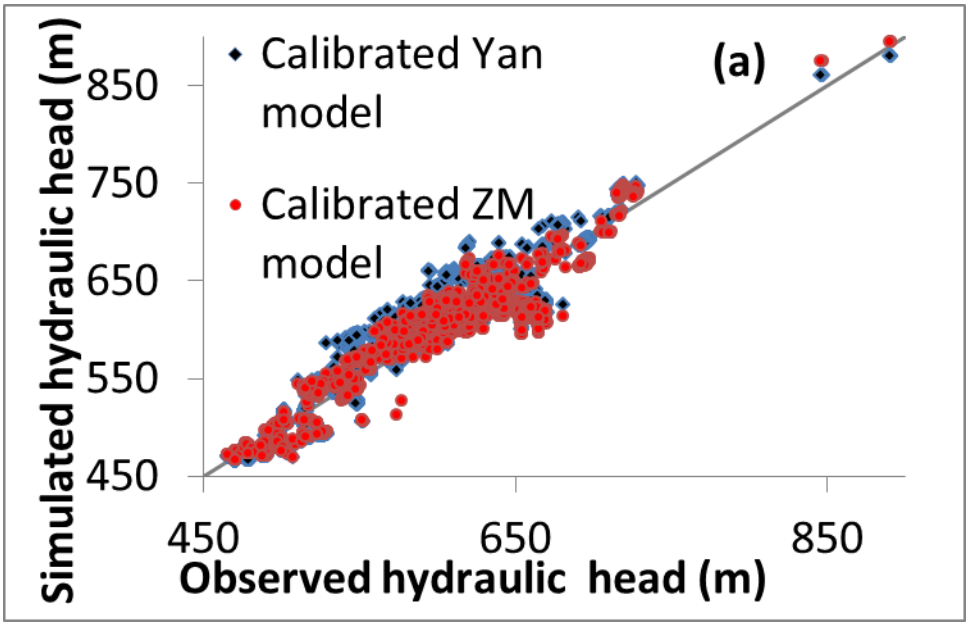

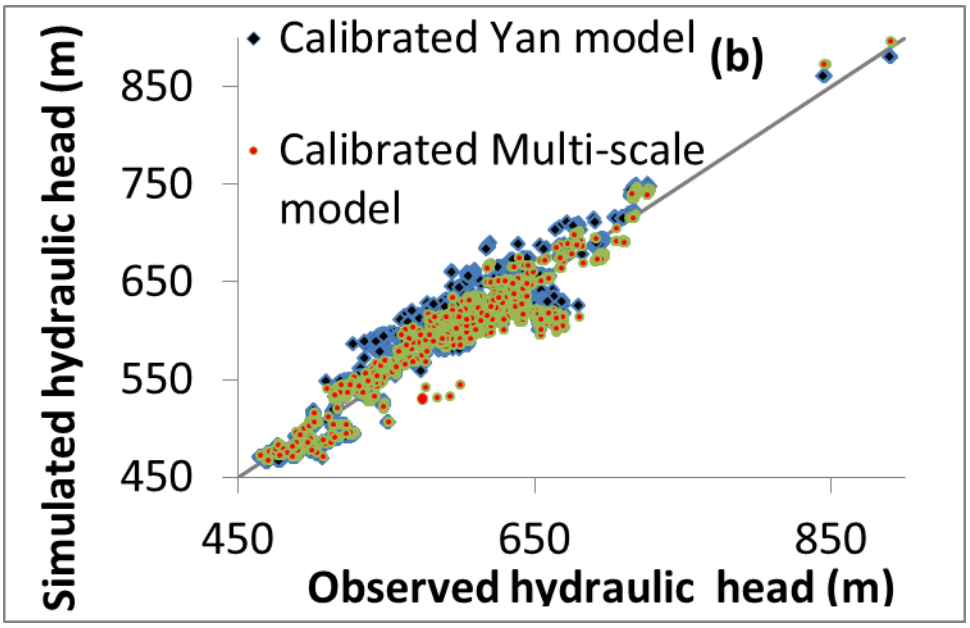

Figure 27. Observed vs. simulated hydraulic heads for the evaluation period using (a) ZM, and (b) adaptive multi-scale method.

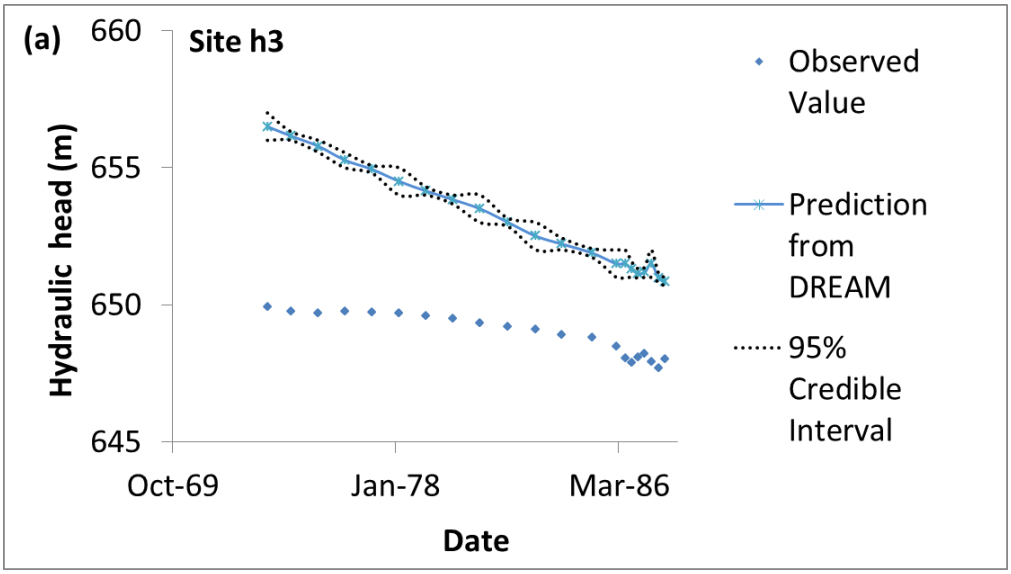

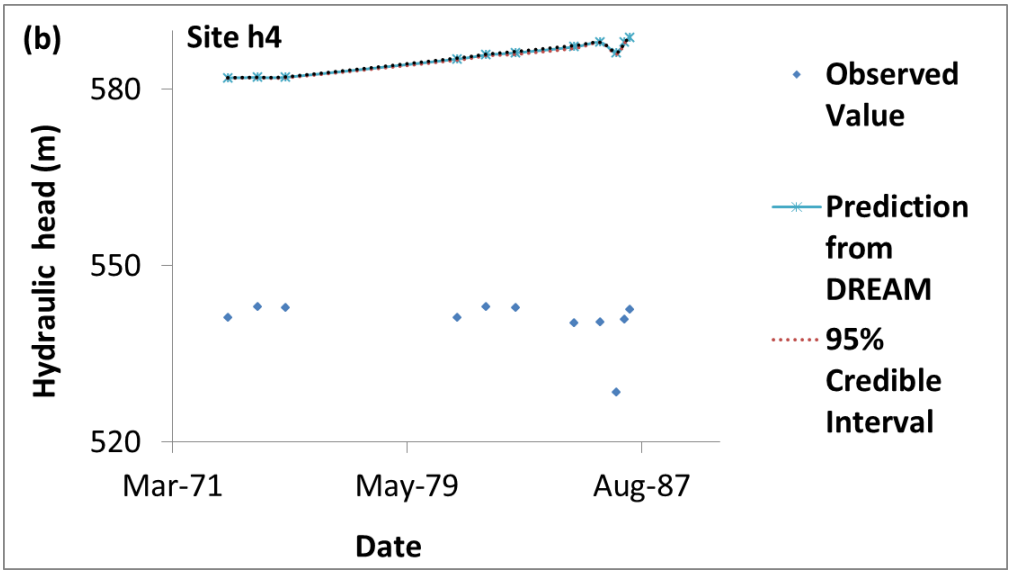

Figure 28. Observed hydraulic head vs. simulated hydraulic head at (a) site h3 and (b) site h4 for the DREAM strategy.

Observed and simulated land subsidence values for the evaluation period using the ZM and the adaptive multi-scale inversion strategies are shown in Figure 29. Results indicate that the greatest fit relative to Yan's model occurs with the ZM (Figure 29b) and the

adaptive multi-scale (Figure 29b) methods. A quantitative assessment of model fit is listed in Table 2 and indicates that none of the three calibrated models are sufficient to accurately predict land subsidence because all three of the inversion methods produce simulated subsidence values that are lower than the observed values on average.

Figure 30 shows plots that compare observed versus predicted land subsidence. The results show that the 95% credible intervals include several observations, but the intervals are too narrow to include all the observed data. The mean predictions (the center of the intervals) are shown to be far from the observations. One reason for the insufficient prediction is that only 113 land subsidence measurements are used for the evaluation period from 1963 to 1980 in the calibration process (Figure 14), which evidently is insufficient to adequately reflect the complex pattern of the land subsidence at the basin scale. Furthermore, the observed land subsidence values are not random, but occur in two transects through the basin, thus many areas where known subsidence is known to have occurred (based on more recent InSAR data) is absent of observed values.

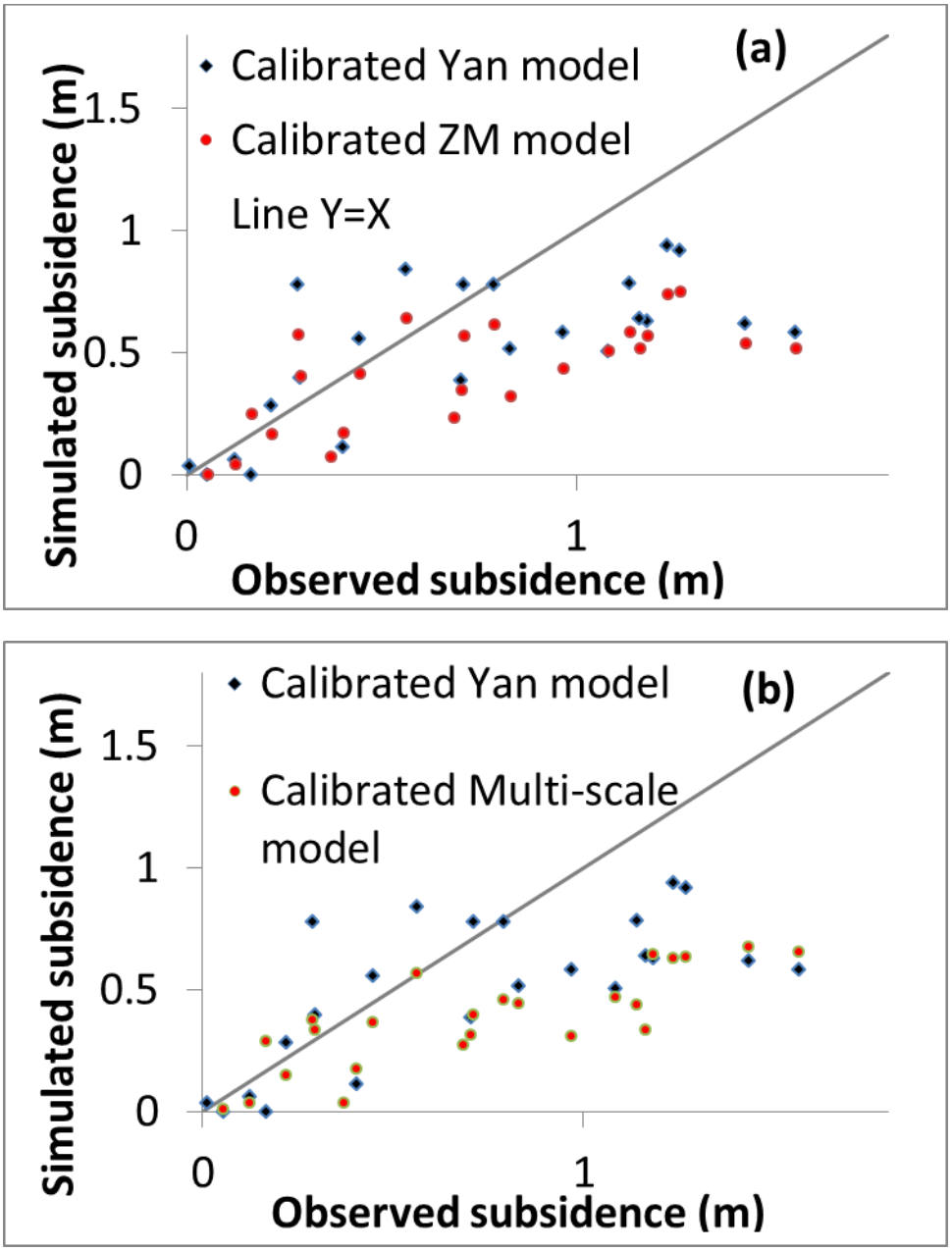

Figure 29. Observed vs. simulated land subsidence for the evaluation period using (a) ZM, and (b) the adaptive multi-scale method.

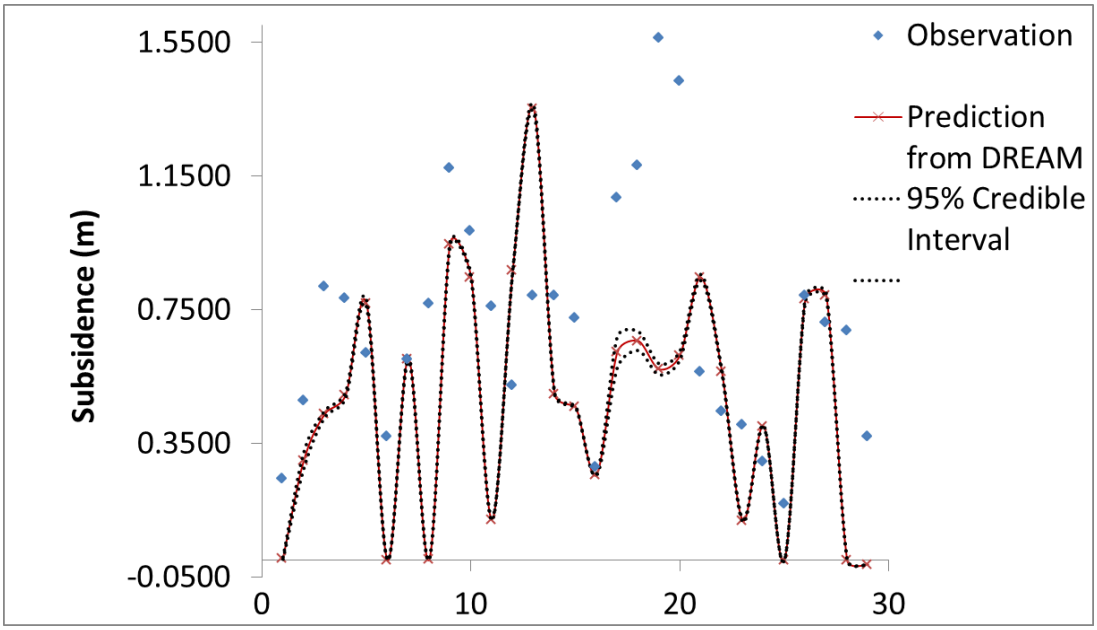

Figure 30. Observed land subsidence vs. predicted land subsidence for the DREAM strategy.

3.5. Discussion

The results of this study provide an opportunity to compare three inversion strategies that were invoked for calibrating *T*, S_{ke} *and* S_{kv} for Las Vegas Valley at the basin scale with the aim of achieving both accuracy and computational efficiency.

3.5.1. Parameter Estimation

The parameters *T*, S_{ke} *and* S_{kv} of the developed zone aquifer (principal aquifer, layer 3) are calibrated for Las Vegas Valley at the basin scale. Many investigations and regression analyses have been used to determine *T*, S_{ke} *and* S_{kv} values by various researchers (Harrill 1976, Plume 1984, Morgan and Dettinger 1994, Hoffmann, Zebker et al. 2001, Pavelko 2004, Bell, Amelung et al. 2008). In order to constrain the range of the parameters for the

ZM and adaptive multi-scale method, prior information obtained from the previous investigations are used for the parameters T , S_{ke} and S_{kv}. Parameters described in Yan's model (Yan 2007) are treated as initial guesses of both zones and parameters in our study (Figure 13a and Figure 18a). Calibrated T values that we obtained have similar values as that from Yan, except at zones E and S (Figure 18a, b), where coarse grained sediments occur in the eastern part of the basin (close to point A' in Figure 13b and in the southern part of the basin near Henderson shown in Figure 13a). Calibrated S_{ke} and S_{kv} values are generally lower than those from Yan (Figure 23a-c), but among the reasonable range for the clay interbed. Because the interbed thicknesses were inferred for a large portion of the basin, especially in the northwest part of the area (See Figure 3.3.4-1 and 3.3.4-2 of (Morgan and Dettinger 1994)), S_{ke} and S_{kv} zones had to be reconstructed using the adaptive multi-scale method. Calibrated T , S_{ke} and S_{kv} zones and values reflect more realistically the hydrogeological conditions of the basin. A CSS analysis indicates that the information provided by the observations and the model are sufficient to calibrate all T , S_{ke} and S_{kv} parameters in our study, with S_{kv} exhibiting the largest CSS, which suggests that this parameter is highly sensitive to observations and important in the calibration process. Pavelko (2004) found that the inelastic skeletal specific storage has a relatively large CSS compared to other parameters. The PCC analysis suggests that no parameter is prevented from being uniquely estimated (Foglia, Hill et al. 2009).

For the DREAM MCMC method, we only simulate marginal posterior distributions of the four parameters in the model. The results shown in Figure 21 indicate that the formal likelihood Gaussian function assumption may not hold due to the complexity and different sources of uncertainty that exist in the model. The PCC analysis shows that

transmissivity parameters are weakly correlated. This is consistent with the result obtained from the ZM and adaptive multi-scale methods.

3.5.2. Model Fit

For the ZM and the adaptive multi-scale methods, the measures *NS*, *m* and *D* are used to evaluate the overall model fit, which are independent of the observation weights, while *s* is a measure of overall model fit to the observations related to error-based weighting. *NS*, *m*, *D* and *s* are included in this study because of their widespread use for hydrogeologic models. The observation data used in this study are the same as Yan's model; however, the simulated results are different than Yan's, because the parameters are calibrated with ZM and the adaptive multi-scale methods. The *s* criteria decreases with the ZM and the adaptive multi-scale method (Table 2), which suggests that the overall model fit to the weighted observational data has improved. For the DREAM method, the prediction uncertainties are quantified using their 95% credible intervals. The results shown in Table 2 indicate that the calibrated model fit, based on *NS*, *D* and *m* criteria, is excellent or very good for observations of hydraulic head during the calibration and evaluation periods. The measures of model fit shown in Table 2 indicate that the model fit is very good or good for observations of land subsidence during the calibration period, but insufficient for land subsidence during the evaluation period based on weighting independent analysis. The prediction uncertainties shown in Figure 28and Figure 30 indicate that the 95% credible intervals are too narrow to include all the observed data and the mean predictions (the center of the intervals) are not close to the observations. One likely reason for the insufficient prediction of the land subsidence during the evaluation period is because of the complex factors influencing subsidence such as interbed thickness, the

location of basin-fill faults, delayed interbed drainage and time constant that contributes to the occurrence of land subsidence. Another reason for the insufficient prediction of the land subsidence is that the observational data used during the calibration period are taken from a set of transects from years 1963 and 1980, which, as pointed out by Bell (2002), does not encompass the entire spatial extent of the basin and the transects miss major subsidence areas and the complex interaction of many of the faults in the region. However, the objective of this paper is to find the optimal inversion strategy for the Las Vegas Valley model, so we incorporated a shorter model for the sake of minimizing computational time and maximizing efficiency. In fact, InSAR and GPS data have revealed new spatial patterns of subsidence that were not evident on earlier conventional subsidence maps based on the data used in this investigation (Hoffmann, Zebker et al. 2001, Bell, Amelung et al. 2002, Bell, Amelung et al. 2008). We are in the process of incorporating high spatial resolution InSAR data for the period from 1992-2010 and anticipate greatly improved calibration results when these new InSAR data are included in the inversion model. Nonetheless, the data used in this investigation reveals that the multi-scale method is the best inversion method to pursue for the full Las Vegas model.

3.5.3. Comparison of the Three Inversion Strategies

Three different inversion strategies were investigated including ZM, the adaptive multi-scale method and DREAM MCMC. The ZM is a fast inversion method but is somewhat subjective when defining actual parameter zones. The multi-scale method is an approach that provides criteria to reconstruct the zones by refining or coarsening the current zones based on actual hydrogeological conditions, which removes subjectivity in identifying zones that is inherent in the other methods. In this study, we first identify those zones

where hydrogeological analysis shows that the refinement or coarsening may be required. We then identify those zones that are important to fitting the observations through a sensitivity analysis (Grimstad, Mannseth et al. 2003, Foglia, Hill et al. 2009). Both refinement and coarsening indicators provide first order information on the minimization of the optimal objective function, so the decrease of the objective function is not guaranteed all the time, but this provides an alternative to reconstructing the current zones by saving time from trial-and-error guesses for zone structures. Due to the complex hydrogeological conditions and large amount of available temporal and spatial groundwater hydraulic head and land subsidence measurements in Las Vegas Valley area, a model with finer cells and more parameter zones is required to reflect the actual hydrogeological conditions and to better predict the hydraulic head and land subsidence patterns. This study reveals that the adaptive multi-scale method represents an effective, flexible and computationally efficient methodology for reconstructing the T, S_{ke} and S_{kv} zones according to hydrogeological and sensitivity analyses.

The DREAM MCMC method is a scheme that significantly improves the efficiency of MCMC simulations (Vrugt, Ter Braak et al. 2009), It can be used to estimate the posterior probability density function of model parameters in high dimensional and multimodal sampling problems. However, the computational time is excessive and impractical for such large models as the Las Vegas model developed in this study. Because many sources of uncertainty (such as measurement error, input error and s error) exist in the model processing, the commonly used formal likelihood function (Equation 30), which is based on the assumption that the residual term follows a multivariate Gaussian distribution, is not practical for complex applications (Beven, Smith et al. 2008). Thus, the DREAM

MCMC could not be used with formal likelihood function to calibrate all the parameters for the Las Vegas model, and is more suited for smaller, less complex, simulation problems.

The commonly used quantitative model fit measurement results show that, in general, the adaptive multi-scale method is superior to the ZM and Yan's model (Table 2 and Figure 25), especially for the hydraulic head and land subsidence fit during the calibration period. The insufficient prediction of the land subsidence during the evaluation period is attributed to the sparsely distributed observational data used during the calibration period. It's anticipated that a better land subsidence fit could be obtained if sufficient observed land subsidence data were available. The adaptive multi-scale method is more efficient than the DREAM MCMC method. Therefore, it is suggested that the adaptive multi-scale method represents the best and most efficient strategy for calibrating the optimal model parameters for making credible predictions, and providing a framework for developing an accurate hydrogeologic model for Las Vegas Valley, and for other similar highly complex non-linear problems.

3.6. Conclusions

This paper explores three inverse strategies, (1) the ZM, (2) the adaptive multi-scale method and (3) DREAM to estimate the distribution of transmissivity (T) and elastic and inelastic skeletal storage coefficients *(S_{ke}* and S_{kv}, respectively) from observations of hydraulic head and land subsidence measurements for Las Vegas Valley between 1912-1987. The key conclusions can be defined as follows:

1. Calibrated T values that we obtained from ZM and the adaptive multi-scale method are similar in magnitude and distribution from those of Yan (2007), except at zones E and S (Figure 17b and Figure 17c). Calibrated S_{ke} and S_{kv} values are lower than those from Yan (Figure 23a-c), but still fall within a reasonable range for the clay interbed. The S_{ke} and S_{kv} zones are reconstructed with the adaptive multi-scale method where the interbed thicknesses were inferred from Morgan and Dettinger (1994). Calibrated T, S_{ke} and S_{kv} zones and values appear to reflect more realistically the hydrogeological conditions of the basin.
2. Because many sources of uncertainty (such as measurement error, input error and structure error) exist in the Las Vegas model, the DREAM MCMC is not compatible with UCODE-2014 using a formal likelihood function (Equation 30), which is based on the assumption that the residual term follows a multivariate Gaussian distribution. Therefore, this method is not a good choice for calibrating parameters for this study.
3. The adaptive multi-scale method is able to quickly and efficiently reconstruct the T, S_{ke} and S_{kv} zones while providing more flexibility and accuracy than the other two methods. The model fit results show that overall, the adaptive multi-scale method is superior to the ZM method, especially for the land subsidence fit during the calibration period and hydraulic head fit. The inadequate prediction of the land subsidence during the evaluation period is attributed to the sparsely distributed observational data used during the calibration period. It's anticipated that a better land subsidence fit could be obtained if sufficient observed land subsidence data were available. The adaptive multi-scale method is more efficient

than the DREAM MCMC method, and can be used to successfully calibrate parameters at the basin scale. Thus, the adaptive multi-scale method is the best strategy for calibrating optimal model parameters and providing a framework for developing an accurate hydrogeologic model for Las Vegas Valley.

4. For the DREAM method, the results show that the 95% credible intervals are too narrow to include all the observed data and the mean predictions are not close to the observation data. Better calibration results are expected once high spatial and temporal resolution InSAR data (basin wide subsidence data) are included in the inversion model.
5. A CSS analysis indicates that information provided by observations are sufficient to calibrate all T , S_{ke} and S_{kv} parameters in our study. A PCC analysis shows that no parameter is prevented from being uniquely estimated from the multi-scale method and ZM.

4. Quantifying high-resolution hydrologic parameters at the basin scale using InSAR and inverse modeling, Las Vegas Valley, NV

Abstract

Las Vegas Valley has had a long history of surface deformation. InSAR interferograms have revealed detailed and complexspatial patterns of subsidence in the Las Vegas Valley area that do not coincide with major pumping regions. This research represents the first effort to use high spatial and temporal resolution subsidence observations from InSAR and hydraulic head data to inversely calibrate transmissivities (T), elastic and inelastic skeletal storage coefficients (S_{ke} and S_{kv}) of the developed-zone aquifer and conductance (CR) of the basin-fill faults for the entire Las Vegas basin. The results indicate that the subsidence observations from InSAR are extremely beneficial for accurately quantifying hydraulic parameters, and the model calibration results are far more accurate than when using only water-levels as observations, and just a few random subsidence observations. The offset between pumping and greatest levels of subsidence is found to be attributed to variations in clay thickness. The Eglington fault separates more compressible deposits to the northwest from less compressible deposits to the southeast and the fault may act as a barrier, although the influence of the barrier to this area is found to be insignificant.

4.1. Introduction

Las Vegas Valley remains a rapidly growing metropolitan area with the population reaching 1.4 million residents in 2014. To meet the growing domestic, irrigation and commercial water demand, groundwater has been intensively pumped since 1905, with the largest volumes of pumping commencing in the 1950s. Until 1990 water levels declined continuously throughout the valley, with a 90-m maximum decline occurring in the west-northwest part of the valley (Figure 31a, from (Burbey 1995)).

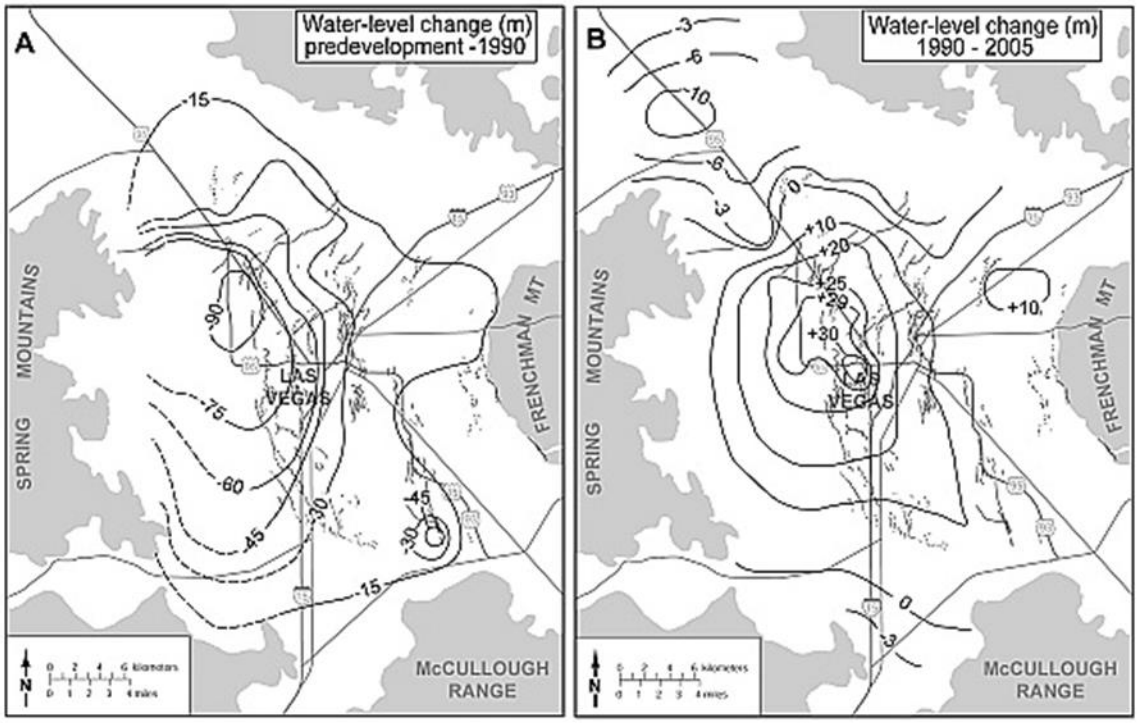

Figure 31. Water-level change in the principle aquifer (a) from predevelopment to 1990 based on water-level measurements (from Burbey, 1995) and (b) from 1990 to 2005 based on water-level measurements (Las Vegas Valley Water District, 2005)

Due to declining water levels, decreasing pore-water pressures within the aquifer system have led to significant increases in effective stress, which accounted for large-scale compaction of mostly fine-grained sediments (Terzaghi 1925, Poland and Davis 1969, Poland, Lofgren et al. 1972, Helm 1975). Because pumping has exceeded natural recharge for many years now, intensive groundwater pumping in Las Vegas has led to highly varying degrees of land subsidence. According to benchmark surveys, an early subsidence map for the period 1935-1963 shows that subsidence occurred as a singular bowl located near downtown Las Vegas (central bowl), with a maximum subsidence during that period of 67cm (Figure 32a)(Bell, Amelung et al. 2002). For the ensuing period 1963-1980, an updated subsidence map shows that three localized subsidence bowls--the Northwest, Central and Southern bowls--exist near the central part of the valley. The maximum total subsidence in 1980 occurred in the Northwest bowl, which was measured to be 78cm (Figure 32b)(Bell, Amelung et al. 2002). For the period 1963-1987, the three principal localized subsidence bowls became more widespread and extensive. Observed subsidence of more than 1.5 meters had occurred in the northwest bowl by 1987 (Figure 32c)(Bell, Amelung et al. 2002).

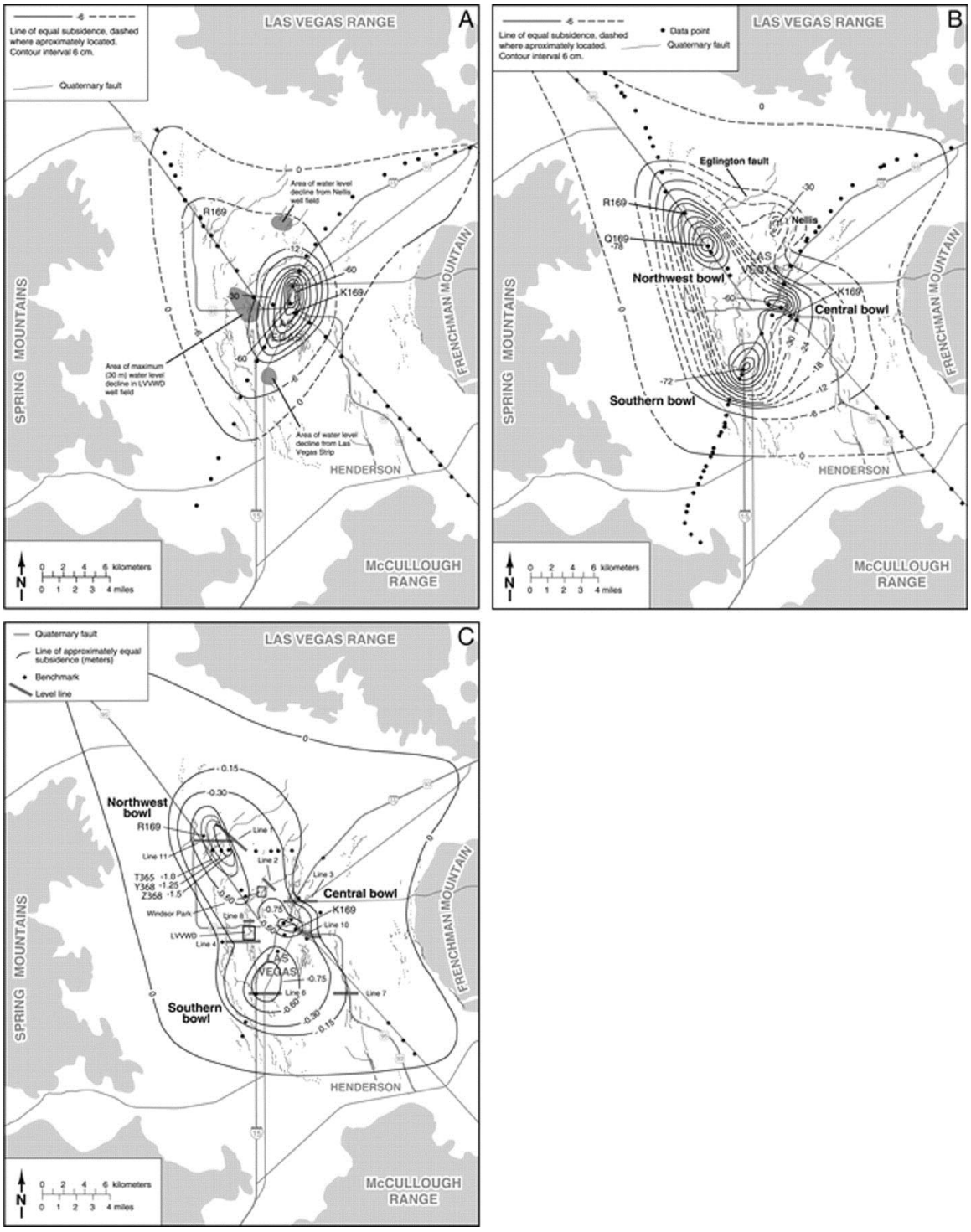

Figure 32. Subsidence maps for 1935 to 1987. (a) Subsidence map for the period 1935–1963. (b) Subsidence map for the period 1963–1980. (c) Subsidence map for the period 1963–1987 (from (Bell, Amelung et al. 2008)).

However, the bench mark surveys did not encompass the entire spatial extent of the basin and the transects miss major subsidence areas and the complex interaction of many of the faults in the region. InSAR and GPS data have revealed new spatial patterns of subsidence in Las Vegas Valley area that were not evident on earlier conventional subsidence map (Amelung, Galloway et al. 1999, Hoffmann, Zebker et al. 2001, Bell, Amelung et al. 2002). InSAR techniques allow for the measurement of surface displacements at spatial resolutions on the order of meters or tens of meters, and the precision is on the order of millimeters to centimeters, and can cover very large areas of up to thousands of square kilometers (Hoffmann 2003). The first InSAR study of subsidence occurred in Las Vegas Valley is by Amelung and others (1999) (Amelung, Galloway et al. 1999). Their research shows that the spatial extent of subsidence is controlled by faults and clay thickness (Figure 33 A-B). Bell (2002) developed a subsidence map for 1963-2000 based on synthesis of In-SAR pattern, GPS and conventional leveling data collected by the cities of Las Vegas and North Las Vegas in 1998 (Figure 34). The map shows that the maximum total subsidence was in the Northwest bowl (bounded on the east by Eglington fault), which was measured to be 170 cm.

The connection between faults and land subsidence has been investigated by previous researchers. Based on the InSAR map shown in Figure 33, Amelung and others (1999) pointed out that the four main subsidence bowls in the valley (Northwest, North Las Vegas, Central and Southern bowls) are bounded by Quaternary faults, among which, the Eglington fault appears to act as a subsidence barrier, where most of the subsidence occurs on the western upthrown block of the fault. He inferred that the fault may separate

more compressible deposits to the northwest from less compressible deposits to the southeast, or the fault may act as a barrier, creating a discontinuity in water level across the fault. Donovan (1996) plotted a hydrostratigraphic map for the subsurface sediments near the Eglington fault using the data collected from a cross section (Figure 35). The map shows that aquifer and aquitard thickness, transmissivity and elastic storage coefficients are generally uniform across the fault (Donovan 1996). The cross-section constructed between the Eglington and Windsor Part faults (Figure 33C) also shows that both sides consist of similar 300 m thick sections of compressible clays and water levels in the cross-section wells do not show significant discontinuities or variations (Bell, Amelung et al. 2002). Bell (2002) inferred that fault gouge or secondary carbonate cementation of the fault zone, or other mineralization occurring along the Eglington fault, may act as a subsidence barrier. Based on the observed conditions of the Eglington fault zone, Hernandez-Marin and Burbey (2009) developed a series of hypothetical numerical models using ABAQUS to evaluate the fault-zone width and the type of fault-zone constituent materials that best represent the field conditions leading the large differential subsidence and earth fissuring. The results suggest that the fault zone material is likely to have mechanical properties similar to sand, and the Eglington fault is best represented by a 100m wide fault zone (Hernandez-Marin and Burbey 2009).

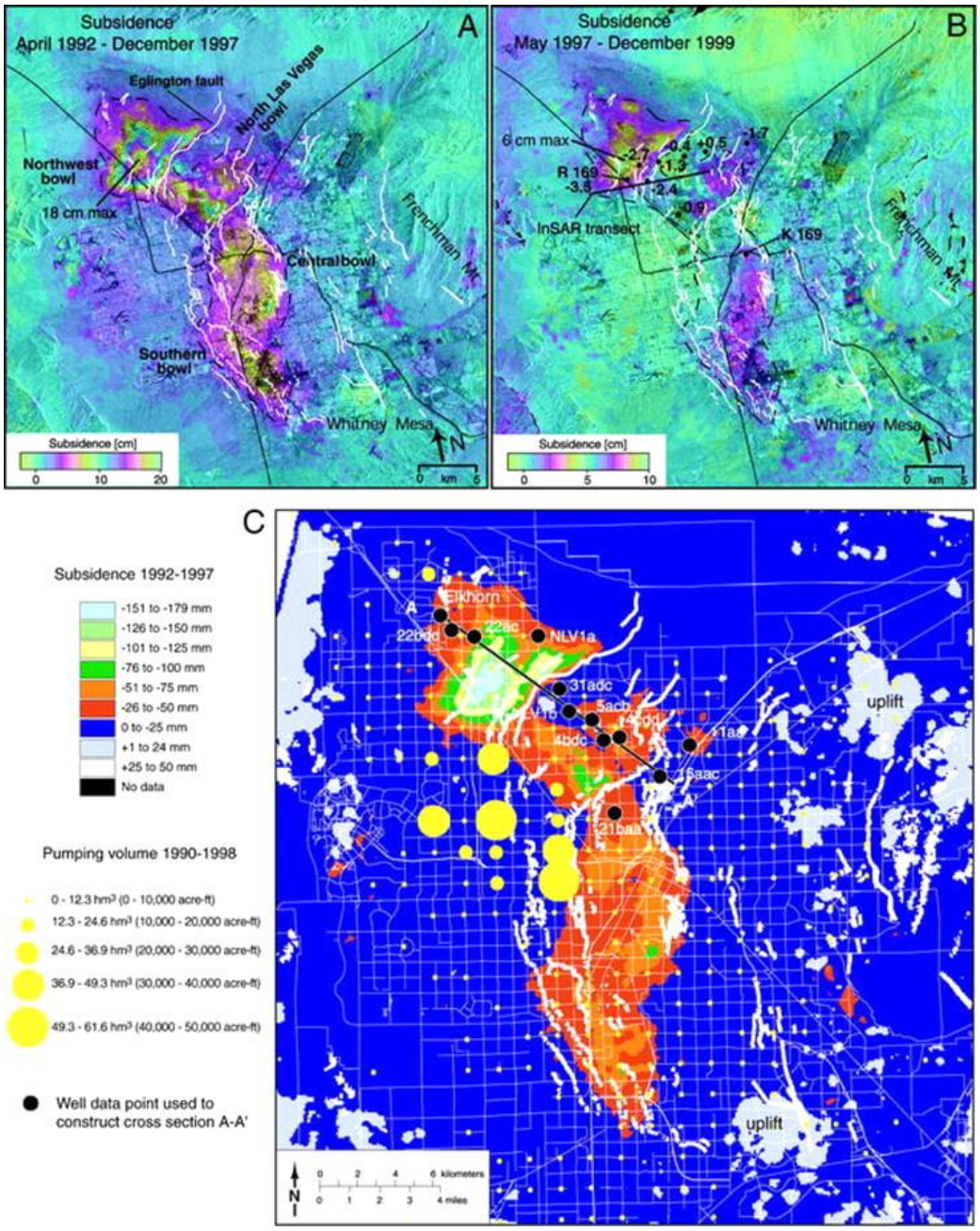

Figure 33. Synthetic aperture radar interferometry (InSAR) data for Las Vegas Valley for the periods (A) 1992–1997, (B)1997–1999 and (C) ArcView map showing InSAR and pumping data (from (Bell, Amelung et al. 2002)).

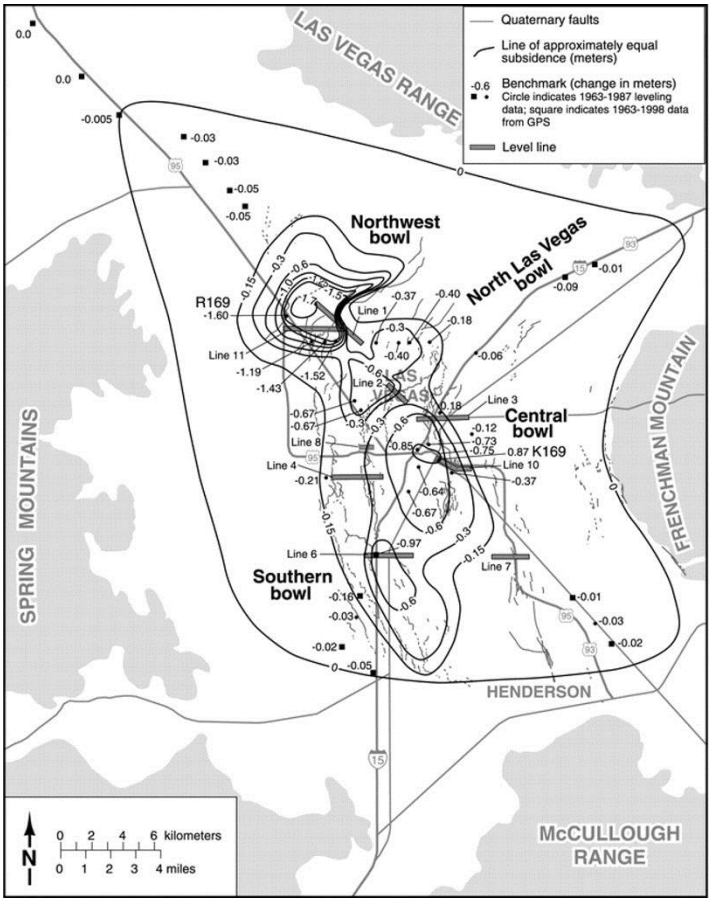

Figure 34. Subsidence map for 1963–2000 (from (Bell, Amelung et al. 2002))

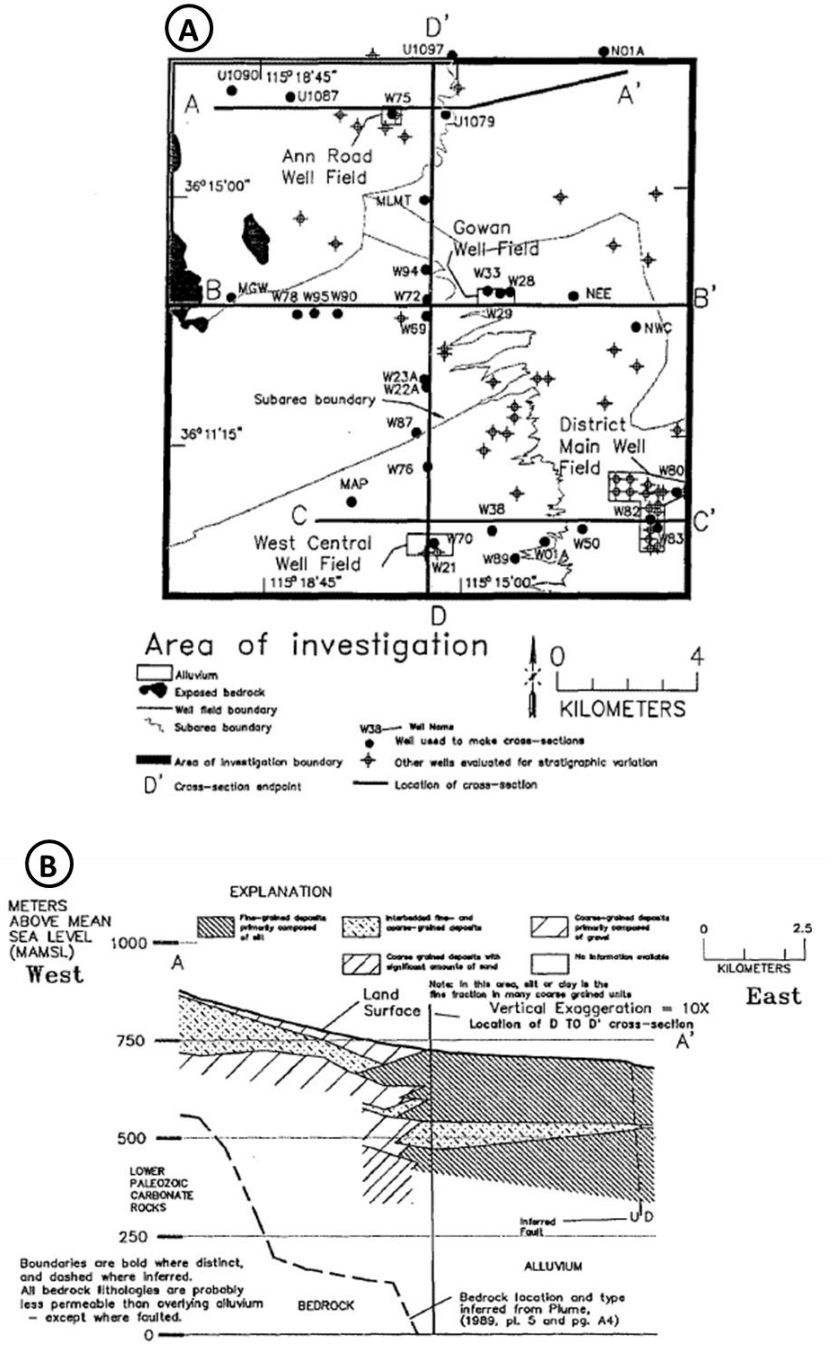

Figure 35 (a) Location of cross-section (A-A') across the Eglington fault and (b) geologic cross-section (A-A') (from Donovan, 1996.

Harrill (1976) was the first to systematically estimate basin-wide transmissivities from aquifer test data. Morgan and Dettinger (1994) developed the first valley-wide numerical groundwater model, which covered the period from 1912-1981 using the Trescott, Pinder

and Larson groundwater model (Trescott, Pinder et al. 1976). In their model, precalibration transmissivity was estimated using regression analysis from pumping tests and lithologic data interpreted by Plume (Plume 1984). The final transmissivities were manually calibrated by adjusting transmissivities and storage values so that the difference between simulated heads and observed heads was minimized as much as possible through trial-and-error methods and a minimum grid spacing of 2.5 km. Mean inelastic specific storage values were calculated based on groundwater level declines, clay thicknesses, and subsidence data measured at four benchmarks. The model yielded a rather generalized and crude distribution of simulated drawdown and land subsidence, but did not capture the now known complex patterns of subsidence that exist today and likely existed at the time this model was developed. Jeng (Jen 1998) later converted the Morgan and Dettinger model to the MODFLOW model (McDonald and Harbaugh 1984) without changing any final simulated parameters from Morgan and Dettinger. Yan (Yan 2007) later updated Jeng's model by extending the simulation period to 2005 using mostly the original parameter estimates of Morgan and Dettinger as well as the same course grid spacing. Pavelko (Pavelko 2004) developed a one dimensional groundwater and subsidence model in conjunction with UCODE (Poeter and Hill 1998) to calibrate hydraulic parameters at the Lorenzi site where the USGS installed an extensometer in 1993. Hoffmann et al. (Hoffmann, Zebker et al. 2001) and Bell et al. (Bell, Amelung et al. 2008) used InSAR and PS-InSAR combined with ground water level declines to evaluate elastic and inelastic skeletal storage coefficients in Las Vegas Valley at several individual locations. Until now no research has been done on calibration of the

transmissivities and elastic and inelastic skeletal storage coefficients of Las Vegas Valley at the basin scale using the high-resolution InSAR data and water head data.

In this study, we invoke the adaptive multi-scale strategy, which we developed in our previous research (Zhang and Burbey, 2014, submit) to be an efficient and accurate strategy, to calibrate the transmissivities and elastic and inelastic skeletal storage coefficients of Las Vegas Valley at the basin scale using the high-resolution InSAR data and water head data from 1912 to 2010.

The second objective of this research is to further investigate the influence of the faults and their potential role on influencing clay thicknesses and subsidence. We have successfully extended Las Vegas Valley model to year 2010 using MODFLOW-2005 (Harbaugh 2005) with the subsidence (SUB) (Hoffmann, Leake et al. 2003) and horizontal flow barrier (HFB) (Hsieh and Freckleton 1993) packages while implementing a 600m × 600m grid cell size, by far the finest scale model developed for the valley to date.

The third goal of this investigation is to use the calibrated parameters to investigate future trends of land subsidence in Las Vegas Valley by extending the simulation period of the developed calibration model to the year 2030.

4.2. Hydrogeological Condition

Las Vegas Valley encompasses an area of about 4,150 km2 in Clark County, southern Nevada. The northwest-trending valley is bounded on all sides by various mountains composed of rocks ranging from carbonates to volcanics. Carbonate bedrock underlies

the entire basin. The carbonate-dominated Spring Mountains to the west of the valley represent the main source of natural recharge to the valley. Winter snows melt and flow through fractures in the carbonates and then enter the adjacent alluvial deposits as infiltration or lateral groundwater inflow (Figure 34). Some additional recharge is occurring from the Sheep Range north in the and perhaps a minor amount from the volcanic McCullough Range to the southeast. No recharge occurs as the result of direct precipitation on the valley floor. Secondary recharge is primarily associated with lawn and golf course watering as well as discharge and disposal of industrial wastewater and has increased with the increasing population (Morgan and Dettinger 1994). By the early 1970s, the secondary recharge rate has exceeded the natural recharge rate and the secondary recharge to the near surface aquifer increased dramatically (Morgan and Dettinger 1994). The Southern Nevada Water Authority has estimated that 1.2×10^{8} m^3 per year of water is lost to the shallow groundwater system due to over irrigation in 2010 (Figure 36). Before the 1970's, groundwater was the principal water resource for the valley. To reduce the dependence on groundwater resources, surface water from Lake Mead was imported beginning in 1971 and now represents over 75% of the total water use in the valley. To help mitigate the ongoing occurrence of land subsidence, an artificial recharge program was initiated by the Las Vegas Valley Water District in 1989 (Figure 36), which involves injecting Colorado River water into the principle aquifer during the winter months when water demand is low. This program resulted in a maximum of approximately 30 m of groundwater level increase between 1990 and 2005 (Figure 31b). Currently, water that recharges the aquifers by natural and artificial processes, including secondary recharge of the shallow aquifer, is greater than the total water withdrawals,

thus helping stabilize or increase groundwater levels in most areas of the basin. Figure 31b shows that groundwater levels have underwent a general increase over the entire basin from 1990 to 2005. Nonetheless land subsidence has not ceased in many parts of the valley (Figure 33 and 38) because of hydrodynamic lag associated with the time-dependent drainage of clay interbeds.

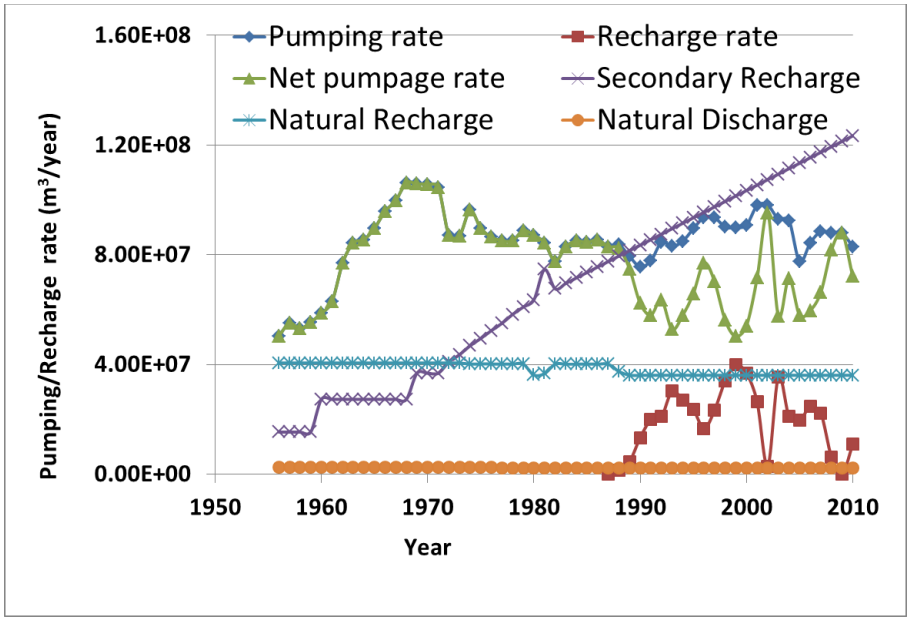

Figure 36. Total groundwater pumping and recharge rates (data from Las Vegas Valley Water District).

Las Vegas Valley is located in a structurally controlled alluvial basin. A series of north- to northeast-trending, east-dipping Quaternary faults cut the valley floor. A thick accumulation of interbedded and interfingered coarse- and fine-grained sediment fills the structural basin. In the northern, western, and southern parts of the valley, sediment consists of mainly coarse-grained sand and gravel. However sediment becomes thicker and finer-grained toward the central and eastern parts of the valley. The principle aquifer,

composed mainly of course-grained deposits with some fine-grained low-permeable interbeds, occurs at depths ranging from 60-300 m below land surface (Malmberg 1965, Harrill 1976, Morgan and Dettinger 1994). In the vertical direction, permeability tends to decrease with depth (Maxey and Jameson 1948). Overlying the principal aquifer is a 30 m to 90 m thick sequence of clay, sand, and gravel, which is often referred to as the near-surface reservoir, which is not pumped nor used as a potable water source.

4.3. PS-InSAR (Persistent Scatterer Interferometric Synthetic Aperture Radar) Data

In this study, we have incorporated the latest PS-InSAR data (2002-2010), which is provided by Zhang (Youquan Zhang, Capital Normal University, China 2012). Two independent data sets obtained from the European Space Agency and UNAVCO are used for the study. Fifty-eight ENVISAT-satellite acquisitions were acquired in a descending track mode taken over the Las Vegas Valley between October 2002 and October 2010. Raw radar images were processed using ROI_PAC software developed by the JPL/Caltech(Rosen, Hensley et al. 2004). Interferograms were formed using Doris software developed by Delft University of Technology, the Netherlands (Kampes, Hanssen et al. 2003). The PS-InSAR data (Hooper 2008) were processed to obtain deformation phase data for each PS in order to calculate the radar line-of-sight (LOS) displacement of each PS relative to the master acquisitions (23 November 2007), and to detect the average velocity fields from the time-series data. PS-InSAR data were processed to remove topographic errors, atmospheric errors, the phase noise introduced

by the filtering operation, the correction for elevation-dependent atmospheric effects and the orbit tilts. A 40 m resolution is used in both the azimuth and range directions to describe the subsidence distribution for Las Vegas Valley. To test the accuracy of the PS results over the Las Vegas area, PS-InSAR results are compared with the independent 3D displacement data from a continuous GPS station (Zhang, 2012) (Figure 37). The comparison between InSAR measurements and GPS measurements shows general agreement with the long-term trend, but the PS data lack the seasonality of the GPS observations. The lack of seasonality in the PS data is caused by the removal of tropospheric errors, that are often mitigated by averaging several interferograms (Hoffmann, Zebker et al. 2001). Unfortunately, this also has the negative side effect of removing the seasonality in the data.

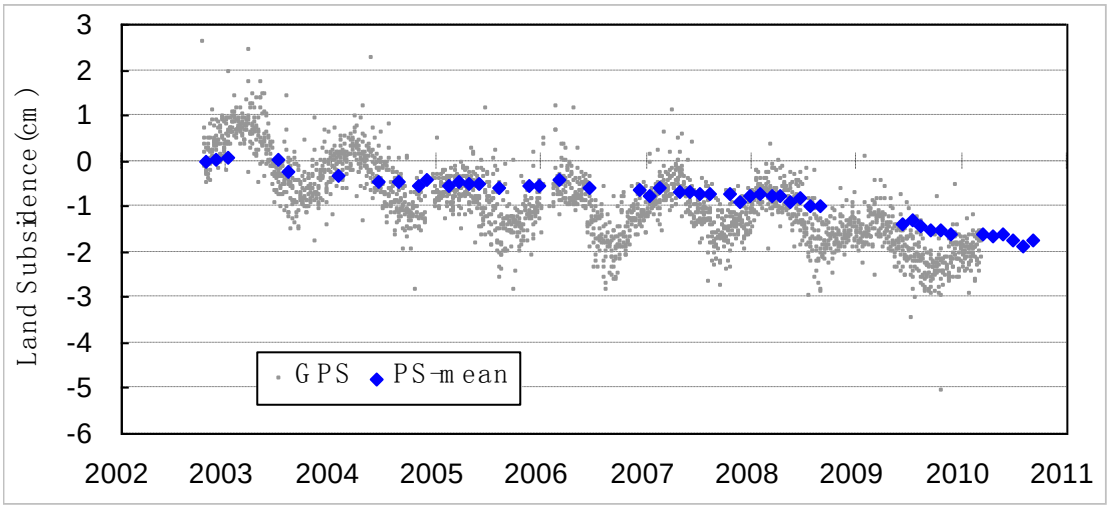

Figure 37. Comparison of time-series InSAR results to the projected LOS, time-series data for a GPS station (provided by Zhang, person. Commun., 2012).

InSAR measurements from 2002 to 2010 reveal new spatial patterns and temporal details of land deformation including velocity and distribution (Figure 38). Compared with the InSAR map of 1990-1998 (Figure 33), the most recent map shows that subsidence

velocities are lower and new uplift bowls (areas 1 and 2) have developed (Figure 38). In addition, seasonal land deformation responses to pumping, artificial recharge and secondary recharge have been lowered. In Las Vegas Valley the summer drawdown season typically occurs from April to November, and the remainder of the year represents the winter recovery season (Hoffmann, Zebker et al. 2001). Seasonally fluctuating water levels along with detailed monthly InSAR data can be used to investigate how seasonal variations in water levels are reflected in subsidence and rebound patterns. These stress-strain signals are found to be highly diagnostic and can be used to more accurately estimate the elastic skeletal storage coefficients of the aquifer system (Hoffmann, Zebker et al. 2001, Yan 2007, Bell, Amelung et al. 2008, Yan and Burbey 2008).

Interestingly, however, the subsidence/uplift bowls depart from the principal locations of artificial recharge (Figure 38) and pumping (Figure 33). Relative land subsidence/uplift revealed by Figure 38 suggests a spatial correlation between fault location, hydraulic head change, interbed thickness and land deformation.

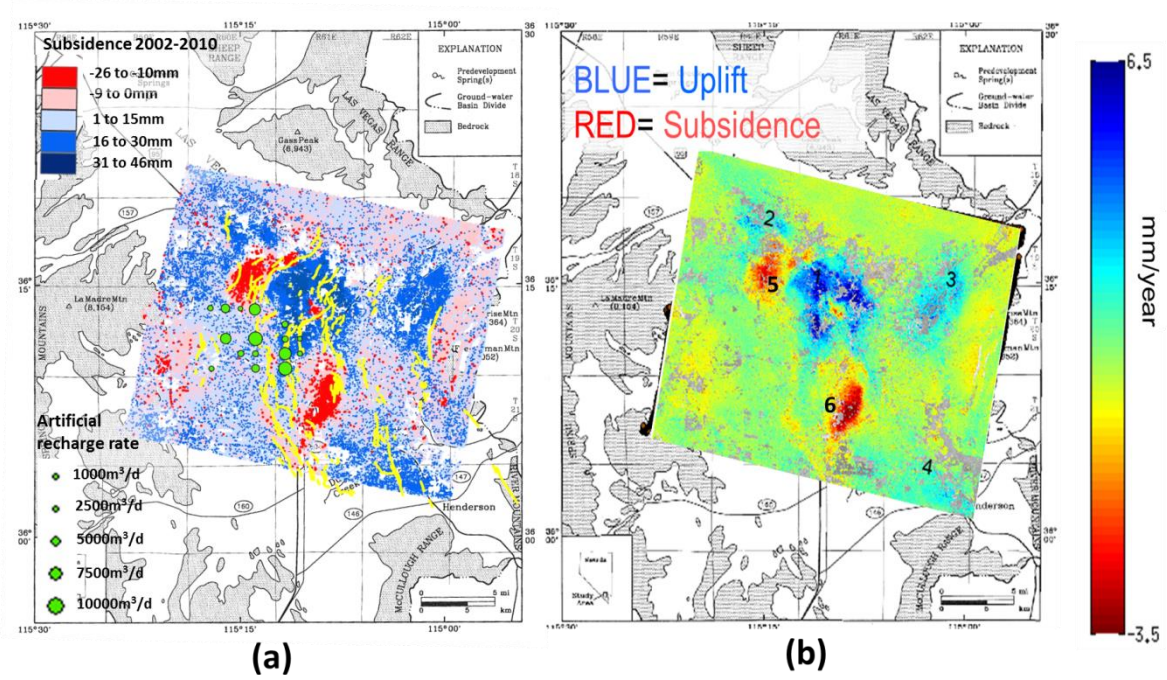

Figure 38. (a) Total subsidence, and (b) subsidence velocity in Las Vegas Valley between October 2002 and October 2010.

The InSAR map (Figure 38) shows four uplift areas (area 1-4). Area 1 is located at the location of the North subsidence bowl, which is controlled by the Windsor Park fault and the Cashman Field fault, which has undergone a net uplift of 16-46 mm with the largest uplift amplitudes of 6mm/year. At the same time, the maximum water-level recovery for this area is approximately 10m (Figure 40m-p). Area 2 is located in the northwest part of the Northwest subsidence bowl. Since 2002, the maximum water-level recovery for this area has reached 8m (Figure 40c-e). The interbed thickness of area 3 is large, but nearly no subsidence has occurred in this region. The lack of significant subsidence in area 3 can be attributed to its lack of water level decline and by the fact that it is located near a bedrock boundary (Figure 40i-l, and Figure 41). Area 4 is located at Whitney Mesa, which is also adjacent to a bedrock boundary. No significant subsidence has occurred

here previously, which can be explained by the absence of thick clay interbeds or significant water level decline (Figure 40v-w, and Figure 41).

Figure 38 shows two main subsidence bowls: the Northwest bowl (labeled 5) and the Central bowl (labeled 6). The Central bowl has undergone a net compaction of -10mm to -26mm with the maximum velocity of -3.5mm/year. Groundwater levels have generally recovered (Figure 40f-h) in the aquifer, so the occurrence of land subsidence during this time period suggests the existence of residual compaction, which is due to the slow draining (dewatering) of relatively thick clay interbeds. The Northwest bowl is bounded to the east and southeast by the Eglington fault, where more than 160 cm of total compaction has occurred since 1963 ((Bell, Amelung et al. 2002)) and the subsidence in this area has not ceased, although the maximum water level recovery for this area has reached up to 30m since the 1990s (Figure 40a-b). The importance of the Eglington fault to subsidence has been studied by a number of researchers, which has been discussed in section 1.1.

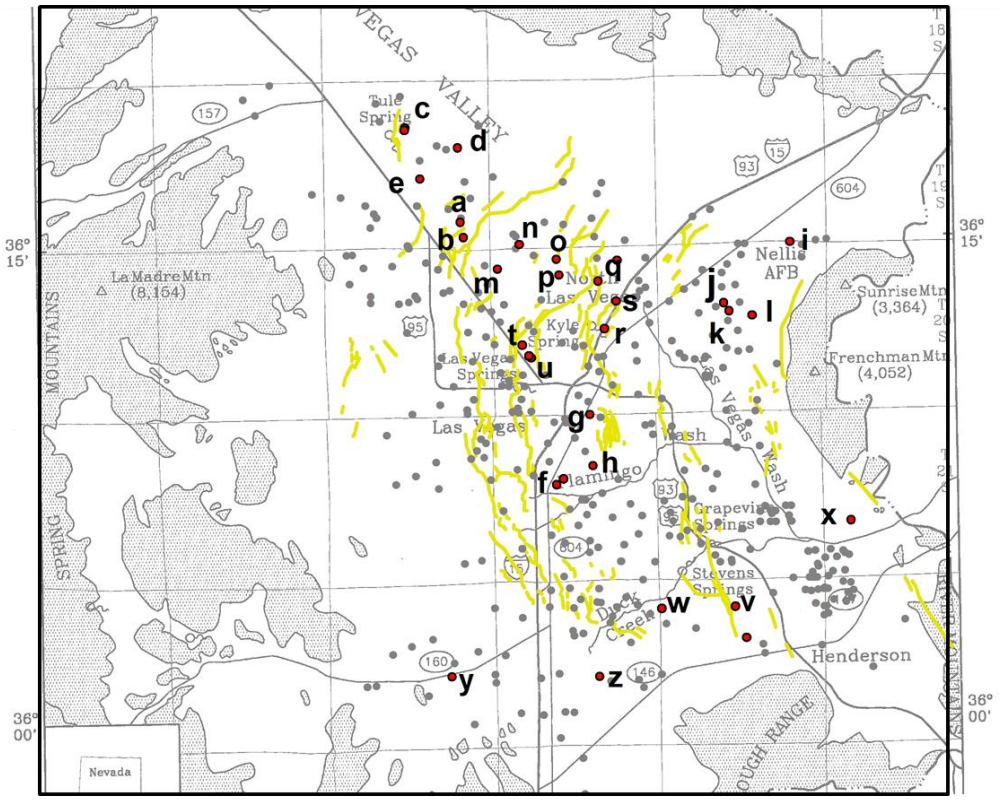

Figure 39. Groundwater monitoring network used as observations in the model. Grey circles represent locations of observed water levels. Yellow lines represent basin-fill faults; labeled points (a-z) are where observed vs. simulated heads are provided in Figure 40.

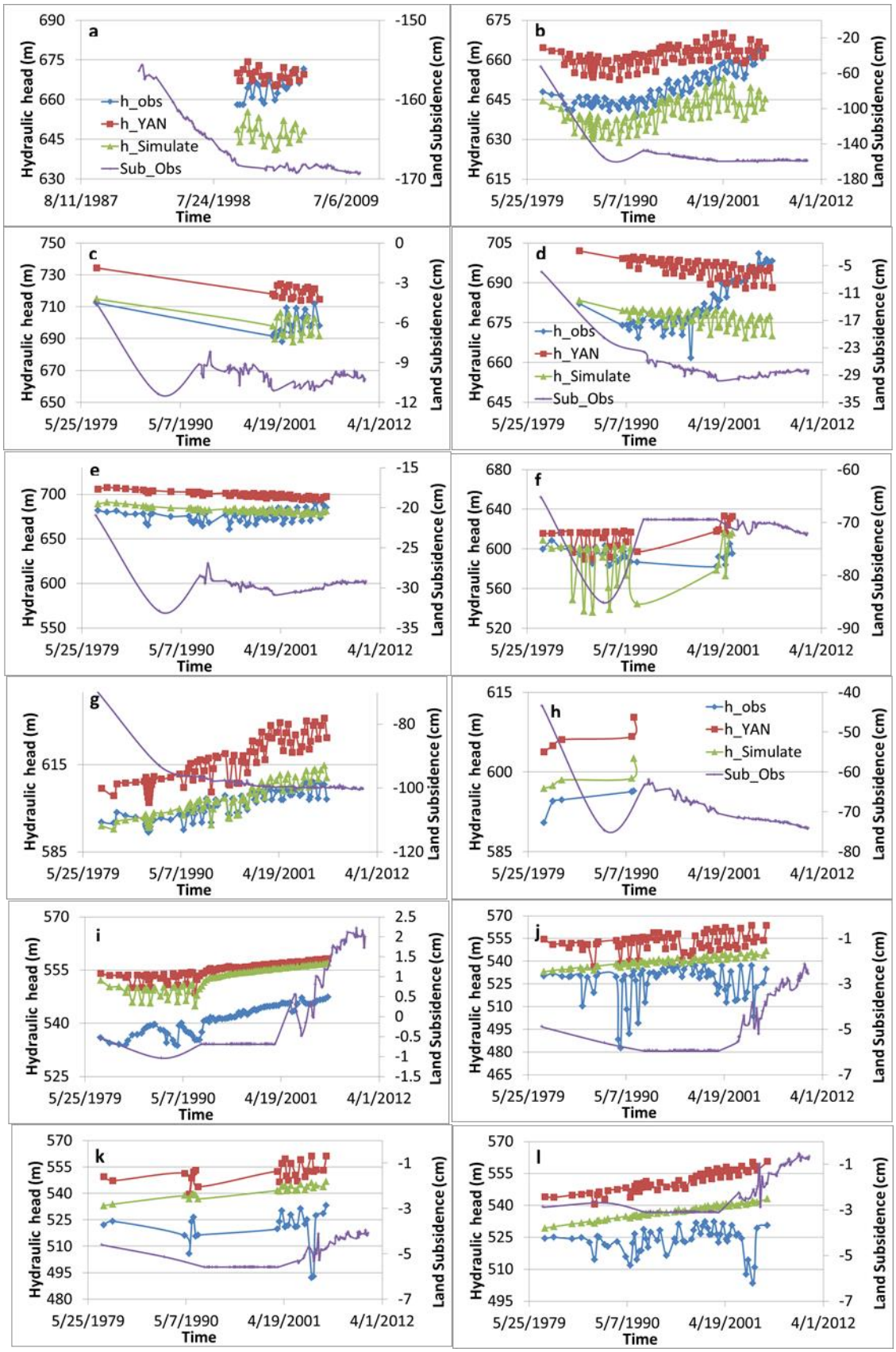
a
b
c
d
e
f
g
h
i
j
k
l
h_obs
h_YAN
h_Simulate
Sub_Obs
Hydraulic head (m)
Land Subsidence (cm)
Time
8/11/1987
7/24/1998
7/6/2009
5/25/1979
5/7/1990
4/19/2001
4/1/2012

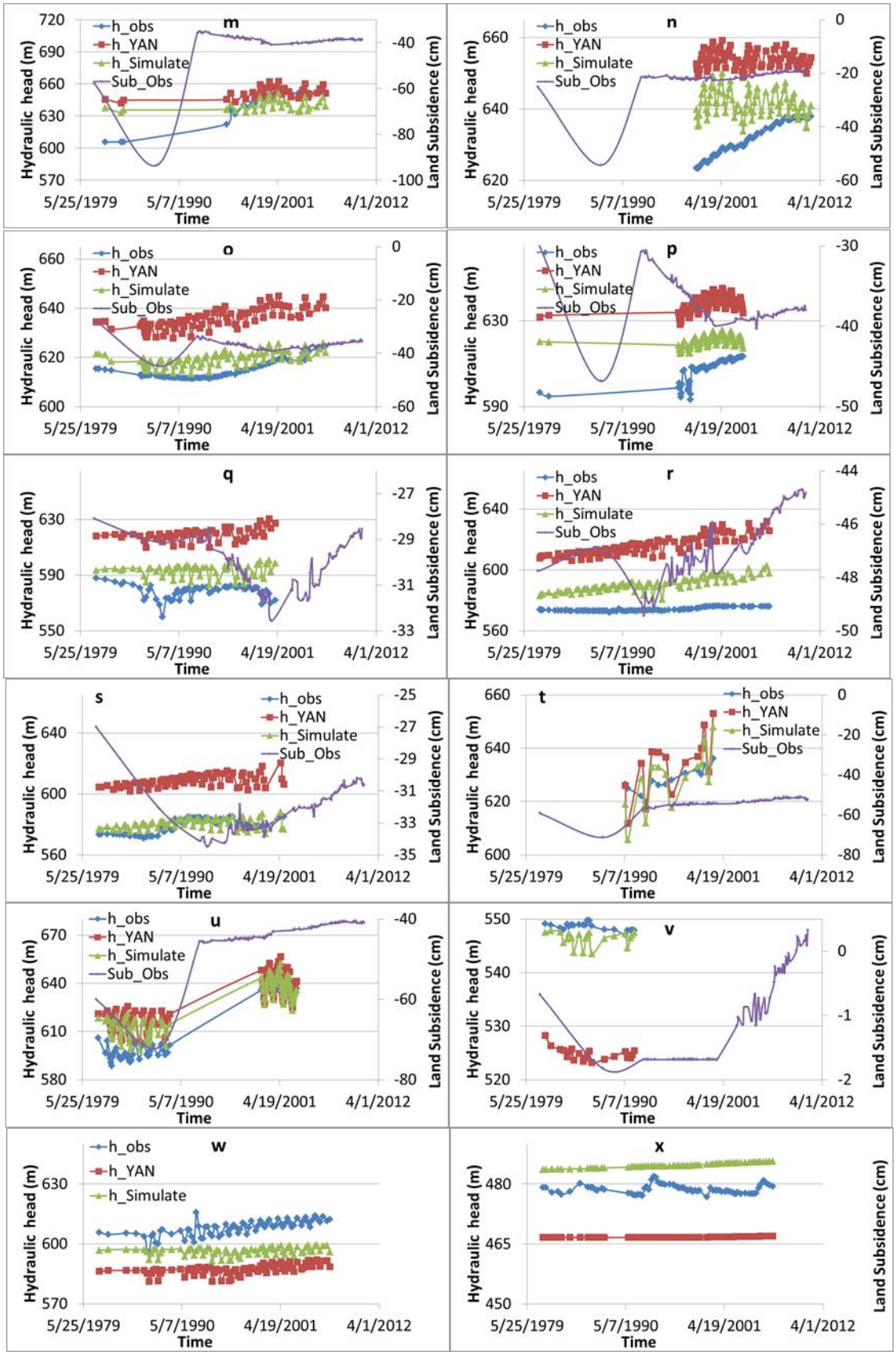
m
h_obs
h_YAN
h_Simulate
Sub_Obs
Hydraulic head (m)
Land Subsidence (cm)
Time
5/25/1979
5/7/1990
4/19/2001
4/1/2012
n
o
p
q
r
s
t
u
v
w
x

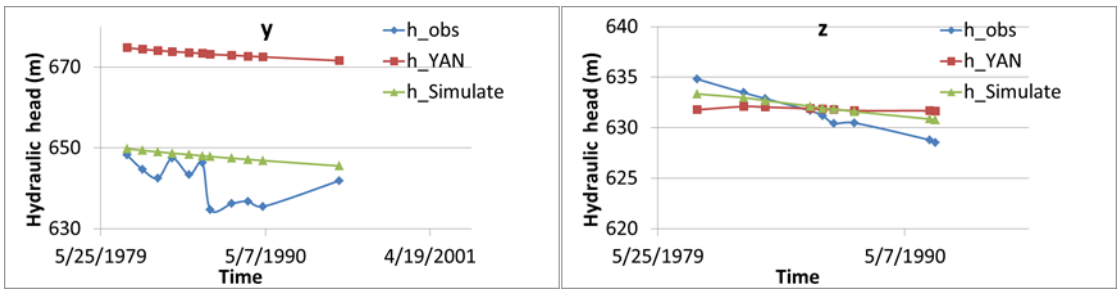

Figure 40. Observed subsidence data and observed hydraulic heads vs. simulated hydraulic heads at sites a-z.

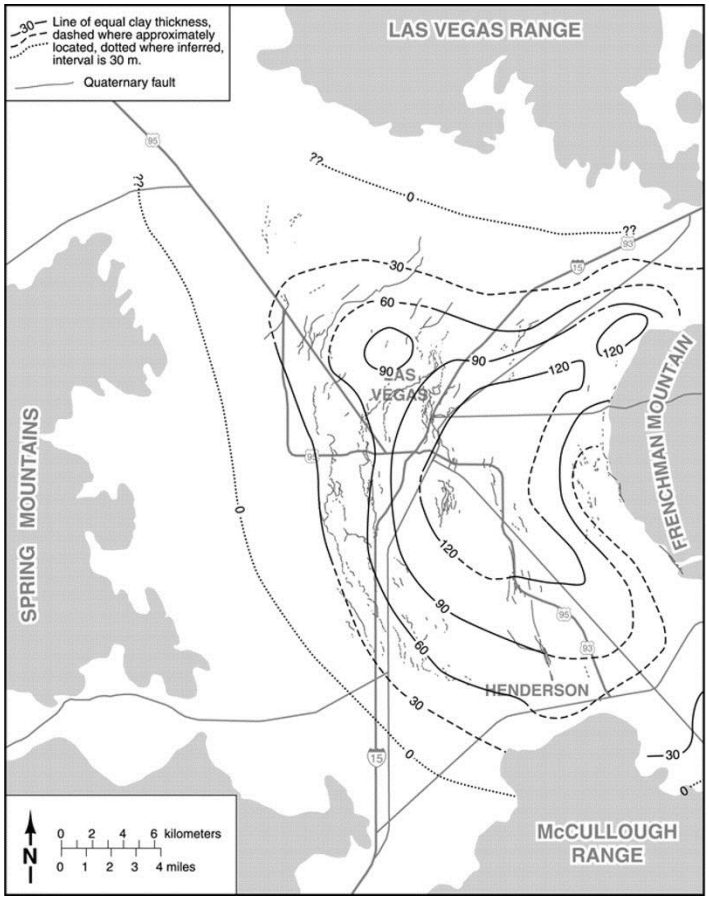

Figure 41. Total clay thickness defined as total interbed thickness (compressible of clay deposits) in the principal aquifer of Las Vegas Valley (from (Morgan and Dettinger 1994).

4.4. Updated Las Vegas Valley Model

4.4.1. Forward Model

Transmissivities and elastic and inelastic skeletal storage coefficients of Las Vegas Valley have been calibrated at the basin scale using temporal PS-InSAR data to evaluate the influence that faults and clay thicknesses have on land subsidence. To accomplish this, we have successfully extended a previous version of the Las Vegas Valley model to year 2012 using MODFLOW-2005 (Harbaugh 2005) with the subsidence (SUB) (Hoffmann, Leake et al. 2003) and horizontal flow barrier (HFB)(Hsieh and Freckleton 1993) packages while implementing a 600m × 600m grid cell size (Figure 42a). A total of 87 stress periods are used to simulate the flow and subsidence in the new model that extends from March 1912 to October 2010. The new conceptual model consists of four model layers: Layers 1 and 2 represent the near-surface aquifers; layer 3 represents the developed-zone aquifer for which aquifer parameters are calibrated, and layer 4 represents the deep-zone aquifer (Figure 42c). Nearly all of the groundwater supply in the valley comes from the developed-zone (or principal) aquifer, which is 200-300m below the land surface (Maxey and Jameson 1948, Morgan and Dettinger 1994). Only the developed-zone (or principal) aquifer is pumped for groundwater. All four layers are assumed to be confined aquifers.

(a)

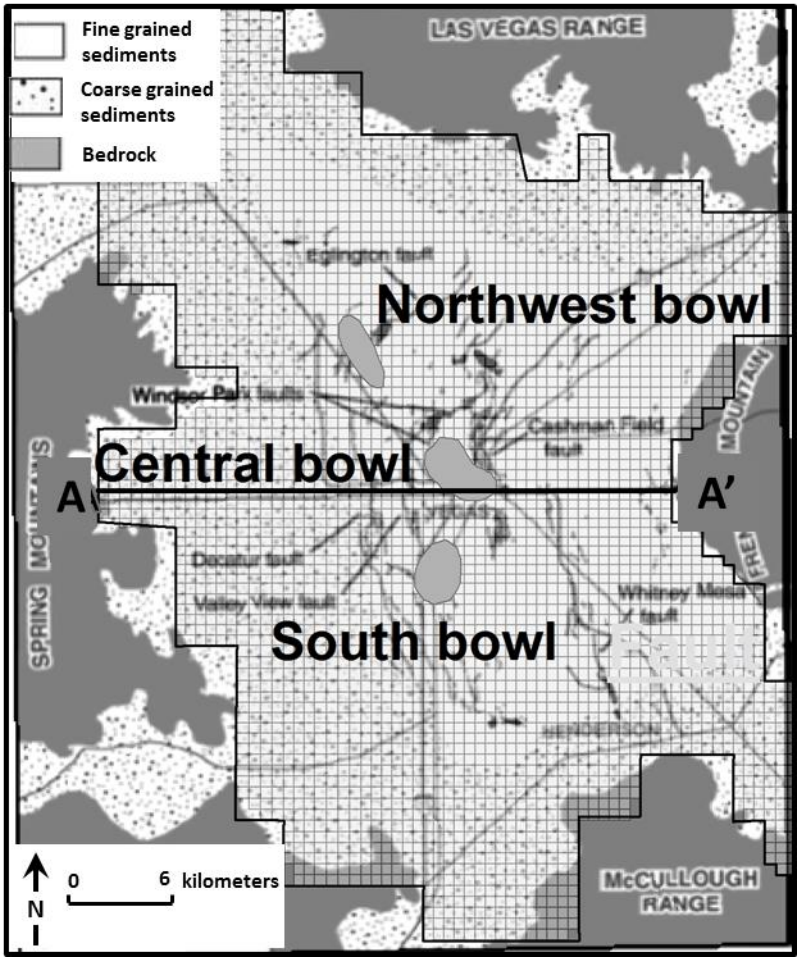
Fine grained sediments
Coarse grained sediments
Bedrock
LAS VEGAS RANGE
Northwest bowl
Central bowl
South bowl
A
A'
SPRING MOUNTAINS
MOUNTAIN
FRE
McCULLOUGH RANGE
0
6 kilometers
N

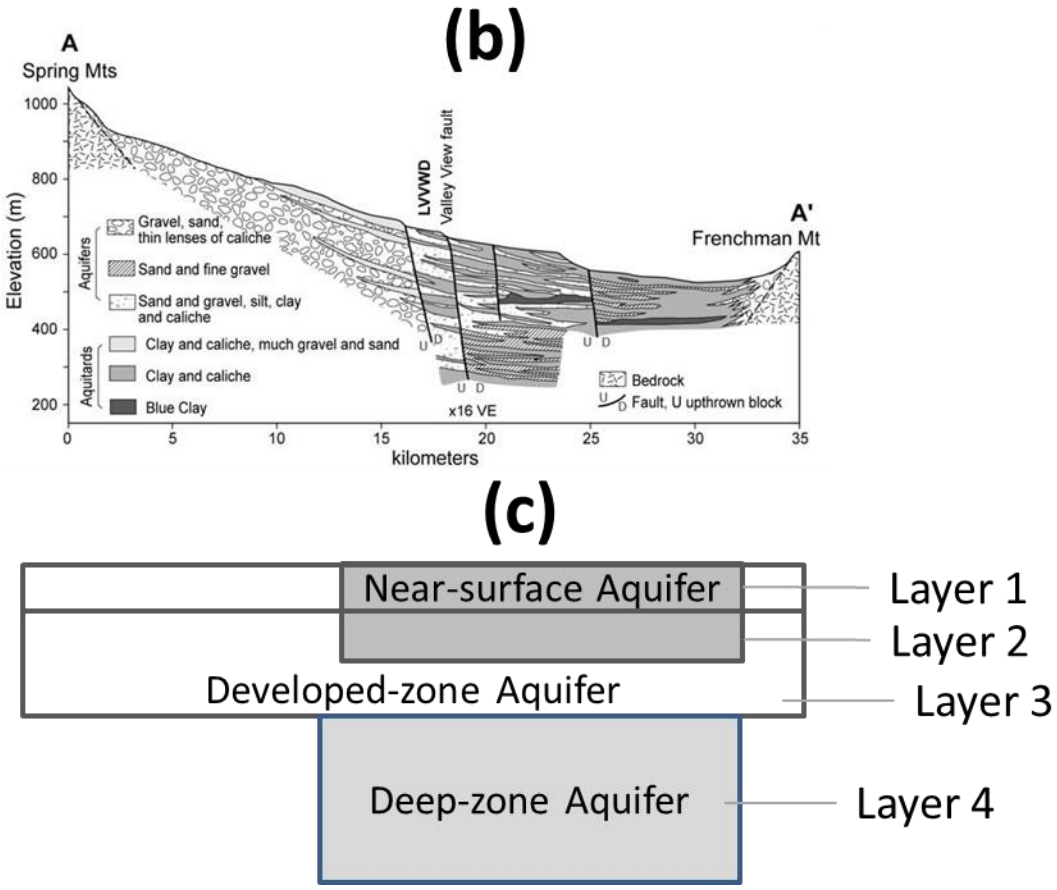

Figure 42 (a) Generalized surficial geologic map of Las Vegas Valley showing distribution of coarse- and fine-grained deposits, and principal Quaternary faults and fissures. (b) geologic cross-section (A-A') as modified from Bell, Amelung et al. (2002) that schematically illustrates the stratigraphy and fault relations interpreted from well log data (Bell, Amelung et al. 2002). (c) conceptual numerical model for the basin.

4.4.2. Observations

Groundwater hydraulic head measurements covering the entire simulation history (Figure 39) and high spatial and temporal land subsidence measurements from InSAR (1990-2010) are invoked in this study. Although the spatial resolution of the InSAR data is 40m, we use a 600m (which is the size of the model grid cells) modeling grid network for this investigation. Only one InSAR data point is selected randomly to represent the

observational subsidence value of each model grid cell. This method of selection is not considered to be problematic because of the generally smooth transition in land subsidence that occurs over the area of one model cell.

4.4.3. Parameters

The key parameters that are calibrated and that are believed to most affect land subsidence and hydraulic head data are transmissivities (T), elastic and inelastic skeletal storage coefficients (S_{ke} and S_{kv}) of layer 3 (the developed-zone aquifer) and the conductance (CR) of the faults (horizontal-flow barrier). The principal aquifer is responsible for transmitting significant quantities of ground water (Maxey and Jameson 1948, Malmberg 1965, Harrill 1976, Morgan and Dettinger 1994) and contributing to virtually all of the observed land subsidence. Seventy-two T parameters, and six S_{ke} and S_{kv} parameters were considered in Yan's model (Yan 2007), which are treated as initial estimates of both zones and parameters of layer 3 in our study. The zones and parameters of the other layers are kept the same as Yan's model (Yan 2007) and are not believed to have significant bearing on the overall simulated water levels or subsidence of the basin.

4.4.4. Inversion Method

The adaptive multi-scale algorithm, which provides criteria to reconstruct the zones by refining or coarsening the current zones is applied in this study (Ameur, Chavent et al. 2002). The least-squares objective function is defined as a least-squares misfit to the data with respect to the parameter values. UCODE-2005 (Poeter, Hill et al. 2005) is used to

minimize the weighted least-squares objective function using a modified Gauss-Newton method. The weighted least-squares objective function can be written as:

$$J(\alpha) = \sum_{i=1}^{ND} \omega_i [y_{obs(i)} - y_i(\alpha)]^2 + \sum_{p=1}^{NPR} \omega_p [P_{prior(p)} - P_p(\alpha)]^2 \qquad (1)$$

where,

$$\alpha = (T, S_{ke}, S_{kv}, CR) \qquad (2)$$

and represents the parameter vector to be optimized: ND is the number of observations, NPR is the number of prior information values, ω_i is the weight for the i^{th} observation, ω_p is the weight for the p^{th} prior estimate, $y_{obs(i)}$ represents the i^{th} observation, $y_i(\alpha)$ represents the simulated value which corresponds to the i^{th} observation, $P_{prior(p)}$ represents the p^{th} prior estimate, $P_p(\alpha)$ represents the p^{th} simulated value.

Prior information is used for parameters T and S_{ke} and S_{kv} on the basis of the T and S_{ke} and S_{kv} distribution map provided by Morgan and Dettinger (Morgan and Dettinger 1994). The parameters are log transformed. We assume that the standard deviation is 0.349, which is used to weight the prior information. The approximate reasonable range of values for the parameters is between one fifth to five times the values provided by Morgan and Dettinger (1994) with a 95% probability. The convergence criterion is set to 0.01, which means that the regression converges if the relative change of the objective function is less than 0.01 for three sequential iterations or the fractional change for all parameters is less than 0.01 for all parameters.

If parameters have composite scaled sensitivities (CSS) that are less than about 0.01 times the largest CSS, it is likely that the regression will not converge (Hill, 1998; Anderman and others, 1996), so when minimizing the objective function using UCODE-

2005, we choose to omit those parameters that have CSS lower than 0.01. The parameter nonuniqueness can be detected using parameter correlation coefficients (PCC). Parameters with PCC's larger than 0.85 will be omitted due to their nonuniquness (Foglia, Hill et al. 2009).

4.5. Results

4.5.1. Calibrated Transmissivity Zones and Values

Transmissivities (*T*) of layer 3 are calibrated at the basin scale. Seventy-two *T* parameters described in Yan's model (Yan 2007) are shown in Figure 43a. The parameter estimation problem is solved through 15 iterations of successive approximations by refining the zone domains (especially zone E and zone S in the eastern part of the basin) during the inverse procedure. The final zone distributions and zone values are shown in Figure 43b. Most zones have similar T values as that from Yan (2007), except at zones C, E and S (Figure 44). Coarser-grained alluvial deposits are known to occur near point A' (Figure 42b) and in the southern part of the basin (Figure 42a), which may explain the higher simulated T values for zones E and S. The sensitivity analysis shows that all parameters have CSS values larger than 0.021 times the largest CSS (Figure 44), indicating that the model and the observed data provide sufficient information to estimate the parameters. A PCC analysis shows that no parameter has a correlation coefficient larger than 0.60, which indicates that the estimated parameters are unique given the information provided by the observations.

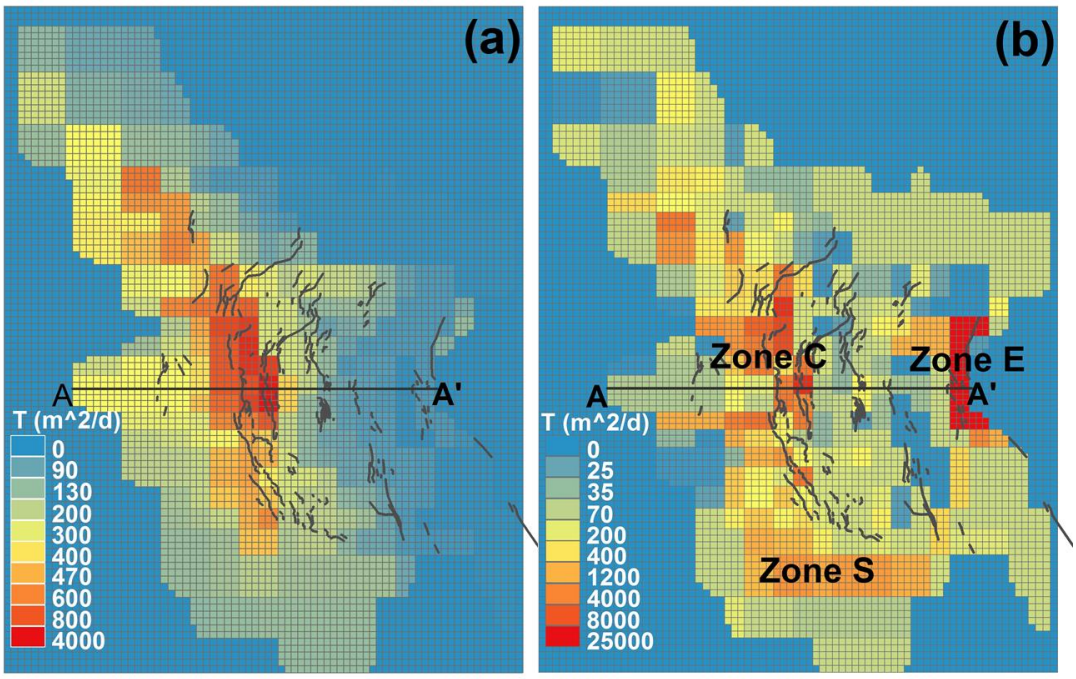

Figure 43 Transmissivity zones and values from Yan (2007); (b) transmissivity zones and values calibrated with DREAM MCMC.

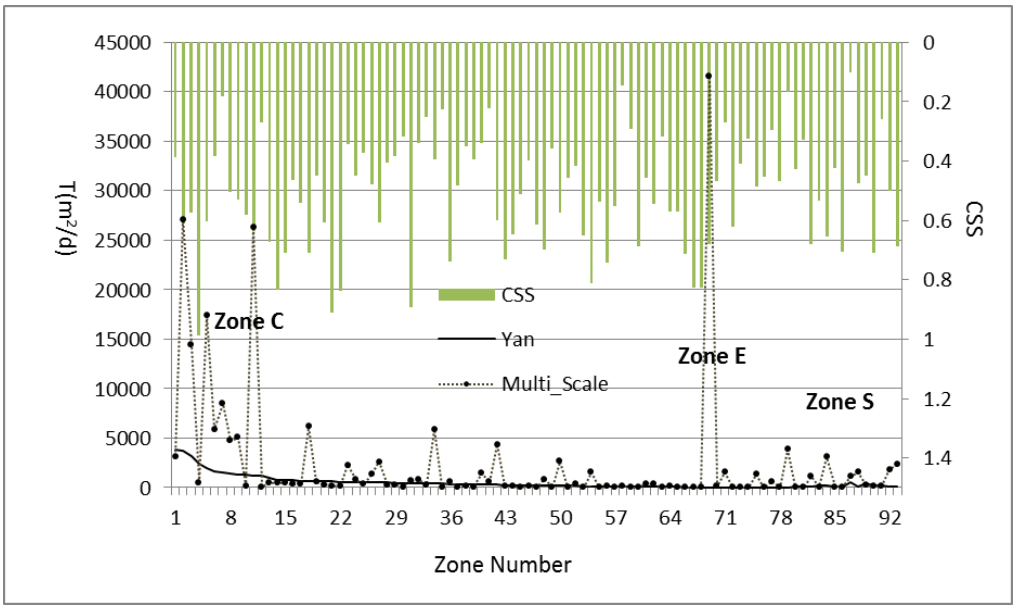

Figure 44 A comparison between transmissivity values from Yan (2007) and calibrated with the multi-scale strategy. Zones C, E and S are shown in Figure 43. CSS represents the composite scaled sensitivities.

4.5.2. Calibrated Ske and Skv Zones and Values

The parameters S_{ke} and S_{kv} of layer 3 are calibrated at the basin scale using the multi-scale strategy. Six pairs of S_{ke} and S_{kv} parameters described in Yan's model (Yan 2007) are shown in Figure 45a. The S_{ke} and S_{kv} parameters that Yan used are from Morgan and Dettinger (1994) (Figure 41). The interbed thicknesses that are used to calculate S_{ke} and S_{kv} are inferred for many locations within the basin where data are limited, especially in the northwest part of the basin (Morgan and Dettinger 1994), where the Eglington fault is located, hence, in order to obtain a better model fit, reconstructing S_{ke} and S_{kv} zones and calibrating parameter values based on actual hydrogeological conditions is preferred. The parameter estimation problem is solved through five iterations of successive approximations by refining or coarsening the zone domains (especially in the northwest part of the basin where initial estimates were largely unknown) during the inverse procedure.

The final calibrated zone distributions and values are shown in Figure 45b. Calibrated S_{ke} and S_{kv} values are lower than those calibrated by Yan, except on the upthrown block of the Eglington fault, where we believe a thicker interbed (clay) may occur. Donovan (1996) and Bell (2002) inferred that aquifer and aquitard thickness and elastic storage coefficients are generally uniform across the Eglington fault, however, the data they collected are from two cross sections, which are constructed beyond the large interbed

thickness area that we inferred. It can be seen from Figure 45 that the Eglington fault may separate more compressible deposits to the northwest from less compressible deposits to the southeast, although the compressible deposits do not extend entirely through the upthrown block. Sensitivity analysis shows that all parameters have CSS values larger than 0.11 times the largest CSS with S_{kv} exhibiting the largest CSS, which suggests this parameter is highly sensitive to the observations and important in the calibration process. A PCC analysis shows that no parameter has correlation coefficients larger than 0.6, indicating that the estimated parameters are unique and relatively unaffected by the model given the information provided by the observations.

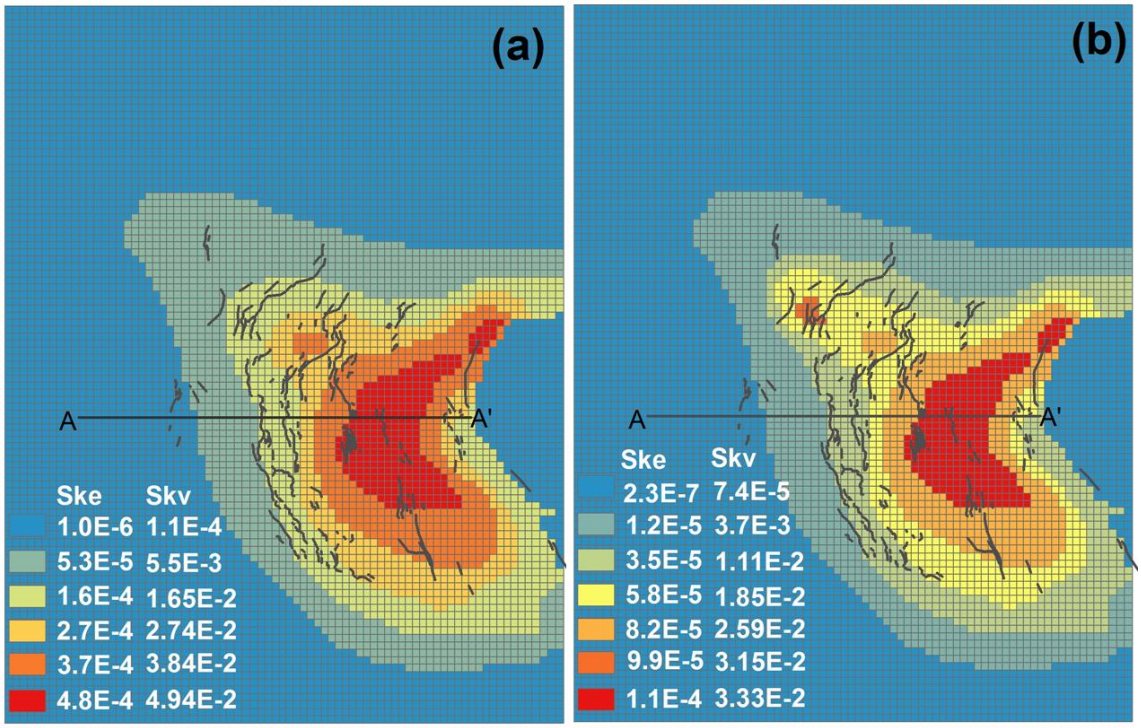

Figure 45. Elastic and inelastic skeletal storage coefficient zones and values (a) from Yan (2007); (b) calibrated with the adaptive multi-scale strategy for this study.

4.5.3. Calibrated Conductance of the Fracture (Horizontal-Flow Barrier)

In order to evaluate the conductance values near the Eglington fault, eight HFB zones are set at the upthrown block of the Eglington fault (Figure 46).

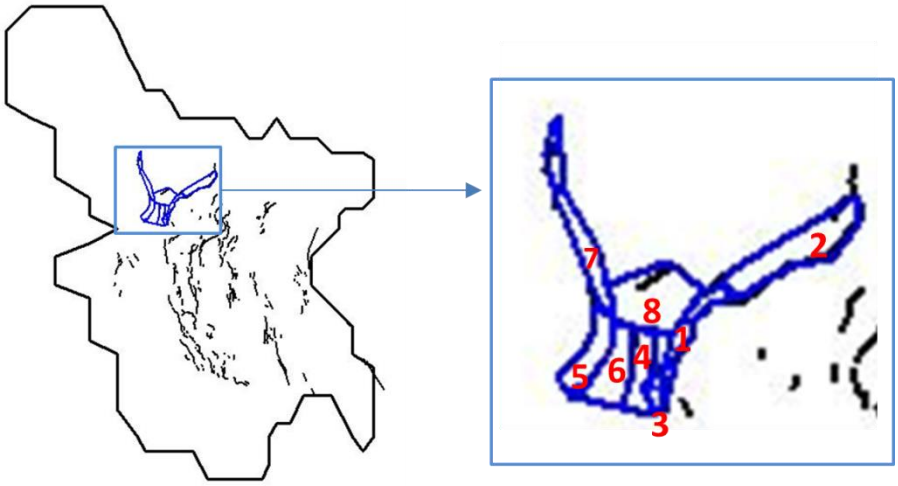

Figure 46. HFB zones used for the Northwest subsidence bowl region.

Calibrated conductance values are shown in **Error! Reference source not found.**. Zone2 nd zone8 have the highest conductance values, and zone5 and zone7 have the lowest conductance values. If the barrier width is assumed to be 100m, the approximate magnitude of *T* for zone 2 and 8 is $10^2 m^2$/day; the approximate magnitude of *T* for zones1, , and 6 is $10^1 m^2$/day; and the approximate magnitude of *T* for zones 5 and is $10^0 m^2$/day, which implies that a conductance barrier may exist at this locality. However, groundwater levels in wells a-e, m and n do not show appreciable changes (Figure 40), so the influence of the conductance barrier to this arear is not significant.

Table 3 Conductance values for the eight HFB zones shown in Figure 46.

HFB zone	Conductance (m^2/day)
1	5.02E-02
2	0.1344
3	1.72E-02

4	8.51E-02
5	5.52E-03
6	9.14E-02
7	8.37E-03
8	0.134

4.5.4. Calibrated Groundwater Levels and Land Subsidence

The final calibrated T, S_{ke} ,S_{kv} and CR values are used to calculate simulated hydraulic heads and basin-wide land subsidence.

Simulated groundwater levels are shown in Figure 40 and Figure 47. It can be seen from Figure 40 that the calibrated model produces a better model fit than Yan's model. The Nash-Sutcliffe efficiency index (NS) (Nash and Sutcliffe 1970), mass balance error (m) and the Schulz criterion (D) (Schulz, Beven et al. 1999) are used to evaluate model fit. NS, m and D are commonly used in evaluating hydrogeologic models. A quantitative assessment of the model fit is listed in

Table 4. Equivalent qualitative assessments associated with NS and D values are listed in Table 5. When the simulated values match the observations, m=0. When m>0 this indicates that the simulated values are, on average, greater than the observed values,

while for the case when $m<0$ the simulated values are, on average, lower than the observed values.

The *NS* criteria indicates that the fit between the simulated and observed hydraulic head is excellent; The *m* criteria indicates that on average, the simulated hydraulic heads are larger than the observed heads; The *D* criteria indicates that the model fit is very good.

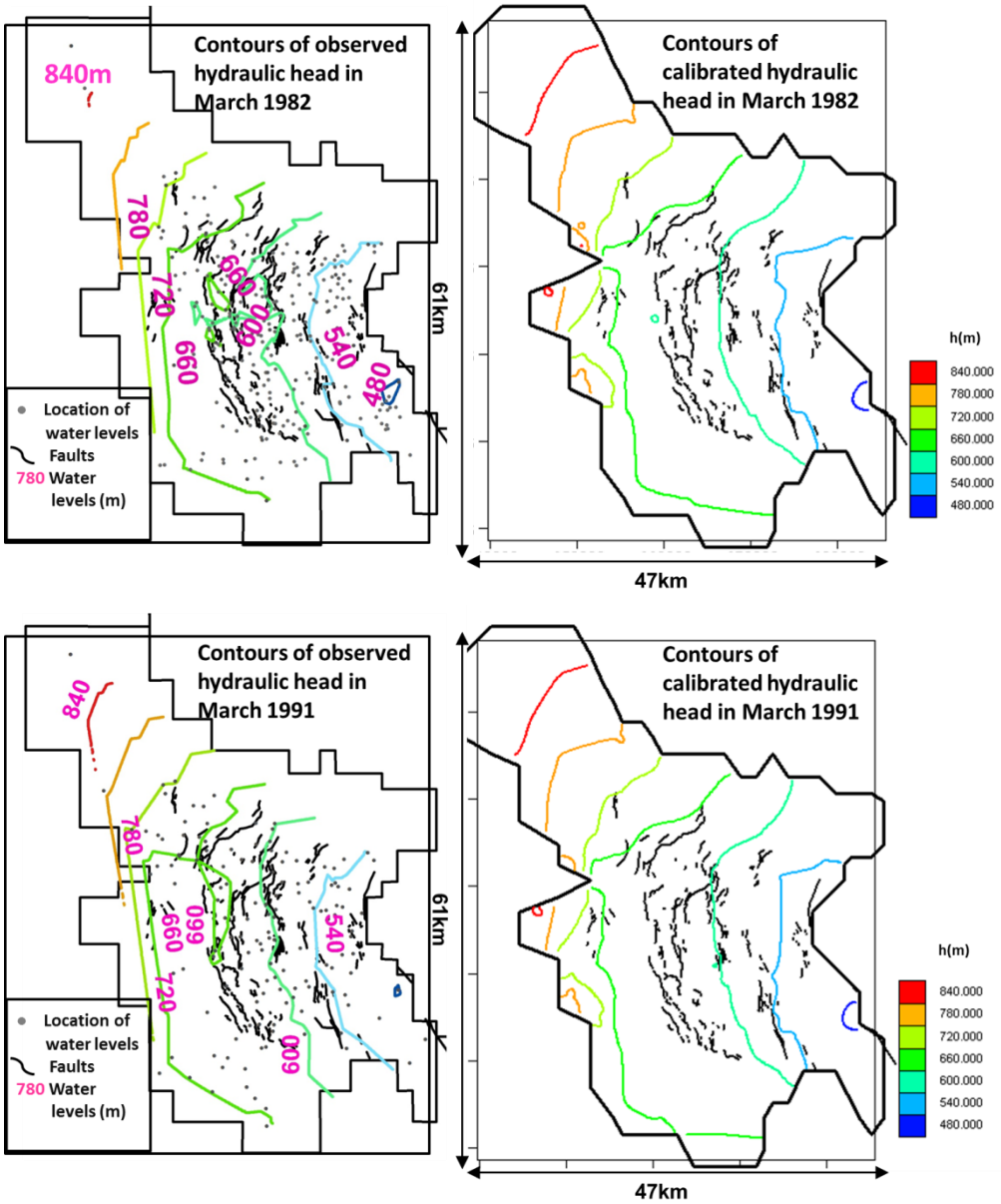

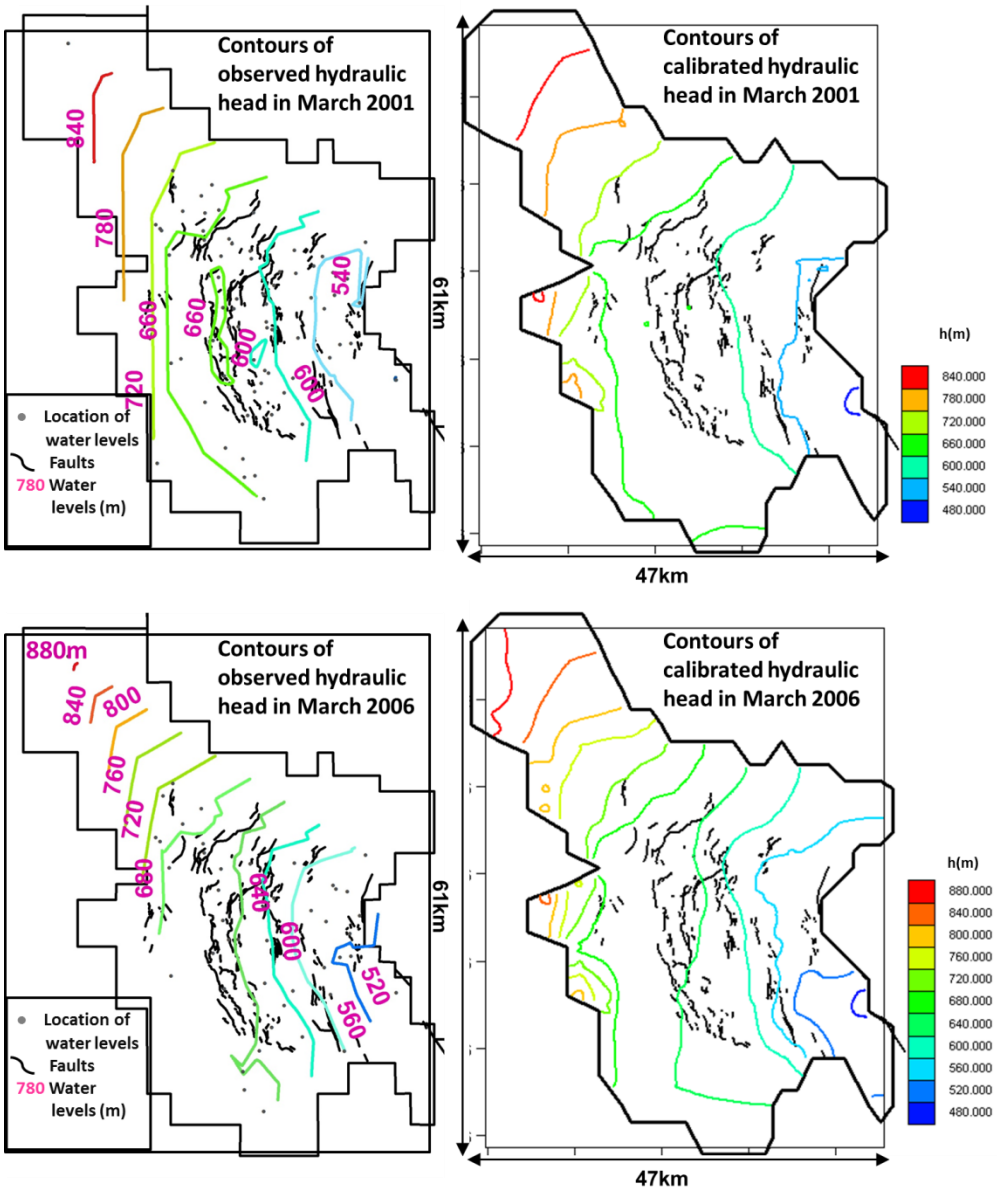

Figure 47. Contours of observed vs. simulated hydraulic heads for years 1982, 1991, 2001 and 2006

Table 4. Measures of model fita between observed and simulated hydraulic heads and land subsidence.

	Hydraulic head	Subsidence (1987)	Subsidence (2000)
NS	0.946	0.734	0.633
m	0.385	6.514	24.528
D	1.897	1.016	0.830

[a] NS is the Nash-Sutcliffe efficiency index; m is the mass balance error; D is the Schulz criterion; s is the quantitative measure of overall model fit to the weighted observations.

Table 5. Correspondence between the Nash-Sutcliffe and Schultz Indices and model performance.

Fit	*NS*	*D*
Excellent	>0.8	
Very good	0.6-0.8	0.0-3.0
Good	0.4-0.6	3.0-10.0
Sufficient	0.2-0.4	10.0-18.0
Insufficient	<0.2	>18.0

Simulated land subsidence is shown in Figure 48, which shows a similar pattern as Figure 44 developed by Bell (2002) based on observed values, except in the eastern part of the basin where larger subsidence values are obtained with our model. A quantitative assessment of the model fit is listed in

Table 4. The *NS* criteria indicates that the fit between the simulated and observed land subsidence is very good; The *m* criteria indicates that on average that the simulated subsidence values are larger than the observed subsidence values; The *D* criteria indicates that the fit is very good.

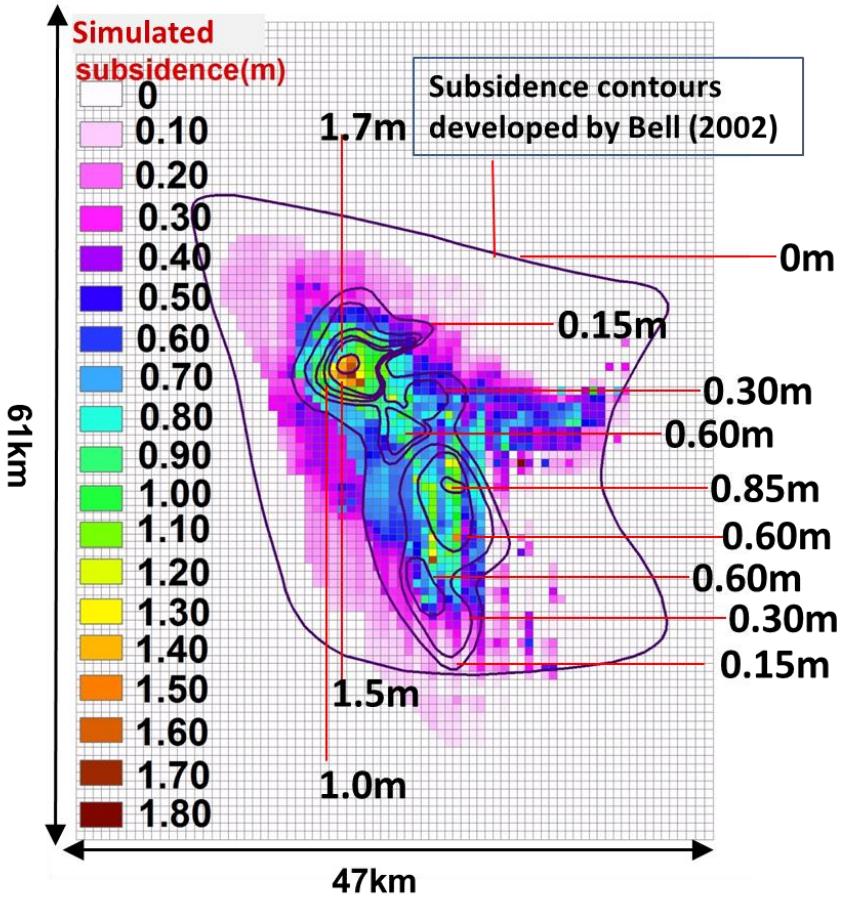

Figure 48. Subsidence map developed by Bell (2002) vs. simulated total subsidence for years 1912-2000 using the calibrated parameter values.

4.5.5. Land Subsidence and Groundwater Level Prediction

One of the goals of this investigation is to use the calibrated parameters to investigate future trends of land subsidence in Las Vegas Valley by extending the simulation period of the developed calibration model to year 2030. The total annual pumping rate, artificial recharge rate, natural recharge rate and natural discharge rate for years 2011 to 2030 are assumed to be 9.00×10^7 m^3/year , 3.99×10^7 m^3/year, 3.61×10^7 m^3/year and 2.32×10^6 m^3/year, respectively. These rates are identical to the average annual measured rates between 1990 and 2010.The quantity of secondary recharge is closely related to land use and is influenced by urban growth and importation of surface water from Lake Mead since 1972. The secondary recharge rate has increased considerably since 1972 (Morgan and Dettinger 1994). We assume a secondary recharge growth rate of 1.23×10^6 m^3/year (Figure 49). The predicted locations of pumping and recharge remain the same as current patterns.

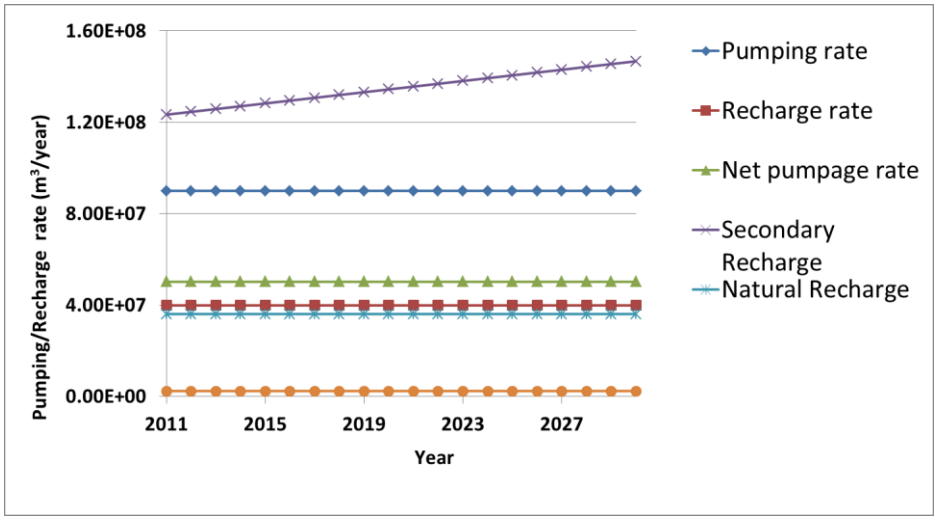

Figure 49. Total predicted groundwater pumping and recharge rates for the period 2011 through 2030.

Figure 50a shows the map of predicted groundwater levelschanges in Las Vegas Valley between 2011 and 2030. Groundwater levels have generally recovered, with the maximum water-level recovery reaching approximately 50 m for this area. Figure 50a exhibits the same pattern as Figure 31b, which shows the groundwater levels change for the period from 1990 to 2005. Groundwater levels in the Northwest subsidence bowl have also increased during this 20-year prediction period (Figure 50a and Figure 51). Figure 52a shows the map of predicted subsidence in Las Vegas Valley for the period from 2011 to 2030. Virtually all of the predicted subsidence occurs in the northwest portion of the Las Vegas basin. The Northwest subsidence bowl experiences a maximum subsidence of 11.3 cm during this 20-year prediction period, suggesting that residual compaction from slowly draining clay interbeds will continue into the future in this region of the basin. Conversely, the North and Central bowls will undergo a net uplift of approximate 0.4cm.

In order to mitigate the continued subsidence problems occurring in the Northwest subsidence bowl, we propose three design strategies (Table 6). The well site W1 located in the Northwest subsidence bowl (Figure 50b) pumps groundwater at a rate of 3.15×10^6 m3/year in 2010. In strategy 1, we move this pumping well to site W2beginning in 2011, but all the other pumping conditions remain unchanged. No significant prior subsidence has occurred at site W2, due to the lack of a thick clay interbed at this locality. Simulation results for strategy 1 are shown in Figure 50b, Figure 51, and Figure 52b, and indicate that the groundwater levels have significantly recovered in the Northwest bowl and the maximum subsidence rate is reduced so that the maximum total

subsidence for this 20-year prediction period is only 9.93cm. However, at the same time, the increase of groundwater levels at site W2 are not as great as in Figure 50a, although no subsidence occurs at this locality between 2011 and 2030.

In strategy 2, a rectangular recharge area R1 is implemented over a portion of the Northwest subsidence bowl and given a recharge rate of 4.07×10^6 m^3/year. Simulation results show that the groundwater level recovery at site h1 increases by 14m and the maximum subsidence decreases to 6.3 cm in the Northwest bowl (Figure 51 and Figure 52c). This result indicates that the rectangular recharge area R1 more greatly influences the hydrodynamics of the system than W1 and more effectively mitigates land subsidence. Strategy 3 represents a combination of strategies 1 and 2, where the pumping is moved from site W1 to site W2and R1 actively recharges groundwater. In strategy 3 the maximum subsidence is similar to that of strategy 2, but in the northwest part of the bowl subsidence has been largely mitigated Figure 52d. At the same time, recovery of groundwater levels at site h1 have reached 15m (Figure 51), but due to the large amount of pumping at site W2, groundwater levels at this site have not recovered as in strategy 2 (Figure 50d).

These proposed strategies show that it will be difficult to completely mitigate subsidence in the Northwest subsidence bowl, even when significant measures are taken to reduce subsidence. This is largely the result of slowly draining thick interbeds that likely have a very long time constant for complete compaction. Thus, even if water levels recover, the interbeds appear to continue to release water from overpressurization from past stress conditions.

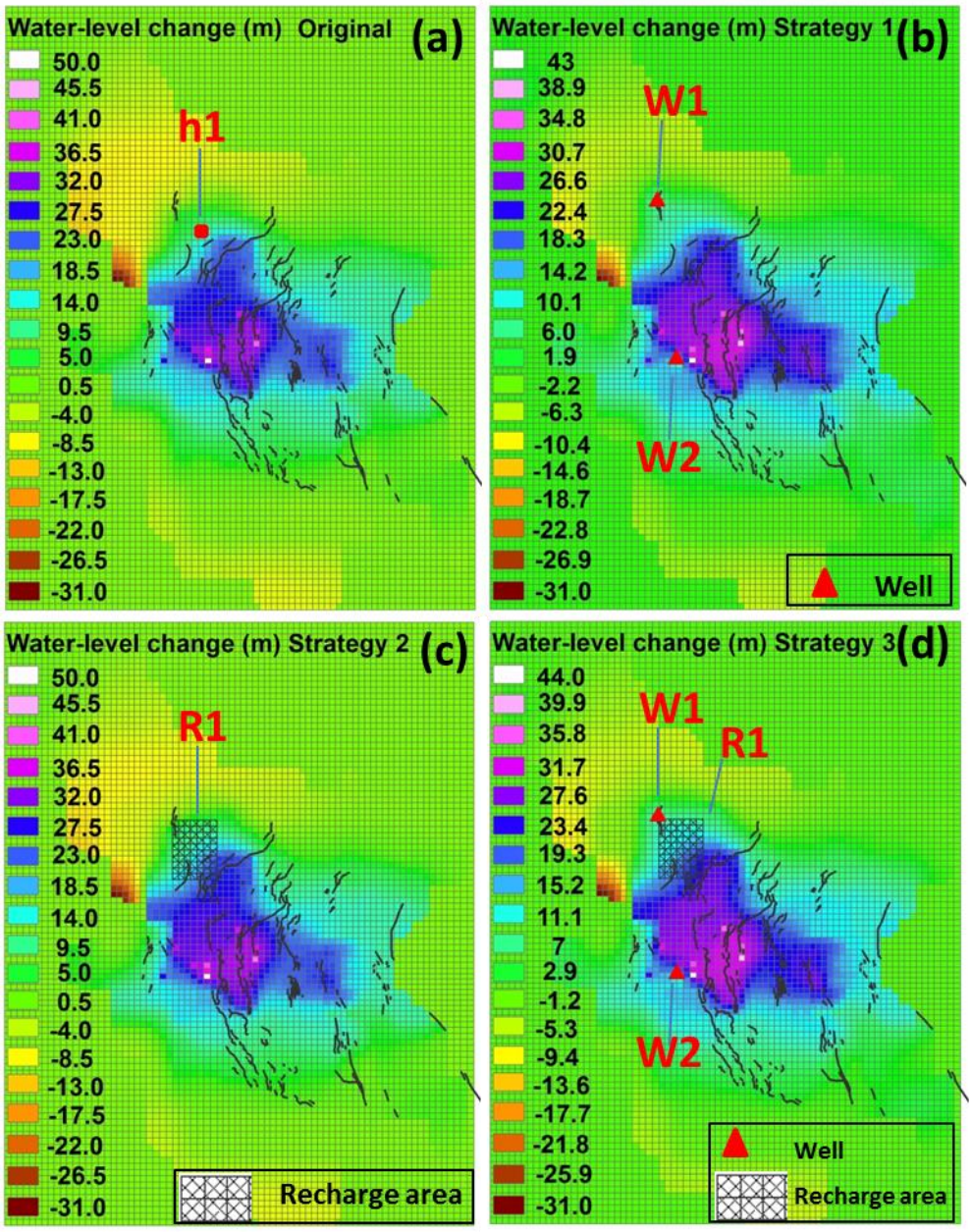

Figure 50. Predicted groundwater-level changes in Las Vegas Valley between years 2011 and 2030.

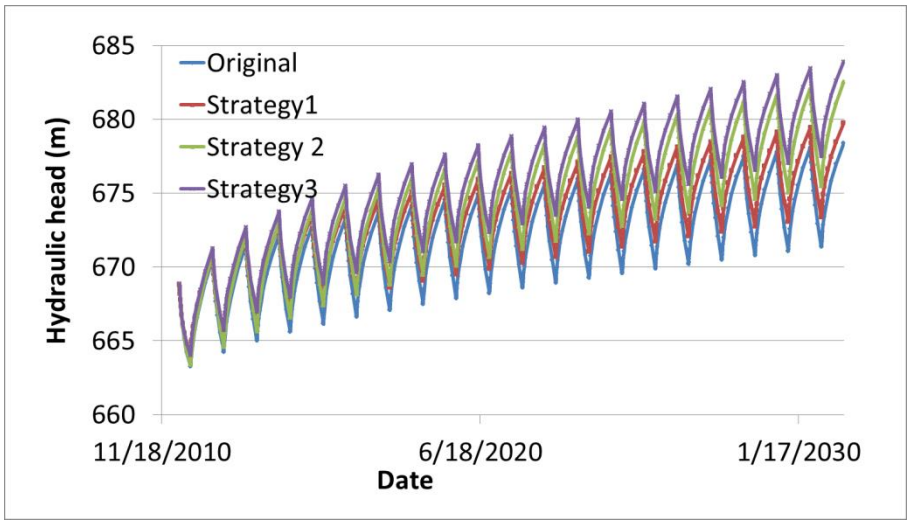

Figure 51. Simulated hydraulic heads at site h1 for the three strategies.

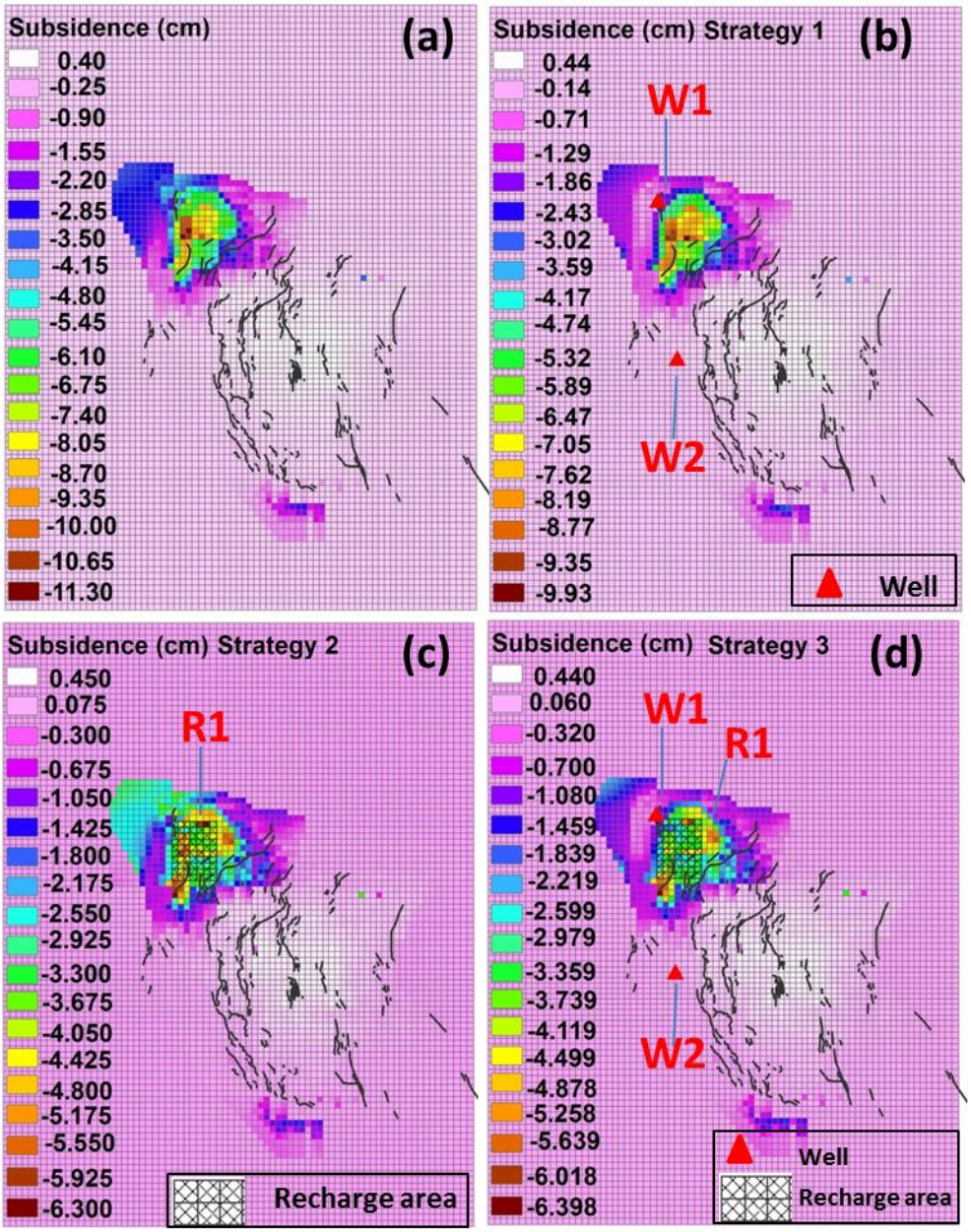

Figure 52. Predicted subsidence in Las Vegas Valley between years 2011 and 2030.

Table 6 Proposed strategies for mitigating land subsidence in the NW portion of Las Vegas Valley.

	Point well W1(m^3/year)	Point well W2(m^3/year)	Recharge Area R1(m^3/year)
Original	-3.15E+06	0	0
Strategy 1	0	-3.15E+06	0
Strategy 2	-3.15E+06	0	4.07E+06
Strategy 3	0	-3.15E+06	4.07E+06

4.6. Discussion

4.6.1. New Spatial Patterns Revealed by InSAR Measurements (2002-2010)

InSAR measurements from 2002 to 2010 reveal four uplift areas (area 1-4) and two subsidence bowls (area 5-6) (Figure 38), which are largely controlled by faults and interbed thickness. In addition, seasonal land deformation responses to pumping and artificial recharge are lower than in previous years. This could be attributed to the continuing recovery of the groundwater levels. Another reason for smaller variations in the seasonal change of subsidence is due to the processing of the InSAR data that involves an averaging technique to remove tropospheric errors has resulted in the elimination of the seasonality in the data set. If more acquisitions become available and the time gap becomes shorter and distributed more evenly, the seasonality of the data will become more pronounced. Furthermore, if the seasonality of the data were retained or brought back by new processing techniques, more accurate elastic skeletal storage coefficients could be obtained.

4.6.2. Parameter Estimation

The parameters T, S_{ke} *and* S_{kv} of the developed zone aquifer (principal aquifer, layer 3) are calibrated for Las Vegas Valley at the basin scale. Calibrated T, S_{ke} and S_{kv} zones and values reflect more realistically the hydrogeological conditions of the basin. The calibrated S_{ke} and S_{kv} zones and values can be used to infer a new interbed thickness map.

The information provided by the high spatial and temporal resolution observations are sufficient to uniquely calibrate all the parameters. S_{kv} exhibits the largest CSS, which suggests that this parameter is highly sensitive to observations and important in the calibration process. The value of S_{kv} depends on the long-term water-level declines and inelastic compaction of the clay interbeds, but a long-term inelastic compression signal resulting from delayed drainage of interbeds may be superimposed on the cyclical subsidence pattern, greatly complicating the parameter estimation process. Detailed monthly InSAR data are used to investigate how the seasonal variations in water levels are reflected in subsidence and rebound patterns. These elastic stress-strain signals are used to estimate the S_{ke}, which depends more heavily on the seasonal response of the clay interbeds. However, part of the seasonality of the InSAR data is eliminated during the process of removing the tropospheric errors. The absence of the seasonality can influence the accuracy of estimating S_{ke}. It should be noted that the seasonality is retained in the 1992-2000 InSAR data set (Bell, Amelung et al. 2008) and therefore contains more information than the 2002-2010 data set. However, both the InSAR data from 1992-2000 and from 2002-2010 are involved in the calibration process.

4.6.3. The Influence of the Fault

The influence of the Eglington fault is investigated in this study. On the upthrown block of the Eglington fault, calibrated S_{ke} and S_{kv} values are higher than those from Yan, so we infer that thicker interbeds (clay) may exist at this locality and may represent the primary factor controlling the formation of the Northwest subsidence bowl. The area that is calibrated to have a thicker interbed is quite small, and apparently falls just outside the

cross-sectional reconstruction by Donovan (1996) and Bell (2002). The high spatial subsidence observations from InSAR are quite critical for calibrating the small scale variation of the interbed compressibility. In this study, only the S_{ke} and S_{kv} zones in the northwest part of basin are reconstructed using the adaptive multi-scale method, so we infer that the Eglington fault acts to separate more compressible deposits to the northwest from less compressible deposits to the southeast. . Calibrated *CR* values indicate that a conductance barrier may exist along the upthrown block of the Eglington fault, just as suggested by Bell (2002) who implied that fault gouge or secondary carbonate cementation of the fault zone may exist, or perhaps some other mineralization may be occurring along the fault to cause it to act as a subsidence barrier. However, no significant hydraulic head discontinuity exists across the fault (Figure 40a-e, m and n, Figure 47), indicating that the influence of the fault as a hydraulic barrier may not be significant. A further study is required to investigate the potential role of other faults on influencing clay thicknesses, subsidence and hydraulic conductance.

4.6.4. Correlation between Subsidence, Fault Location, Hydraulic Head Change, Pumping Rate and Interbed Thickness

The subsidence history of Las Vegas Valley (Figure 34) and the spatial patterns revealed by InSAR measurements (Figure 38) suggests a complex spatial and temporal correlation between fault location, hydraulic head change, pumping/recharge rate and interbed thickness.

Four main subsidence bowls (Northwest, North Las Vegas, Central and Southern bowls) are bounded by Quaternary faults and are significantly offset from the center of artificial

recharge (Figure 38) and center of pumping (Figure 33). The Northwest bowl, which is located not far from the pumping/recharge center (Figure 33c), is controlled by the Eglington fault, which separates more compressible deposits to the northwest from less compressible deposits to the southeast (Figure 45b), and the fault may act as a barrier, although the influence of the fault as a hydraulic barrier to is not significant. Although the maximum water level recovery for the Northwest bowl has reached 30m since 1990s (Figure 40a-b), land subsidence has not ceased.

The North bowl located not far from the pumping/recharge center has recently undergone land uplift and hydraulic head recovery (Figure 38, Figure 40m-p). At the Central and Southern bowls, groundwater levels have generally recovered (Figure 40f-h), so the occurrence of land subsidence suggests the existence of residual compaction as a result of slowly draining clay interbeds.

The lack of significant subsidence/uplift at or near the center of active pumping/recharge could be explained by the absence of thick clay interbeds (Figure 33c, Figure 38, and Figure 41). The interbed thickness is large in the eastern part of the valley (Figure 41). The lack of significant subsidence in this area can be explained by the general lack of appreciable water level decline (Figure 40i-l) and by the fact that it juxtaposes a bedrock boundary.

4.6.5. Prediction Model

A management model developed for the period 2011-2030 indicates that residual compaction will continue to occur in the Northwest subsidence bowl. Strategies aimed at mitigating subsidence by moving pumping wells to less compressive areas or assigning a

recharge area to the Northwest subsidence bowl are shown to help mitigate land subsidence by reducing compaction rates. However, moving the pumping well to another site may also influence local groundwater levels, so an appropriate site or sites to install pumping wells should be in areas far away from the current Northwest subsidence bowl, preferably in areas where interbed thicknesses are small.

4.6.6. Model Fit and Limitation

The high spatial and temporal resolution of subsidence observations from InSAR are extremely beneficial for accurately quantifying both elastic and inelastic skeletal specific storage values as well as hydraulic conductivity values, and the model calibration results are far more accurate than when using only water-levels as observations, and just a few random subsidence observations (such as from traditional survey benchmarks and GPS benchmarks).The calibrated model produces a better hydraulic head fit than Yan's model (Figure 40). Calibrated land subsidence (Figure 48) shows a similar pattern as that developed by Bell (2002) (Figure 34), except in the eastern part of the basin where larger simulated subsidence values occur. The lack of significant subsidence in this area can be explained by a lack of water level decline and by the fact that it is located near a bedrock boundary, which could limit the deformation of the aquifer system. Only vertical compaction is considered in this investigation so the influence of the rock boundary on horizontal deformation is not included, but may be a reason why we get larger subsidence values here than observed.

Accurate pumping and recharge distributions are not available, particularly the rates and locations of domestic pumping wells and secondary recharge associated with lawn and golf course watering, which may impact the simulation results.

Even though the current model uses a 600m × 600m grid cell size, which is the finest grid network ever developed for the Las Vegas Valley, it is still coarse compared to the spatial resolution of the subsidence data from InSAR. In addition, subsidence observations from InSAR are extremely beneficial for accurately quantifying hydraulic parameters; however, the groundwater monitoring network is not fine enough (Figure 39) to guarantee amore accurate parameter calibration.

4.7. Conclusions

The key conclusions can be summarized as follows:

1. InSAR measurements from 2002 to 2010 reveal four uplift areas (area 1-4) and two subsidence bowls (area 5-6) (Figure 38), which are controlled by the faults and interbed thickness. Subsidence velocities are currently lower than in 1990s and two new uplift bowls (area 1 and 2) have recently developed (Figure 38). Seasonal land deformation responses to pumping and artificial recharging is less than in 1990s. Residual compaction and delayed drainage of interbeds still exists and may continue to be a problem in certain areas for years to come.
2. Calibrated *T* values that we obtained from the adaptive multi-scale method are similar in magnitude and distribution from those of Yan (2007), except at zones C, E and S, where coarser-grained alluvial deposits are known to exist.

3. Calibrated S_{ke} and S_{kv} values are generally lower than those from Yan (Figure 45), except along the upthrown block of the Eglington fault, where thicker interbed (clay) may exist and is believed to be the primary factor controlling the formation of the Northwest subsidence bowl.
4. Calibrated *CR* values indicate that a conductance barrier may exist along the upthrown block of the Eglington fault, however, the fault is not an effective hydraulic barrier.
5. The high spatial and temporal resolution subsidence observations from InSAR are extremely beneficial for accurately quantifying both elastic and inelastic skeletal specific storage values as well as hydraulic conductivity values, and the model calibration results are far more accurate than when using only water-levels as observations, and just a few random subsidence observations (such as from traditional survey benchmarks and GPS benchmarks).
6. A management model developed for the period 2011-2030 indicates that the residual compaction will still occur in the Northwest subsidence bowl. Investigated strategies suggest that moving pumping wells to less compressive area or assigning a recharge area to the Northwest subsidence bowl region can be effective at mitigating land subsidence.

Reference

Alcolea, A., J. Carrera and A. Medina (2006). "Pilot points method incorporating prior information for solving the groundwater flow inverse problem." Advances in Water Resources **29**(11): 1678-1689.

Amelung, F., D. L. Galloway, J. W. Bell, H. A. Zebker and R. J. Laczniak (1999). "Sensing the ups and downs of Las Vegas: InSAR reveals structural control of land subsidence and aquifer-system deformation." Geology **27**(6): 483-486.

Ameur, H. B., G. Chavent and J. Jaffré (2002). "Refinement and coarsening indicators for adaptive parametrization: application to the estimation of hydraulic transmissivities." Inverse Problems **18**(3): 775.

Ballio, F. and A. Guadagnini (2004). "Convergence assessment of numerical Monte Carlo simulations in groundwater hydrology." Water resources research **40**(4).

Barends, F. B. J., F. J. J. Brouwer, and F. H. Schröder (Eds.) (1995). "Land Subsidence: By Fluid Withdrawal, by Solid Extraction: Theory and Modeling, Environmental Effects and Remedial Measures, Int. Assoc. of Hydrol. Sci., Gentbrugge, Belgium."

Bell, J. W. (1981). Subsidence in Las Vegas Valley, Mackay School of Mines, University of Nevada.

Bell, J. W., F. Amelung, A. Ferretti, M. Bianchi and F. Novali (2008). "Permanent scatterer InSAR reveals seasonal and long-term aquifer-system response to groundwater pumping and artificial recharge." Water Resources Research **44**(2).

Bell, J. W., F. Amelung, A. R. Ramelli and G. Blewitt (2002). "Land subsidence in Las Vegas, Nevada, 1935–2000: New geodetic data show evolution, revised spatial patterns, and reduced rates." Environmental & Engineering Geoscience **8**(3): 155-174.

Beven, K. J., P. J. Smith and J. E. Freer (2008). "So just why would a modeller choose to be incoherent?" Journal of Hydrology **354**(1–4): 15-32.

Burbey, T. J. (1995). Pumpage and Water-level Change in the Principal Aquifer of Las Vegas Valley, Nevada, 1980-90, Nevada Department of Conservation and Natural Resources, Division of Water Resources.

Burbey, T. J. (2001). "Stress-Strain Analyses for Aquifer-System Characterization." Groundwater **39**(1): 128-136.

Carrera, J. and S. P. Neuman (1986). "Estimation of aquifer parameters under transient and steady state conditions: 1. Maximum likelihood method incorporating prior information." Water Resources Research **22**(2): 199-210.

Casella, G. and R. Berger (2002). "Statistical Inference. Duxbury." Pacific Grove, CA.

Certes, C. and G. de Marsily (1991). "Application of the pilot point method to the identification of aquifer transmissivities." Advances in Water Resources **14**(5): 284-300.

Chavent, G. and J. Liu (1989). Multiscale parametrization for the estimation of a diffusion coefficient in elliptic and parabolic problems. 5th IFAC Symposium on Control of Distributed Parameter Systems, Perpignan.

De Marsily, G., G. Lavedan, M. Boucher and G. Fasanino (1984). "Interpretation of interference tests in a well field using geostatistical techniques to fit the permeability distribution in a reservoir model." Geostatistics for natural resources characterization, Part **2**: 831-849.

Doherty, J. (2003). "Ground water model calibration using pilot points and regularization." Ground Water **41**(2): 170-177.

Doherty, J. (2004). "PEST Model-Independent Parameter Estimation User Manual, Watermark Numerical Computing." Brisbane, Australia.
Donovan, J. D. (1996). "Hydrostratigraphy and allostratigraphy of the Cenozoic alluvium in the northwestern part of Las Vegas Valley, Clark County, Nevada." Unpublished M.S. Thesis, University of Nevada-Las Vegas, 196 p.
Duffy, A. C. (2009). An introduction to gradient computation by the discrete adjoint method, Technical report, Florida State University.
Foglia, L., M. Hill, S. Mehl and P. Burlando (2009). "Sensitivity analysis, calibration, and testing of a distributed hydrological model using error-based weighting and one objective function." Water resources research **45**(6).
Foster, I., C. Kesselman and S. Tuecke (2001). "The anatomy of the grid: Enabling scalable virtual organizations." International journal of high performance computing applications **15**(3): 200-222.
Fu, J. and J. Jaime Gómez-Hernández (2009). "Uncertainty assessment and data worth in groundwater flow and mass transport modeling using a blocking Markov chain Monte Carlo method." Journal of hydrology **364**(3): 328-341.
Galloway, D., D. R. Jones and S. E. Ingebritsen (1999). Land subsidence in the United States, US Geological Survey Reston, VA.
Grimstad, A.-A., T. Mannseth, G. Nævdal and H. Urkedal (2003). "Adaptive multiscale permeability estimation." Computational Geosciences **7**(1): 1-25.
Harbaugh, A. W. (2005). MODFLOW-2005, the US Geological Survey modular ground-water model: The ground-water flow process, US Department of the Interior, US Geological Survey.
Harrill, J. R. (1976). Pumping and Depletion of Ground-water Storage in Las Vegas Valley, Nevada, 1955-74, State of Nevada, Department of Conservation and Natural Resources, Division of Water Resources.
Hayek, M. and P. Ackerer (2007). "An adaptive subdivision algorithm for the identification of the diffusion coefficient in two-dimensional elliptic problems." Journal of Mathematical Modelling and Algorithms **6**(4): 529-545.
Hayek, M., F. Lehmann and P. Ackerer (2008). "Adaptive multi-scale parameterization for one-dimensional flow in unsaturated porous media." Advances in water resources **31**(1): 28-43.
Helm, D. C. (1975). "One-dimensional simulation of aquifer system compaction near Pixley, California: 1. Constant parameters." Water Resources Research **11**(3): 465-478.
Hernandez-Marin, M. and T. J. Burbey (2009). "The role of faulting on surface deformation patterns from pumping-induced groundwater flow (Las Vegas Valley, USA)." Hydrogeology journal **17**(8): 1859-1875.
Heywood, C. E. (1995). Piezometric-extensometric estimations of specific storage in the Albuquerque Basin, New Mexico. US Geological Survey Subsidence Interest Group Conference, Proceedings of the Technical Meeting, Las Vegas, Nevada, February 14–16, 1995.
Hill, M. C. (1998). Methods and guidelines for effective model calibration, US Geological Survey Denver, CO, USA.
Hill, M. C. and C. R. Tiedeman (2006). Effective groundwater model calibration: with analysis of data, sensitivities, predictions, and uncertainty, John Wiley & Sons.

Hill, M. C. and C. R. Tiedeman (2007). Effective groundwater model calibration: with analysis of data, sensitivities, predictions, and uncertainty. Indianapolis (2007) John Wiley & Sons, Inc.
Hoffmann, J. (2003). The application of satellite radar interferometry to the study of land subsidence over developed aquifer systems.
Hoffmann, J., S. Leake, D. Galloway and A. M. Wilson (2003). MODFLOW-2000 Ground-Water Model--User Guide to the Subsidence and Aquifer-System Compaction (SUB) Package, DTIC Document.
Hoffmann, J., H. A. Zebker, D. L. Galloway and F. Amelung (2001). "Seasonal subsidence and rebound in Las Vegas Valley, Nevada, observed by synthetic aperture radar interferometry." Water Resources Research **37**(6): 1551-1566.
Hooper, A. (2008). "A multi-temporal InSAR method incorporating both persistent scatterer and small baseline approaches." Geophysical Research Letters **35**(16).
Hsieh, P. A. and J. R. Freckleton (1993). Documentation of a computer program to simulate horizontal-flow barriers using the US Geological Survey's modular three-dimensional finite-difference ground-water flow model, US Department of the Interior, US Geological Survey.
Jen, D. I. (1998). "A Ground-water Flow and Land Subsidence Model of Las Vegas Valley, Nevada-A Converted MODFLOW Model."
Johnson, A., R. Moston and D. Morris (1968). "Physical and hydrologic properties of water-bearing deposits in subsiding areas in central California: US Geol." Survey Prof. Paper **497**.
Johnson, A. I., (Ed.) (1991). "Land Subsidence, Int. Assoc. of Hydrol. Sci., Gentbrugge, Belgium."
Jorgensen, D. G. (1980). "Relationships between basic soils-engineering equations and basic ground-water flow equations." Geological Survey water-supply paper (USA).
Kampes, B. M., R. F. Hanssen and Z. Perski (2003). Radar interferometry with public domain tools. Proceedings of FRINGE.
Keating, E. H., J. Doherty, J. A. Vrugt and Q. Kang (2010). "Optimization and uncertainty assessment of strongly nonlinear groundwater models with high parameter dimensionality." Water Resources Research **46**(10).
Lavenue, M. and G. Marsily (2001). "Three-dimensional interference test interpretation in a fractured aquifer using the Pilot Point Inverse Method." Water Resources Research **37**(11): 2659-2675.
Liu, J. (1993). "A multiresolution method for distributed parameter estimation." SIAM Journal on Scientific Computing **14**(2): 389-405.
Lu, D., M. Ye, M. C. Hill, E. P. Poeter and G. P. Curtis (2014). "A computer program for uncertainty analysis integrating regression and Bayesian methods." Environmental Modelling & Software **60**(0): 45-56.
Malmberg, G. T. (1965). "Available water supply of the Las Vegas ground-water basin Nevada."
Maxey, G. B. and C. Jameson (1948). Geology and Water Resources of Las Vegas, Pahrump, and Indian Spring Valleys, Clark and Nye Counties, Nevada, Nevada Office of the State Engineer.
McDonald, M. G. and A. W. Harbaugh (1984). A modular three-dimensional finite-difference ground-water flow model, Scientific Publications Company Washington.

Morgan, D. S. and M. D. Dettinger (1994). "Ground-water conditions in Las Vegas Valley, Clark County, Nevada: Part II. Geohydrology and simulation of ground-water flow."
Nash, J. and J. Sutcliffe (1970). "River flow forecasting through conceptual models part I—A discussion of principles." Journal of hydrology **10**(3): 282-290.
Pavelko, M. T. (2004). Estimates of hydraulic properties from a one-dimensional numerical model of vertical aquifer-system deformation, Lorenzi Site, Las Vegas, Nevada, US Department of the Interior, US Geological Survey.
Plume, R. W. (1984). "Ground-water conditions in Las Vegas Valley, Clark County, Nevada; Part I. Hydrogeologic Framework." U.S. Geological Survey Open-File Rep. **84**(130).
Poeter, E. P. and M. C. Hill (1998). Documentation of UCODE: A computer code for universal inverse modeling, DIANE Publishing.
Poeter, E. P., M. C. Hill, E. R. Banta, S. Mehl and S. Christensen (2005). Ucode_2005 and six other computer codes for universal sensitivity analysis, calibration, and uncertainty evaluation: US geological survey techniques and methods 6-A11, US Geological Survey.
Poeter, E. P., Hill, M.C., Lu, D., Mehl, S.W. (2014). "UCODE_2014, with New Capabilities to Define Parameters Unique to Predictions, Calculate Weights using Simulated Values, Estimate Parameters with SVD, and Evaluate Uncertainty with MCMC." International Ground Water Modeling Center Report.
Poland, J. F. and G. H. Davis (1969). "Land subsidence due to withdrawal of fluids." Reviews in engineering geology **2**: 187-270.
Poland, J. F., B. Lofgren and F. S. Riley (1972). "Glossary of selected terms useful in studies of the mechanics of aquifer systems and land subsidence due to fluid withdrawal."
Pope, J. P. and T. J. Burbey (2004). "Multiple-Aquifer Characterization from Single Borehole Extensometer Records." Groundwater **42**(1): 45-58.
Prasad, K. L. (2001). "Estimating net aquifer recharge and zonal hydraulic conductivity values for Mahi right bank canal project area, India by genetic algorithm." J. Hydrol. **243**: 149-161.
Rao, S. V. N. (2003). "Optimal groundwater management in deltaic regions using simulated annealing and neural networks." Water Resour. Manage. **17**(6): 409-428.
Renard, P. (2007). "Stochastic hydrogeology: what professionals really need?" Groundwater **45**(5): 531-541.
Renard, P. and G. De Marsily (1997). "Calculating equivalent permeability: a review." Advances in Water Resources **20**(5): 253-278.
Riley, F. S. (1969). "Analysis of borehole extensometer data from central California." Land subsidence **2**: 423-431.
Rosen, P. A., S. Hensley, G. Peltzer and M. Simons (2004). "Updated repeat orbit interferometry package released." Eos, Transactions American Geophysical Union **85**(5): 47-47.
Schulz, K., K. Beven and B. Huwe (1999). "Equifinality and the problem of robust calibration in nitrogen budget simulations."
Terzaghi, K. (1925). "Principles of soil mechanics, IV—Settlement and consolidation of clay." Eng. News Rec **95**(3): 874-878.

Trescott, P. C., G. F. Pinder and S. Larson (1976). Finite-difference model for aquifer simulation in two dimensions with results of numerical experiments, US Government Printing Office.
Vrugt, J. A., C. Ter Braak, C. Diks, B. A. Robinson, J. M. Hyman and D. Higdon (2009). "Accelerating Markov chain Monte Carlo simulation by differential evolution with self-adaptive randomized subspace sampling." International Journal of Nonlinear Sciences and Numerical Simulation **10**(3): 273-290.
Yan, T. (2007). "Effects of delayed drainage on subsidence modeling and parameter estimation."
Yan, T. and T. J. Burbey (2008). "The value of subsidence data in ground water model calibration." Groundwater **46**(4): 538-550.
Zhang, M., T. J. Burbey, V. D. S. Nunes and J. Borggaard (2013). "A New Zonation Algorithm with Parameter Estimation Using Hydraulic Head and Subsidence Observations." Groundwater.